AD-A171 075   CANARD/TAIL TRANSONIC ANALYSIS(U) GRUMMAN AEROSPACE CORP BETHPAGE NY   P AIDALA OCT 85 AFWAL-TR-85-3087 F33615-81-C-3013   1/2

UNCLASSIFIED   F/G 20/4   NL

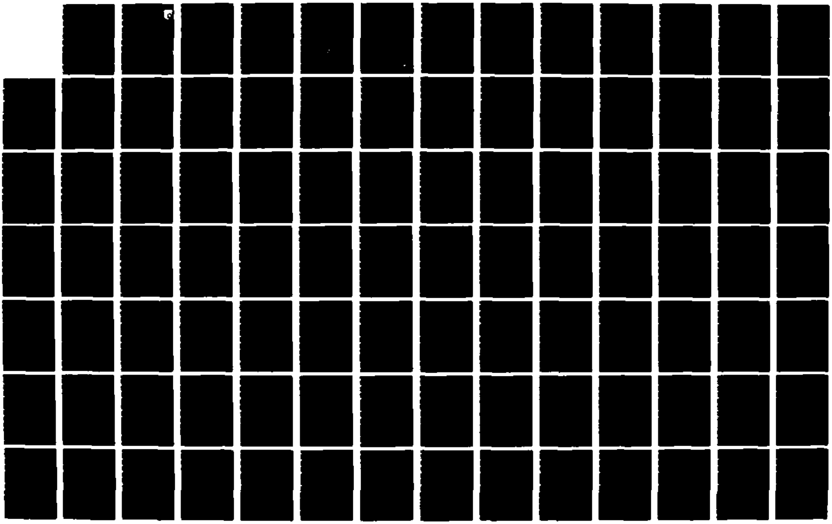

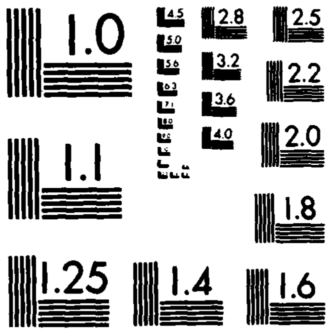

MICROCOPY RESOLUTION TEST CHART
NATIONAL BUREAU OF STANDARDS-1963-A

AFWAL-TR-85-3087

CANARD/TAIL TRANSONIC ANALYSIS

P. Aidala
Grumman Aerospace Corporation
Bethpage, New York 11714

October 1985

Final Report June 1981 to June 1985

Approved for public release; distribution unlimited

FLIGHT DYNAMICS LABORATORY
AIR FORCE WRIGHT AERONAUTICAL LABORATORIES
AIR FORCE SYSTEMS COMMAND
WRIGHT-PATTERSON AIR FORCE BASE, OHIO 45433

NOTICE

When Government drawings, specifications, or other data are used for any purpose other than in connection with a definitely related Government procurement operation, the United States Government thereby incurs no responsibility nor any obligation whatsoever; and the fact that the government may have formulated, furnished, or in any way supplied the said drawings, specifications, or other data, is not to be regarded by implication or otherwise as in any manner licensing the holder or any other person or corporation, or conveying any rights or permission to manufacture, use, or sell any patented invention that may in any way be related thereto.

This technical report has been reviewed and is approved for publication.

James M Gruden

JAMES M. GRUDEN, CAPT
Project Engineer
Power Components Branch

Lowell D. Massie

LOWELL D. MASSIE
Technical Area Manager
Power Components Branch
Aerospace Power Division

FOR THE COMMANDER

James D. Reams

JAMES D. REAMS
Chief, Aerospace Power Division
Aero Propulsion Laboratory

If your address has changed, if you wish to be removed from our mailing list, or if the addressee is no longer employed by your organization please notify AFWAL/POOC-1, Wright-Patterson AFB OH 45433-________ to help maintain a current mailing list.

Copies of this report should not be returned unless return is required by security considerations, contractual obligations, or notice on a specific document.

ADA 171075

UNCLASSIFIED

SECURITY CLASSIFICATION OF THIS PAGE

REPORT DOCUMENTATION PAGE

1a REPORT SECURITY CLASSIFICATION Unclassified	1b RESTRICTIVE MARKINGS None.
2a SECURITY CLASSIFICATION AUTHORITY	3 DISTRIBUTION/AVAILABILITY OF REPORT Approved for public release; distribution is unlimited.
2b DECLASSIFICATION/DOWNGRADING SCHEDULE	
4 PERFORMING ORGANIZATION REPORT NUMBER(S)	5 MONITORING ORGANIZATION REPORT NUMBER(S) AFWAL-TR-85-3087
6a NAME OF PERFORMING ORGANIZATION Grumman Aerospace Corp. 6b OFFICE SYMBOL (If applicable)	7a NAME OF MONITORING ORGANIZATION AF FLIGHT DYNAMICS LABORATORY AFWAL (AFSC)
6c ADDRESS (City, State, and ZIP Code) 111 Stewart Avenue Bethpage, NY 11714	7b ADDRESS (City, State, and ZIP Code) Wright-Patterson AFB, OH 45433
8a NAME OF FUNDING SPONSORING ORGANIZATION Flight Dynamics Laboratory 8b OFFICE SYMBOL (If applicable) AFWAL/FIMM	9 PROCUREMENT INSTRUMENT IDENTIFICATION NUMBER F33615-81-C-3013
8c ADDRESS (City, State and ZIP Code) Air Force Wright Aeronautical Laboratories Wright-Patterson Air Force Base, OH 45433	10 SOURCE OF FUNDING NUMBERS PROGRAM ELEMENT NO 62201F; PROJECT NO 2404; TASK NO. 10; WORK UNIT ACCESSION NO 60

11 TITLE (Include Security Classification)
Canard/Tail Transonic Analysis

12 PERSONAL AUTHOR(S)
P. Aidala

13a TYPE OF REPORT	13b TIME COVERED	14 DATE OF REPORT (Year, Month, Day)	15 PAGE COUNT
Final Technical	FROM 6/81 TO 6/85	October 1985	103

16 SUPPLEMENTARY NOTATION

17 COSATI CODES

FIELD	GROUP	SUB-GROUP
01	01	
02	03	

18 SUBJECT TERMS (Continue on reverse if necessary and identify by block number)
Computational Aerodynamics; Numerical Optimization; Wake Flows; Vortex Modeling; Approximate Factorization

19 ABSTRACT (Continue on reverse if necessary and identify by block number)

The theoretical and operational characteristics of the CANTATA code are described. The code provides 3-D transonic analysis of wing-body-canard or wing-body-tail configurations. The relative placement of the two lifting surfaces is arbitrary. The potential flow solution of the code uses a new ADI algorithm, AF2YZ. The algorithm is a three step procedure which uses a split streamwise operator, with a simple factorization of the cross-plane terms. The analysis includes the ability to allow the vortex sheets from the lifting surfaces to move under the influence of the local velocity. Wake rollup is modeled by merging vortex lines such that a single-valued spanwise shape is maintained. Viscous effects are included through the use of a strip boundary layer method. The overall code includes a numerical optimization routine that can be used to alter the lifting surface geometry in an automated design procedure.

20 DISTRIBUTION/AVAILABILITY OF ABSTRACT ☒ UNCLASSIFIED/UNLIMITED ☐ SAME AS RPT ☐ DTIC USERS	21 ABSTRACT SECURITY CLASSIFICATION Unclassified
22a NAME OF RESPONSIBLE INDIVIDUAL James R. Sirbaugh	22b TELEPHONE (Include Area Code) 513/255-3761 22c OFFICE SYMBOL AFWAL/FIMM

DD FORM 1473, 84 MAR — 83 APR edition may be used until exhausted. All other editions are obsolete.

SECURITY CLASSIFICATION OF THIS PAGE

UNCLASSIFIED

PREFACE

The work documented in this report was performed over four years with the participation of many other individuals. Several whose contributions should be acknowledged are: William Mason and Christina Prete of Grumman Aerospace; Professor Antony Jameson of Princeton University; Professor Jack Werner of Polytechnic Institute of New York; and Glenn Gustafson and James Sirbaugh of AFWAL/FIMM. The use of the NASA Ames CRAY computer was an important factor in the performance of this work. The cooperation of the personnel at NASA Ames was always timely and helpful.

CONTENTS

ILLUSTRATIONS

ILLUSTRATIONS (contd)

TABLES

LIST OF SYMBOLS

b	Wing span.
A,B,C,D	Constant coefficients in Equations (4) and (7).
C_p	Pressure coefficient.
M	Freestream Mach number.
x,X	Streamwise physical coordinate.
y,Y	Spanwise physical coordinate.
YV,ZV	Y,Z coordinates of a vortex line.
z,Z	Vertical physical coordinate.
ZW	Z coordinate of the wake sheet.
α	Angle-of-attack or ADI acceleration parameter.
ω	Overrelaxation parameter.
Γ	Circulation.
γ	Specific heat ratio.
ϕ	Perturbation velocity potential.
ξ	Symbolic streamwise computational coordinate.
η	Symbolic spanwise computational coordinate.
ζ	Symbolic vertical computational coordinate.
ξ_∞	Value for ξ in Equation (7) that corresponds to upstream and downstream infinity.
$\delta\phi$	Change in potential.

<u>SUBSCRIPTS</u>

GLE	Fine grid leading edge.
GTE	Fine grid trailing edge.
X,Y,Z,ξ,η,ζ	Partial derivatives.
n	Normal derivative.

1 - INTRODUCTION

The code is named CANTATA - CANard/TAil Transonic Aerodynamics. It operates on the CRAY X-MP computer at NASA Ames Research Center. Part of the computer time for the code development and evaluation was provided through the Applied Computational Fluids Branch at Ames. The code is stored on the Ames CRAY in UPDATE format.

The CANTATA code was developed from the PANDORA wing-body-canard code (Ref 1). The PANDORA code was developed from an earlier version (1978) of the Boppe wing-body code (Ref 2). Some parts of the three codes are essentially identical. Unnecessary details of the code which are the same as described in Ref 1, 2 and 4 are not repeated here. Those references should be consulted if the particular code details are of interest.

The major improvements incorporated in the CANTATA code are arbitrary canard (or tail) placement, an Alternating Direction Implicit (ADI) solution and a "floating" wake analysis capability. In addition, the CANTATA code takes advantage of the vector processing capability of the CRAY computer.

1 Aidala, P., "Numerical Aircraft Design Using 3-D Transonic Analysis with Optimization," AFWAL-TR-81-3091, August 1981.

2 Boppe, C. W., "Transonic Flowfield Analysis for Wing-Fuselage Combinations," NASA Contractor Report 3243, May 1980.

2 - WING-BODY-CANARD TRANSONIC ANALYSIS

The basic computational method employed in the transonic analysis is that of Boppe (Ref 2). The significant new developments are described in detail here. The common parts (flow equation, embedded grid interfacing, body modeling, viscous effects) are described briefly. Additional details can be found in Ref 1 and 2.

2.1 FLOW EQUATION

The flow equation used in the analysis is an "extended" small-disturbance equation:

$$(1-M^2 - (\gamma+1)M^2\phi_X - \frac{\gamma+1}{2} M^2\phi_X^2)\phi_{XX} - 2M^2\phi_Y + (1-(\gamma-1)M^2\phi_X)\phi_{YY} + \phi_{ZZ} = 0 \tag{1}$$

The additional terms have been added to better capture swept shock waves and more accurately determine the critical velocity. Empirical modifications and similarity variables are not employed. Pressure coefficients on wing surfaces are computed using the complete isentropic formula. To simplify velocity computations on the non-planar body surface, a simplified equation is used:

$$C_p = -(2\phi_X + (1-M^2)\phi_X^2) \tag{2}$$

The computational space is filled with a relatively crude Cartesian mesh. Instead of adopting a formal far-field solution for the grid outer boundaries, the original X, Y, Z region is stretched to ξ, η, ζ, a region in which the boundaries correspond to infinity. The flow field potential is set to zero on all bounding planes except the downstream plane, at which all X-derivatives are set to zero.

The following conditions are enforced at the symmetry plane.

$$\phi_Y = 0 \tag{3a}$$

$$\phi_{XY} = 0 \tag{3b}$$

2.2 GLOBAL CRUDE GRID

The key item to enable wing-canard analysis without undue computer storage requirements was the development of suitable grid point distributions. The global crude mesh uses 65, 26 and 31 planes in the streamwise, spanwise and vertical directions, respectively. This results in 52,390 mesh points.

In order to distribute the crude grid streamwise mesh planes as effectively as possible, separate grids are used for wing and wing-canard analysis. Without a canard, a symmetric streamwise grid is generated with the function

$$X = B_0\xi \tag{4a}$$

$$X = X_1 + B_1 \text{ TAN } (\frac{\pi}{2} (\xi - \xi_1)) + B_2\text{TAN } (\frac{\pi}{2} (\xi - \xi_1)^3) \tag{4b}$$

where B_o is chosen to place 80% of the grid points between $\pm X_1$. The value of X_1 is chosen to center the grid between the most forward and aft points of the exposed wing. The constant B_1 is used to match the grid spacing ($dx/d\xi$) at X_1, and B_2 is used to provide additional stretching to the far field.

The length scale for the streamwise grid is the chord at midspan of the wing. The transformation places the first and last points at infinity. The second and first-to-last points are the effective numerical boundaries, and are at 8.6 mid-chords from the mid-point of the chord at mid-span. The far-field boundary is not swept or tapered.

When a canard is present, the grid of Equation (4 a,b) usually results in too few crude grid planes intercepting the canard planform. The streamwise grid transformation used for wing-canard combinations is:

$$X = A_0 + A_1\xi + A_2\xi^2 + A_3\xi^3 + A_4\xi^4 + A_5\xi^5 + A_S\xi/(1-\xi) \tag{5a}$$

$$\xi = \xi/\xi_\infty \tag{5b}$$

This transforms the finite domain $-\xi_\infty \leq \xi \leq \xi_\infty$ to the *infinite region* $-\infty < X < \infty$. Constant A_S is empirical, controlling the rate of stretching near infinity. The points at $\xi = \pm 1$ are made the points of maximum density of mesh planes by specifying the second derivative of X to be zero. The value of X and the first derivative of X at $\xi = \pm 1$ are also specified to determine the coefficients A_0 to A_5. The value of ξ_∞ is adjusted iteratively to place approximately 60% of the total mesh planes between the most forward and the most aft points on the wing-canard combination.

For an aft swept wing-canard combination, the wing tip and canard tip determine the transformation. The mid-points of the two tip chords are the values of X for $\xi = \pm 1$. The first derivative of X is set to result in a nominal six mesh planes intercepting each of the tip chords. An example of the resulting wing-canard grid transformation and the corresponding physical mesh plane distribution is shown in Figure 1. The mesh generation has been applied to several aft-swept configurations, several forward-swept configurations and to several arbitrary wing-canard parametric variations. Good results were observed in all cases. For forward swept wings, the canard tip and wing tip may be at the same streamwise location. In this case, the two

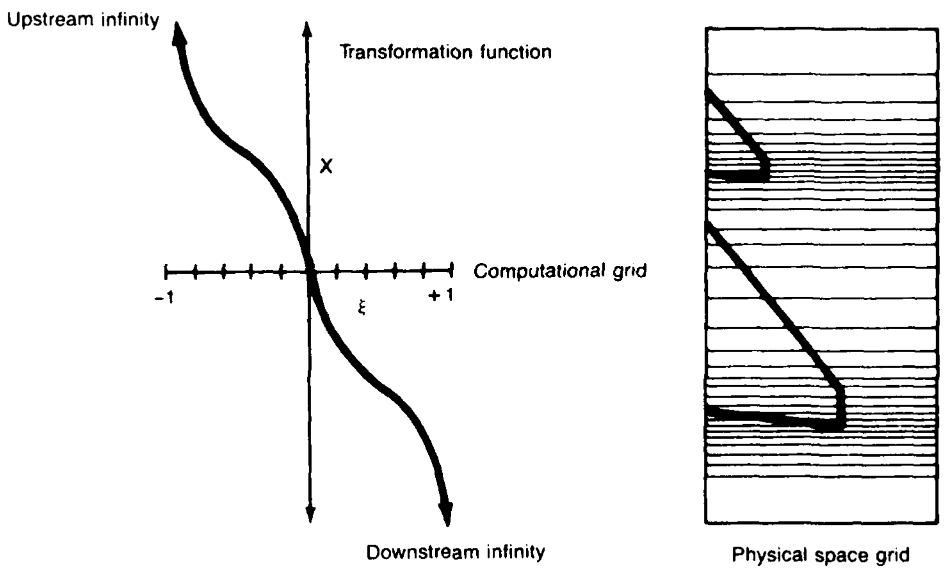

Figure 1. Wing-canard crude mesh transformation.

streamwise points used for $\xi = \pm 1$ in the transformation are the wing/canard tip location and near the trailing edge of the centerline of the wing.

The two arbitrary factors, A_S and ξ_∞ do not allow an analytic expression for the distance to the far field. In addition, the local spacing is adjusted for the canard or wing chord, so that the grid is not symmetrical. As explained in the above discussion, the grid scales with the two tip chords and their streamwise separation. This is independent of the spanwise location of the tips.

The spanwise grid transformation is much simpler:

$$Y = (1/A_2)\mathrm{TANH}^{-1}(\eta) + C_1\eta + C_3\eta^3 \tag{6}$$

This transforms the domain $0 \leq \eta \leq 1$ to $0 \leq Y \leq \infty$. Constant A_2 is determined to place 18 spanwise mesh planes between the centerline and wing tip, with the wing tip falling midway between computational planes. Constants C_1 and C_3 are used to perturb the grid so that the canard tip falls midway between two mesh planes and the wing tip location is not changed. Constants C_1 and C_3 are set to zero when a canard is not present. For a wing-only grid, the spanwise boundary (next-to-last point) is at 2.2 semispans. When a canard is present, the change in the spanwise boundary is usually insignificant.

The vertical grid transformation combines a constant spacing interval near the lifting surfaces with a tangent function stretching to the far field. The computational domain $-1 \leq \zeta \leq 1$ is transformed to the physical domain through the relation

$$Z = Z_{MID} + B_0\zeta \qquad \zeta_{LO} \leq \zeta \leq \zeta_{UP} \tag{7a}$$

$$Z = Z_{MID} + B_0\zeta_{UP} + B_1(\zeta-\zeta_{UP}) + B_3\mathrm{TAN}(B_4(\zeta-\zeta_{UP})) \qquad \zeta \geq \zeta_{UP} \tag{7b}$$

$$Z = Z_{MID} + B_0\zeta_{LO} + B_1(\zeta-\zeta_{LO}) + B_3\mathrm{TAN}(B_4(\zeta-\zeta_{LO})) \qquad \zeta \leq \zeta_{LO} \tag{7c}$$

$$B_1 = B_0 - B_3B_4 \tag{7d}$$

$$B_3 = \frac{B_0\zeta_{UP} + \Delta Z_{BNDRY} - (1-\Delta\zeta-\zeta_{UP})B_0}{\mathrm{TAN}(B_4(1-\Delta\zeta-\zeta_{UP}) - B_4(1-\Delta\zeta-\zeta_{UP})} \qquad \zeta \geq \zeta_{up} \tag{7e}$$

$$B_3 = \frac{B_0\zeta_{LO} + \Delta Z_{BNDRY} - (1-\Delta\zeta+\zeta_{LO})B_0}{\mathrm{TAN}(B_4(1-\Delta\zeta+\zeta_{LO}) - B_4(1-\Delta\zeta+\zeta_{LO})} \qquad \zeta \leq \zeta_{LO} \tag{7f}$$

The coefficient B_0 is initially chosen for a grid spacing of 0.088 mid-chords. It is then adjusted to align grid planes with the two lifting surfaces, with the center of the grid midway between the surfaces (at Z_{MID}). The constant spacing of Equation (7a) is extend two grid planes above and below the surfaces to ζ_{UP} and ζ_{LO}, respectively. The stretchings of Equations (7b) and (7c) place the next to last points a distance ΔZ_{BNDRY}, which is eight mean aerodynamic chords, from Z_{MID}.

An input parameter (ITWAKE) is used to turn on the free wake calculation. Details of the calculation are given in Appendix A. A wake shape calculation is performed every ITWAKE iterations of the potential solution. After each wake shape calculation, the Z grid is sheared to follow the vortex sheet that leaves the trailing edges of the lifting surfaces. The wake shape of the shorter semispan is extended spanwise parallel to the larger semispan. The larger semispan is extended spanwise at a constant value of Z equal to the most outboard value on the wake. The Z grid is then reconstructed, using the same stretching formula described previously. The resulting Z grid is sheared in X and Y, and does not permit two wakes to merge.

2.3 EMBEDDED FINE GRID SYSTEM

Individual fine grid arrays are constructed for the wing and canard. The code always designates the forward lifting surface as the "canard" and the aft surface as the "wing." Thus, the wing of a wing-tail configuration is considered the "canard" and the tail is considered the "wing." These secondary mesh systems serve two purposes. First, detailed computations are performed only in a region very close to the surface where gradients are large and details are important. The resulting numerical efficiency permits a very dense computational mesh, a benefit in both the resolution of shock waves and the calculation of configuration forces and moments. Second, the embedded mesh systems are independent and optimized for a particular geometric component. The system is not constrained by a single geometry-fitting transformation.

Fine grid arrays are set up at each position where a crude spanwise mesh plane cuts the wing and canard surface. With 18 spanwise crude planes between the centerline and wing tip, an isolated wing analysis would have 18 fine wing grids. (A fuselage would reduce the number of fine wing grids by the number

of mesh planes within the computational wing root junction.) The number of canard fine grids is proportional to the extent of the canard semispan. If the canard semispan were half that of the wing, then the canard would have approximately half the number of wing fine grids. This would increase the computation time for the fine grid solution by 50%.

The local section leading edge is placed midway between mesh points and the trailing edge is placed at a mesh point. The streamwise mesh spacing is scaled by the local chord. Thus, each section has the same number of grid points along the chord (72). The nominal boundaries of the fine grids are at 20% of the local chord in front of each leading edge and 40% behind each trailing edge. The total number of fine grid points will vary for different canard/wing semispan ratios. The dimensions of the code will allow 101,250 fine grid points. This corresponds to 30 fine grids on the wing and canard, with each having 135 streamwise points and 25 vertical points.

The starting fine grid system is illustrated in Figure 2. As described above, the fine grids are sheared and tapered to conform to the wing and canard planforms. This represents a transformation function between the fine grid computational domain ξ and the physical domain X:

$$X = \xi\,(X_{GTE} - X_{GLE}) + X_{GLE} \tag{8}$$

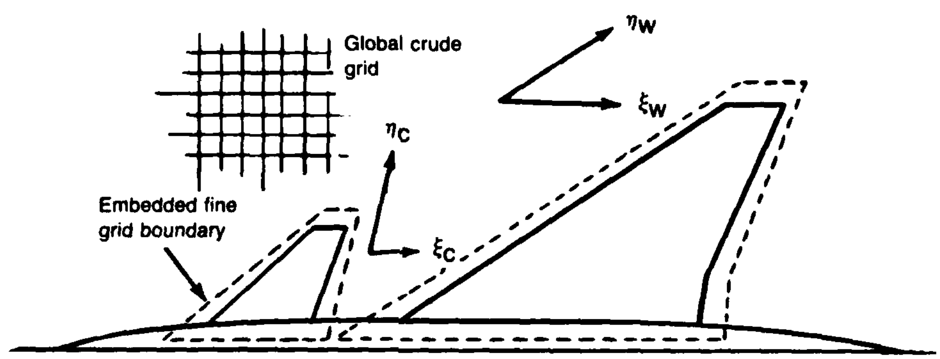

Figure 2. Embedded fine grid system.

The spanwise (Y) transformation is the same as that for the crude grid. The fine Z grid is aligned with the crude Z grid along any surfaces and wakes. In addition, the top and bottom of the fine grid is aligned with the appropriate crude grid plane. Linear interpolation is used in the streamwise direction. The fine grid spacing is constant between surfaces. The constant spacing is continued two points above and below the surfaces. Then the grid is stretched with a parabolic function to the top and bottom boundaries. The nominal locations of the boundaries are five crude grid planes above the surface, and three crude grid planes below the surface.

2.4 SOLUTION TECHNIQUE

The crude grid solution uses Successive Line Over-Relaxation (SLOR). As the vertical line relaxation marches downstream, each streamwise location (streamwise index) is tested to see if a surface or wake will be intercepted. The test is done for both a "high" and "low" surface or wake. The vertical line segments are subdivided by each surface or wake. Thus, when two surfaces (or wakes) are present at a streamwise index, three separate tridiagonal inversions occur. When the two surfaces are in-plane, the "low" surface is the forward one, and the "high" surface is the aft one, with the appropriate logic testing for the in-plane arrangement. The crude grid solution starts at the spanwise boundary and then marches toward the centerline. The fine grid solution update is developed separately on the wing and canard. The solution is first done on the wing and then on the canard. When the fine grid solution on the canard has been updated, one iteration of the fine solution is completed.

The fine grid solution of Equation (1) employs an approximate factorization algorithm that was suggested by Professor Antony Jameson of Princeton University as a consultant to this study. The factorization can be written as:

$$(\alpha + B_1 T\delta_X^{\pm})\,[(\alpha + B_2\delta_Y^2)\,(\alpha + B_3\delta_Z^2) + E_X^{-1}]\delta\phi^n = \omega\alpha^2 L\phi^n \tag{9a}$$

$$\phi^{n+1} = \phi^n + \delta\phi^n \tag{9b}$$

$$B_1 = -\left(\frac{\xi_X}{\Delta\xi}\right)\left(\frac{\Delta\zeta}{\zeta_Z}\right) \tag{9c}$$

$$B_2 = -\left(\frac{\zeta_Z}{\Delta\zeta}\right)^{3/2} \left(\frac{\Delta\xi}{\xi_X}\right)^{1/2} \quad (9d)$$

$$B_3 = -\frac{\eta^2{}_Y}{\Delta\eta^2}\left(\frac{\Delta\xi\Delta\zeta}{\xi_X\ \zeta_Z}\right)^{1/2} \quad (9e)$$

The operator L produces the residual of Equation (1). The coefficient T is the nonlinear coefficient of ϕ_{XX} in Equation (1). The δ_X^+ operator is used at elliptic (subsonic) points in the flowfield, and the δ_X^- operator is used at hyperbolic (supersonic) points.

The solution of this factorization is developed in three steps:

$$\text{Step 1.}\quad (\alpha + B_1T\delta_X^{\pm})\delta\phi_1^n = \omega\alpha^2L\phi^n \quad (10a)$$

$$\text{Step 2.}\quad (\alpha + B_2\delta_Y^2)\delta\phi_2^n = \delta\phi_1^n - E_X^{-1}\delta\phi^n \quad (10b)$$

$$\text{Step 3.}\quad (\alpha + B_3\delta_Z^2)\delta\phi^n = \delta\phi_2^n \quad (10c)$$

Each step involves only tridiagonal inversions, and can be vectorized by inverting several matrices in parallel. Within the separate wing or canard fine grid system, Step 1 is solved for all points in the flowfield. Then Steps 2 and 3 are marched downstream.

The embedded fine grid interface with the crude grid is accomplished by alternately updating the crude grid and fine grid solutions. Potential values at interior points (i.e., on a lifting surface) of the crude grid are fixed by interpolating the most recent fine grid solution. The potential values at the perimeter of the fine grids are fixed by interpolating the most recent crude grid solution. In order to speed up the overall solution convergence, the fine grid solution is not calculated until the crude grid solution has established the "coarse" characteristics of the flow (approximately 100 iterations). Then the crude/fine interaction is begun until both grids are satisfactorily converged (typically an additional 105 cycles). Three-point *LaGrange interpolation* of the crude grid potential values is used to initialize and update the fine grid.

One cycle of the crude/fine grid interaction consists of two steps (see Figure 3):

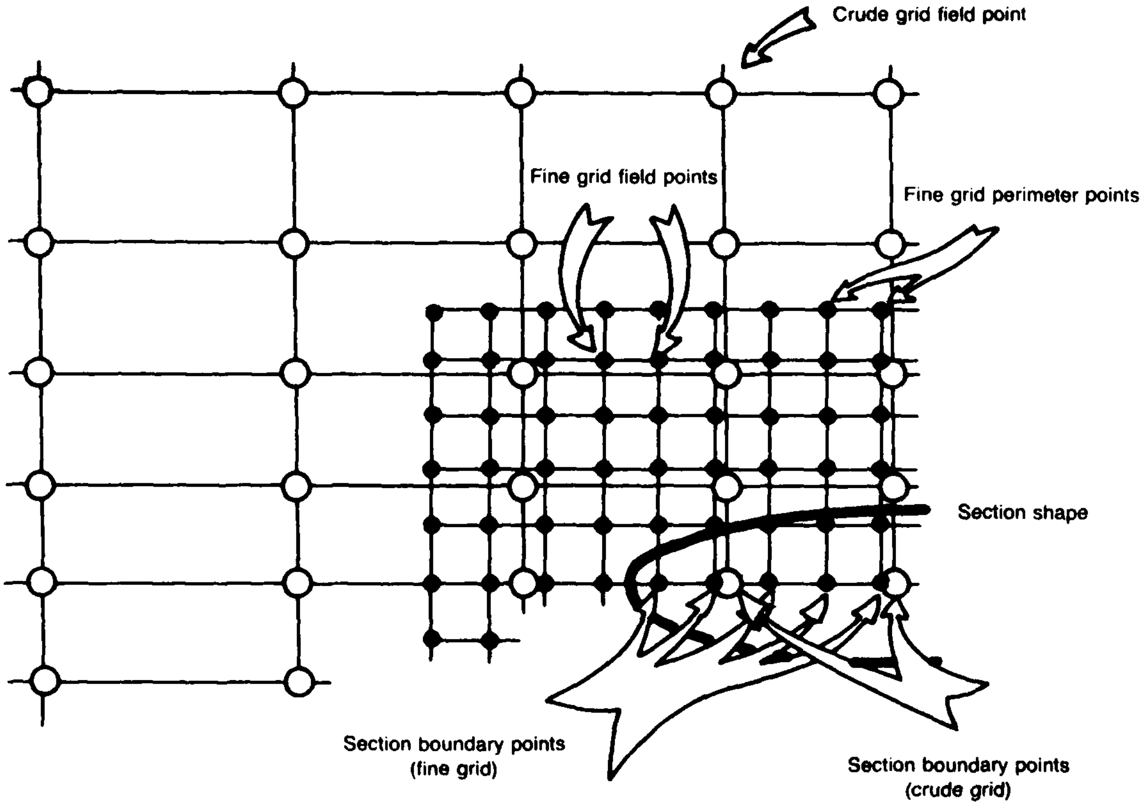

Figure 3. Fine/crude grid interface (from Ref 2).

Step 1. The embedded wing grid is swept holding fine grid perimeter points fixed as an outer boundary. Conventional Neumann boundary conditions (ϕ_n) are imposed at fine grid section boundary points forming an inner boundary.

Step 2. The crude grid section boundary points are computed using the potentials at the fine grid section boundary points (linear interpolation). These crude potentials (ϕ) are held fixed for the global crude grid sweep forming an array of Dirichlet inner boundary conditions. Infinity boundary conditions at the limits of the crude computational space form the outer boundary. At the end of the crude grid sweep, crude grid potentials are used to update the fine grid perimeter points.

One solution iteration of only the crude grid takes 0.35 sec of CRAY X-MP CPU time (6.7×10^{-6} CPU sec per point). One crude/fine cycle takes 1.4 sec CPU time for 23 wing and canard fine grids. Each fine grid has 135 streamwise points and 25 vertical points. Thus, one crude/fine solution cycle solves 130,015 points total (1.9×10^{-5} CPU sec per point). For different wing-canard combinations, the crude/fine CPU time is essentially proportional to the number of wing and canard fine grid arrays.

The development of the solution is monitored by calculating the maximum update to the flow field potential (CCMAX in the printout) and its position in the three-dimensional flow field. The magnitude of the potential update is inversely proportional to the acceleration parameter α in Equation (10). The parameter is cycled through eight values during the solution. In addition, an overall scaling of the α parameters occurs during the solution based on the change in the maximum residual. The initial values of the parameter are set to relatively large values (i.e., slower convergence) in order to provide more reliable results for difficult cases. The automatic scaling will later decrease, or increase, the α parameters as appropriate. However, the scaling occurs only after each set of eight values, which corresponds to eight solution iterations. This results in a relatively slow decrease of the α parameters when it may occur. Consequently, "easy" solutions are penalized with a slower rate of convergence than would be optimal.

The solution is essentially converged when the circulation (CIR in the printout) shows no significant change in about 24 solution cycles. It is possible that a non-decreasing CCMAX value is due to "noise" in the crude/fine interface that does not decay. The position of CCMAX is useful in pinpointing the problem area when divergence occurs. Problem areas may develop when the flow conditions are extreme or when the geometric representation is in error. The solution will terminate itself if divergence is detected.

Three other parameters that indicate the solution convergence appear in the code output as CCAV, RSD and RSDAV. The CCAV parameter is the average of the absolute value of the flow potential corrections at every point. It is a more reliable indication of the solution convergence than CCMAX, and is used to satisfy the convergence test input option. The RSD parameter is the largest residual in the solution. The location of the RSD value is also printed.

The RSDAV parameter is the average of the absolute value of the residual at every point. The vertical index for the location of CCMAX and RSD are negative when the point is located at the lower side of the wing or canard plane. The jump in potential at these locations is handled by an extra array of potential values that have their own index system. As discussed for CCMAX, the values of CCAV, RSD and RSDAV will vary due to changes in the acceleration parameter α.

No precise non-dimensional parameter is available to compare the solution convergence for different grids. The CCMAX and CCAV values are scaled by the wing average cord. This results in the same values for CCMAX and CCAV if the scale of the input geometry is changed (e.g., full scale or model scale). Changes to the planform (e.g., aspect ratio or taper) would result in CCMAX and CCAV values that are not directly comparable. As mentioned above, the reduction in CCMAX and CCAV relative to the starting value should be used to evaluate the solution convergence.

2.5 TRANSFORMED EQUATION AND FINITE DIFFERENCE APPROXIMATIONS

Due to the grid stretching and shearing, the derivatives in terms of the physical domain coordinates (X,Y,Z) are calculated by the following formulas used with the computational domain variables (ξ,η,ζ):

$$\phi_X = \phi_\xi \xi_X + \phi_\zeta \zeta_X \tag{11a}$$

$$\phi_Y = \phi_\xi \xi_Y + \phi_\eta \eta_Y + \phi_\zeta \zeta_Y \tag{11b}$$

$$\phi_Z = \phi_\zeta \zeta_Z \tag{11c}$$

$$\phi_{XX} = \phi_\xi \xi_{XX} + \phi_\zeta \zeta_{XX} + \phi_{\xi\xi} \xi_X^2 + 2\phi_{\xi\zeta} \xi_X \zeta_X + \phi_{\zeta\zeta} \zeta_X^2 \tag{11d}$$

$$\phi_{YY} = \phi_\xi \xi_{YY} + \phi_\eta \eta_{YY} + \phi_\zeta \zeta_{YY} + 2\phi_{\xi\eta} \eta_Y \xi_Y + \phi_{\xi\xi} \xi^2{}_Y + \phi_{\eta\eta} \eta_Y^2 + 2\phi_{\eta\zeta} \eta_Y \zeta_Y + \phi_{\zeta\zeta} \zeta_Y^2 \tag{11e}$$

$$\phi_{XY} = \phi_\xi \xi_{XY} + \phi_\zeta \zeta_{XY} + \phi_{\xi\xi} \xi_X \xi_Y + \phi_{\xi\eta} \xi_X \eta_Y \tag{11f}$$

$$\phi_{ZZ} = \phi_\zeta \zeta_{ZZ} + \phi_{\zeta\zeta} \zeta_Z^2 \tag{11g}$$

In the crude grid the X grid is independent of Y, so that the ξ_Y, ξ_{XY}, and ξ_{YY} terms are not needed. They are not coded for the crude grid. The ζ_X, ζ_Y, ζ_{XX}, ζ_{XY}, and ζ_{YY} terms are zero when there is no wake deflection (the Z grid

is then independent of X and Y). The shearing terms for the X and Z grid are calculated with second order differences and implicit differentiation formulas.

The finite difference approximations to the first derivatives in the above expressions are always second-order, e.g.:

$$\phi_{\zeta_k} = (\phi_{k+1} - \phi_{k-1})/(2\Delta\zeta) \tag{12}$$

When the flow is subsonic all of the second derivatives are second order, e.g.:

$$\phi_{\zeta\zeta_k} = (\phi_{k+1} - 2\phi_k + \phi_{k-1})/\Delta\zeta^2 \tag{13}$$

The only change when the flow is supersonic is "upwind differencing" of the streamwise second derivative:

$$\phi_{\xi\xi_I} = (2\phi_I^+ - \phi_I - 2\phi_{I-1}^+ + \phi_{I-2})/\Delta\xi^2 \tag{14}$$

where the + superscript indicates new values in the crude grid SLOR solution. The upwind differencing is used only for the $\phi_{\xi\xi}$ contribution to ϕ_{XX}. The term for ϕ_{YY} is always central differenced.

The crude grid overrelaxation of the solution is incorporated at subsonic points as:

$$\phi_{\xi\xi_I} = (\phi_{I+1} - \frac{2}{\omega}\phi_I^+ - 2(1-\frac{1}{\omega})\ \phi_I + \phi_{I-1}^+)/\Delta\xi^2 \tag{15}$$

with ω usually 1.6. The spanwise differences make use of the new potential values at J + 1:

$$\phi_{\xi\eta} = (\phi_{I-1,J-1} - \phi_{I-1,J+1}^+ - \phi_{I+1,J-1} + \phi_{I+1,J+1}^+)/(4\Delta\xi\Delta\eta) \tag{16}$$

$$\phi_{\eta\eta} = (\phi_{I,J-1} - \phi_{I,J}^+ - \phi_{I,J} + \phi_{I,J+1}^+)/\Delta\eta^2 \tag{17}$$

The vertical line relaxation implicitly uses all new potential values for $\phi_{\zeta\zeta}$.

Boundary conditions are imposed by setting the value of a potential or its first derivative at a field point which represents the configuration surface. The wing and canard are approximated by planar surfaces. As discussed previously, the wakes can be either fixed planar surfaces or "floating" surfaces updated periodically during the solution. The body or fuselage is rep-

resented by a fixed cross-sectional surface extending from upstream to downstream infinity. Corrections are applied to the body boundary conditions for the simulation of finite length bodies. Modeling is sufficiently flexible to permit the treatment of wings at varying height relative to the body (high-low mid wing).

Special difference approximations are required at boundary points. The lifting surfaces and wakes are represented numerically by a grid surface of double valued potentials. For a wing surface defined by

$$Z = F(X,Y) \tag{18}$$

the wing flow tangency condition is approximated by

$$\phi_Z\ (X,Y,0) = F_X - \alpha + \delta_X^* \tag{19}$$

where the slope of the boundary layer displacement thickness, δ_X^*, is added only for the inviscid/viscous interaction mode of operation.

The wing upper and lower surface boundary conditions enter the solution formulation by way of the ϕ_{ZZ} term in Equation (1). At a surface, this term can be written

$$\phi_{ZZ} = \frac{1}{\Delta Z}\left[\frac{\phi_{k+1}-\phi_k}{\Delta Z} - \frac{\phi_k-\phi_{k-1}}{\Delta Z}\right] \tag{20}$$

where the I and J subscripts have been dropped for convenience. By incorporating the following relation

$$F_X - \alpha + \delta_X^* = \frac{\phi_{k+1}-\phi_{k-1}}{2\Delta Z} \tag{21}$$

the wing boundary condition on the upper surface becomes

$$\phi_{ZZ}\ (X,Y,0^+) = \frac{2}{\Delta Z}\left[\left(\frac{\phi_{k+1}-\phi_k}{\Delta Z}\right) - (F_X^u - \alpha + \delta_X^*)\right] \tag{22}$$

Similarly, the wing lower surface boundary condition becomes

$$\phi_{ZZ}\ (X,Y,0^-) = -\frac{2}{\Delta Z}\left[\frac{\phi_k-\phi_{k-1}}{\Delta Z} - (F_X^\ell - \alpha - \delta_X^*)\right] \tag{23}$$

At the end of each sweep of the flow field, the Kutta condition is enforced by calculating the circulation at the trailing edge of the wing section

$$\Gamma = \phi(X_{TE},Y,0^+) - \phi(X_{TE},Y,0^-) \tag{24}$$

The boundary condition in the wake is to impose the jump in potential, $\Delta\phi$, across the sheet. When the wake is a fixed, planar sheet, the jump in potential is held constant to the downstream boundary at each spanwise station. For a free wake calculation, the jump in potential is constant across the vortex lines, which can move spanwise. This results in a distribution of the jump in potential that varies both spanwise and streamwise.

The use of the shearing transformation (Equation 11) for the embedded fine grid system complicates the imposition of symmetry conditions and root juncture conditions. The simple Cartesian (crude) grid symmetry condition (Equation 3a) becomes

$$\phi_Y = \phi_\xi \xi_Y + \phi_\eta \eta_Y = 0 \tag{25}$$

at the symmetry plane and

$$\phi_Y = \phi_\xi \xi_Y + \phi_\eta \eta_Y = F_X \tag{26}$$

for fuselage combinations in the root juncture region. Here F_X represents the slope of the fuselage or body at the root. The Z shearing is not used because the grid is always continued inside the root as a constant Z value.

Computations indicate that numerical instabilities will result if special attention is not given to the selection of difference approximations in this region. These difficulties result from the nature of the shearing transformation. To solve this problem, a plane of dummy mesh points is positioned across the symmetry plane or within the body surface. These flow-field potentials are artificial in the sense that there is no physical flow field associated with them. They simply provide a side boundary of potentials which, when used for differencing, produce the proper side condition given by Equation (25) or (26).

A special first order accurate one-sided difference operator is used to generate the dummy interior point potential values. For grid lines that are swept back in the physical plan ($\xi_Y < 0$), the following equation is used

$$\phi^D_{I,J-1} = \left[\frac{\eta_Y}{\Delta\eta}\,\phi_{I,J} - \frac{\xi_Y}{\Delta\xi}\,\phi^D_{I-1,J-1}\right] \Bigg/ \left[\frac{\eta_Y}{\Delta\eta} - \frac{\xi_Y}{\Delta\xi}\right] \tag{27a}$$

and for grid lines that are swept forward ($\xi_Y > 0$),

$$\phi^D_{I,J-1} = \left[\frac{\eta_Y}{\Delta\eta}\,\phi_{I,J} + \frac{\xi_Y}{\Delta\xi}\,\phi^D_{I+1,J-1}\right] \Bigg/ \left[\frac{\eta_Y}{\Delta\eta} + \frac{\xi_Y}{\Delta\xi}\right] \tag{27b}$$

Note that the operator changes depending on whether the grid lines are swept forward or backward. In each case, the coefficient of the dummy potential at the point (I, J-1) is larger than the coefficients of other potentials in the difference equation. This enhances the effective diagonal dominance of the system even though the dummy points are not directly relaxed in the conventional sense.

Differencing at the wing tip is complicated by the fact that the fine mesh system does not extend beyond the wing tip. Unlike the conventional global transformation approach, the coordinate lines do not have to be unswept or unsheared far from the wing. Provisions must be made, however, for properly ending the fine grid computation at the wing and canard tips. For this reason, another temporary fine mesh is positioned just beyond the wing tips. Like its neighboring fine grid nearest the tip, this grid array is located at a crude mesh Y-line. Its extent in the streamwise and vertical directions is consistent with the fine grid system. Both the dummy planes beyond the root and the temporary fine grids beyond the tips are computed for each sweep of the array of fine grid structures. While the root dummy plane is computed using difference formulas, the tip plane is simply filled using linear interpolation and potentials from the crude Cartesian grid.

2.6 FUSELAGE MODELING

The body is modeled in the solution by a constant cross-section computational surface in the Cartesian crude grid. The input data allow for simple axisymmetric body definition or detailed "Quick Geometry" (Ref 3) body definition. Body boundary conditions are imposed by fixing the velocity poten-

3 Vachris, A. F. and Yaeger, L. S., "Quick-Geometry - A Rapid Response Method for Mathematically Modeling Configuration Geometry," NASA SP-390, October 1975, pp. 49-73.

tial values on the body computational surface. The procedure follows that of Ref 2 and is described in detail in Ref 1. Body pressures from Equation (2) are used to produce a calculation of the body force and moment contribution.

2.7 BOUNDARY LAYER CALCULATION

Viscous effects are computed in the analysis code by coupling a modified Bradshaw boundary layer computation with the inviscid potential flow solution. The boundary layer calculation is virtually identical to the method developed by Mason (Ref 4). The method employs the modified chord technique of Nash (Ref 5), which represents an infinite sheared wing boundary layer calculation. The wing sweep angle is that of the local mid-chord span line, such that it may vary across the span. The two dimensional Bradshaw turbulent boundary layer analysis (Ref 6) provides the foundation for the method. The use of a modified two dimensional boundary layer analysis greatly reduces the necessary computer time and has demonstrated good results for several different codes (Ref 1, 2, 3, 7).

The boundary layer calculation provides a displacement thickness and skin friction calculation at each analysis station of the wing and canard. The slope of the displacement thickness is used to modify the surface boundary conditions in the inviscid solution. The local skin friction calculation is used to provide a viscous drag estimate for the configuration at the end of the analysis run.

4 Mason, W. H., et al., "An Automated Procedure for Computing the Three-Dimensional Transonic Flow Over Wing-Body Combinations, including Viscous Effects," Report AFFDL-TR-77-122, Vol. 1, October 1977.

5 Nash, J. F. and Tseng, R. R., "The Three-Dimensional Turbulent Boundary Layer on an Infinite Yawed Wing," The Aeronautical Quarterly, November 1971.

6 Bradshaw, P. and Ferriss, D.H., "Calculation of Boundary Layer Development Using the Turbulent Energy Equation. Compressible Flow on Adiabatic Walls," J. Fluid Mech., Vol. 46, 1971.

7 Hinson, B. L. and Burdges, K. P., "Acquisition and Application of Transonic Wing and Far-Field Test Data for Three-Dimensional Computational Method Evaluation," Technical Report, AFOSR-TR-80-0421, March 1980.

3 - SAMPLE CASES

Two fighter configurations and one transport configuration were selected as sample cases for demonstration of the CANTATA code multiple surface analysis capability. The two fighter configurations were the X-29 Forward Swept Wing technology demonstrator (Figure 4), and the Configuration Development of Advanced Fighters (CDAF) Configuration (Figure 5). The transport configuration was the C-5A, Figure 6.

The X-29 configuration was analyzed at Mach 0.9, 7.6 degrees angle of attack. The predicted pressures are compared with wind tunnel data (Ref 8) in Figure 7. Both fixed and free wake analysis results are shown. The discrepancies between the analysis and data are, in part, due to flow separation. The test Reynolds number was approximately four million, based on the mean aerodynamic chord. The computational model does not include the rearward strake of the wind tunnel model, and the code does not allow any modeling of inlet spillage. Lower surface actuator fairings were included in the wind tunnel test, but not modeled in the analysis. In general, the code predicts a shock location that is aft of the experimental data, except at 0.907 semispan. There the agreement with data is very good. Considering the presence of the actuator fairings in the data, the lower surface agreement is very good. The upper surface leading edge expansion is under-predicted outboard of 0.306 semispan. The results at 0.907 semispan might be considered typical of a small disturbance prediction, but the discrepancies at 0.490 and 0.698 are much greater. Model inspection results were not available to verify the leading edge contours. The free wake analysis produces a more forward shock

8 Charletta, Roy, "Post Test Report Series I Transonic/Supersonic Testing on a 12.5% Scale Grumman Design 712, X-29A Forward Swept Wing Demonstrator Aircraft Model in the NASA-ARC 11 foot and 9x7 foot Wind Tunnels, at Moffett Field, CA," Grumman Aerospace Report No. 712/ENG-RPT82-021, August 1982.

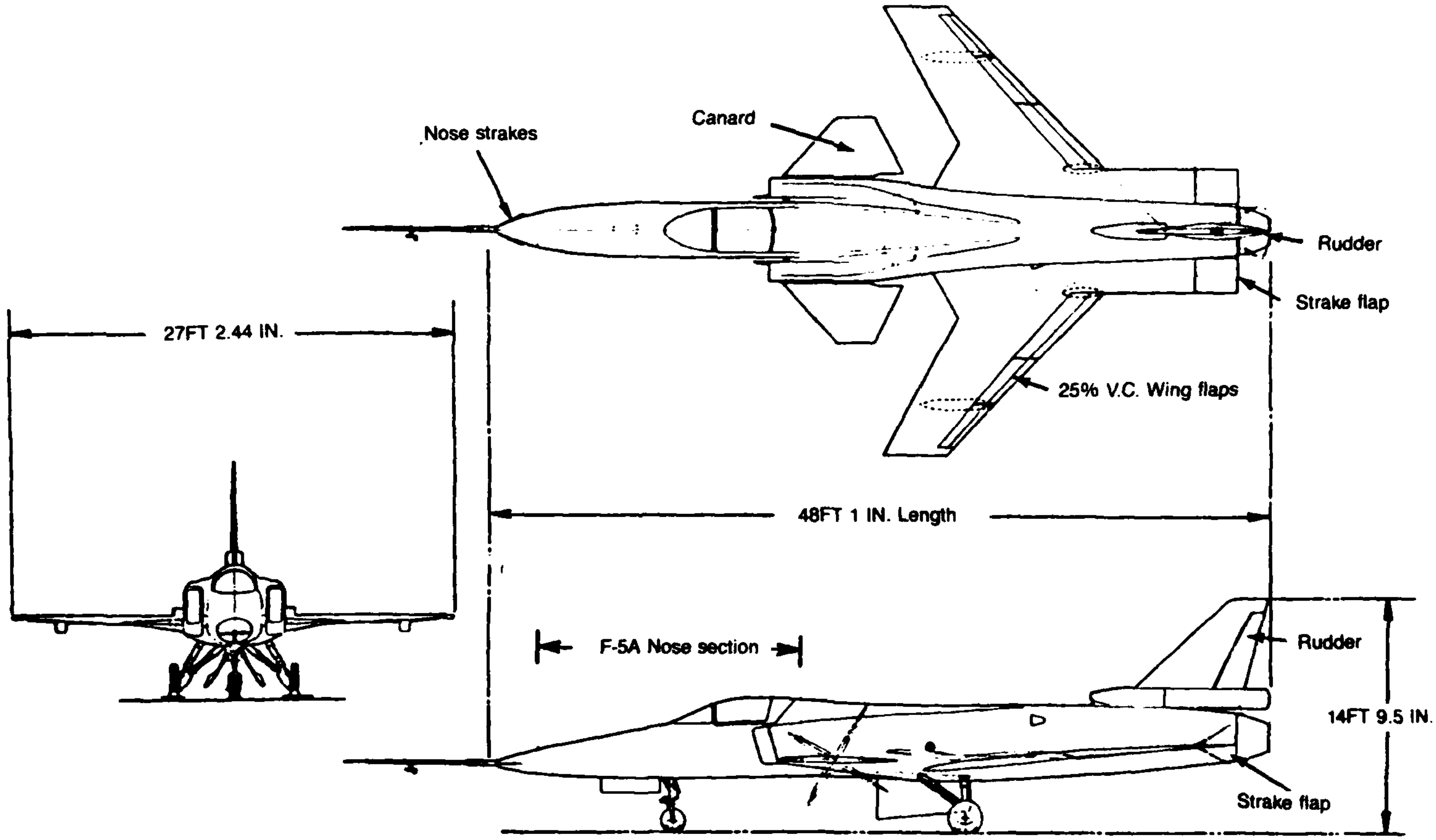

Figure 4. X-29 General arrangement.

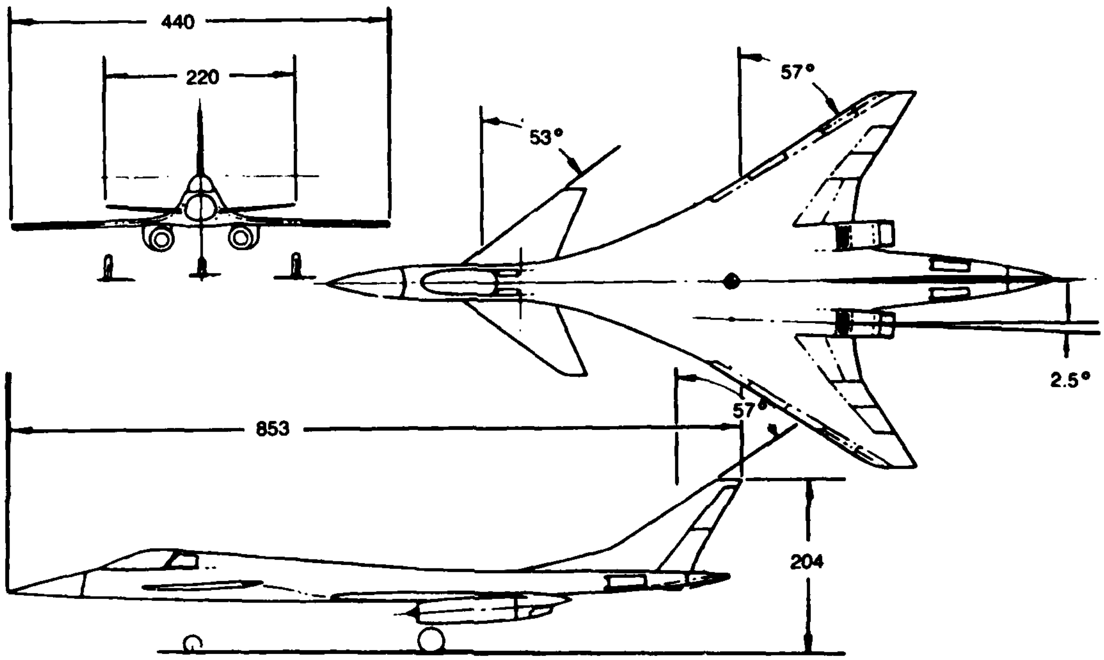

Figure 5. CDAF general arrangement.

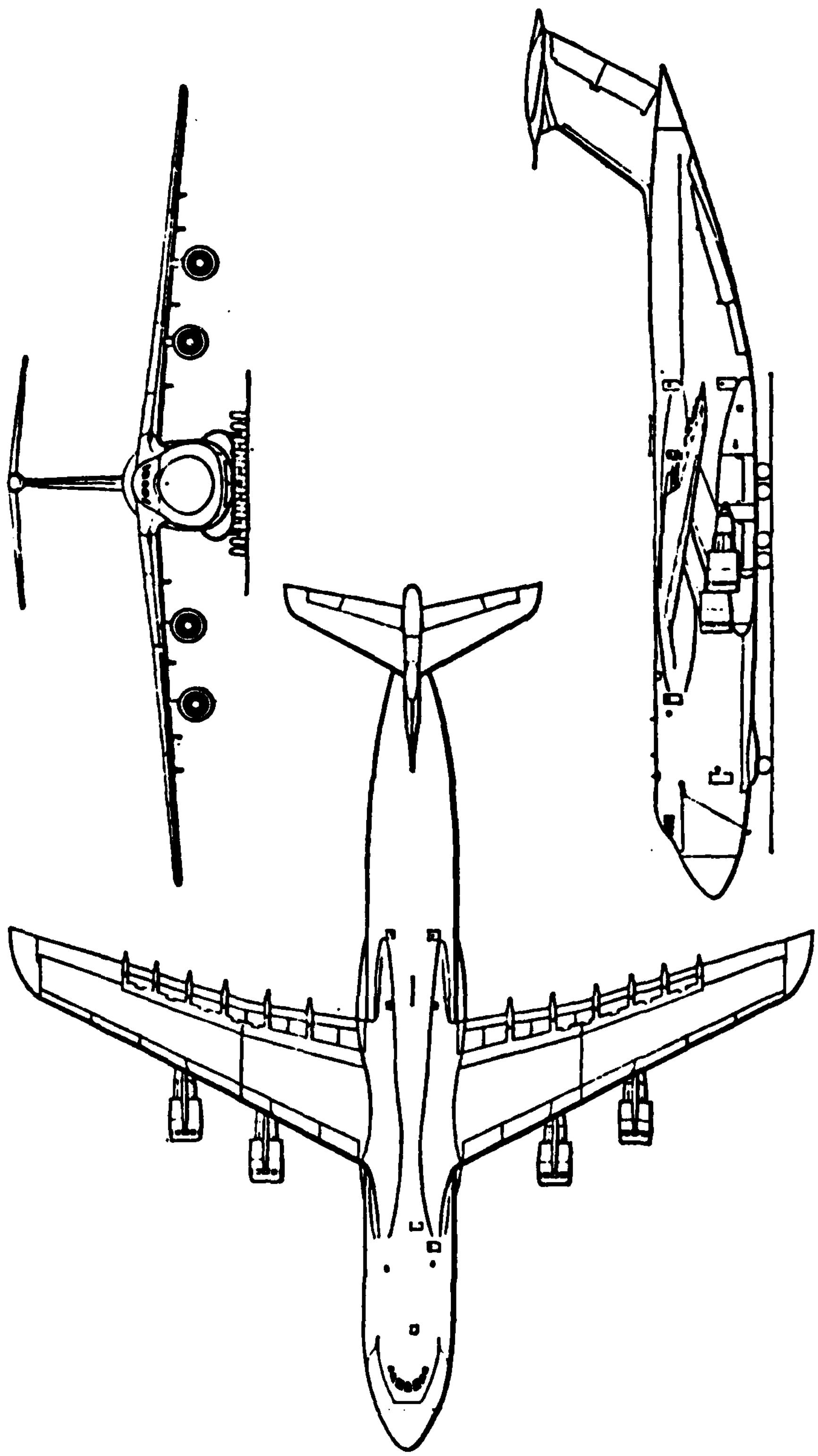

Figure 6. C-5A General arrangement.

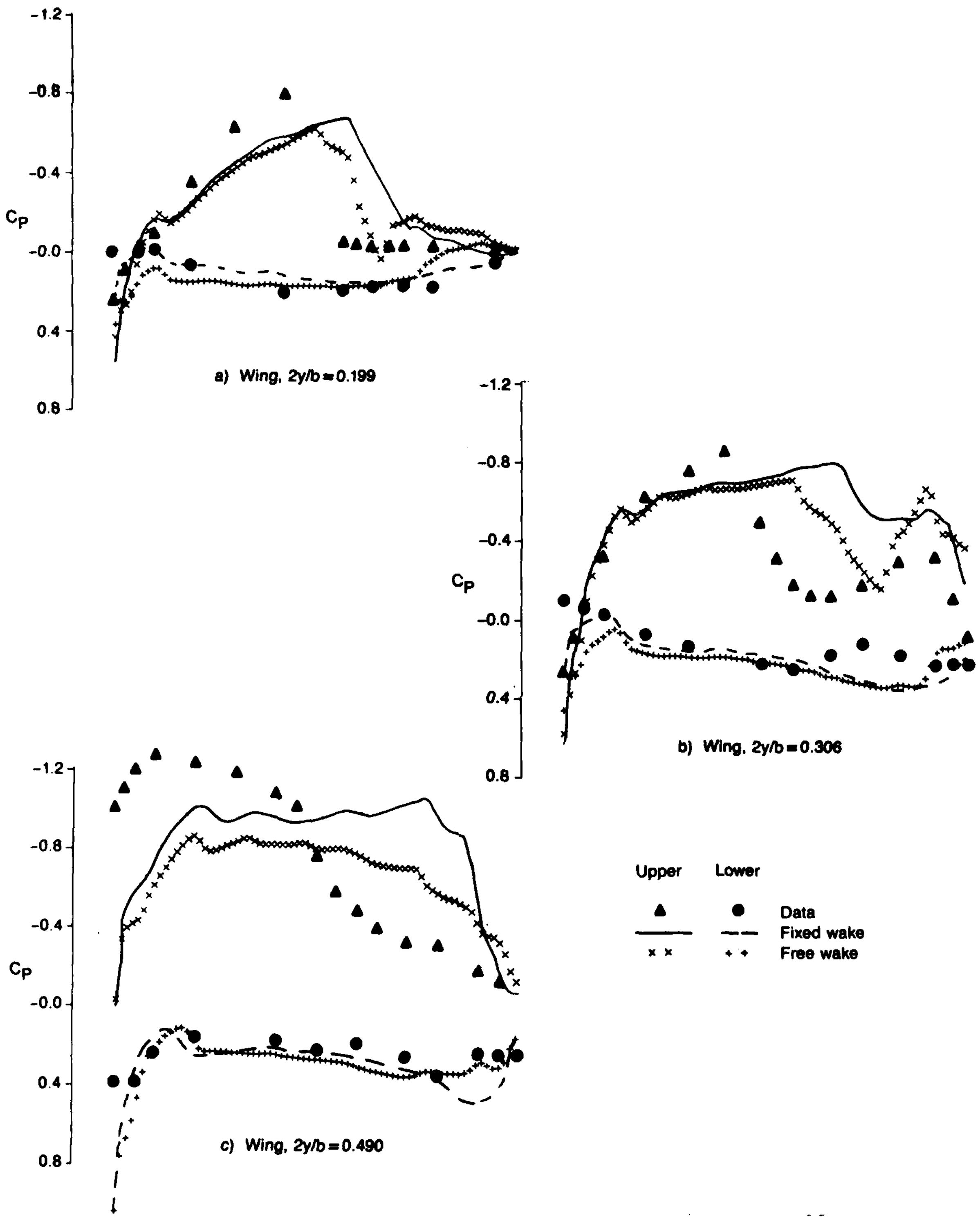

Figure 7. Data-analysis pressure comparison, X-29, Mach 0.9, α 7.6 (sheet 1 of 2).

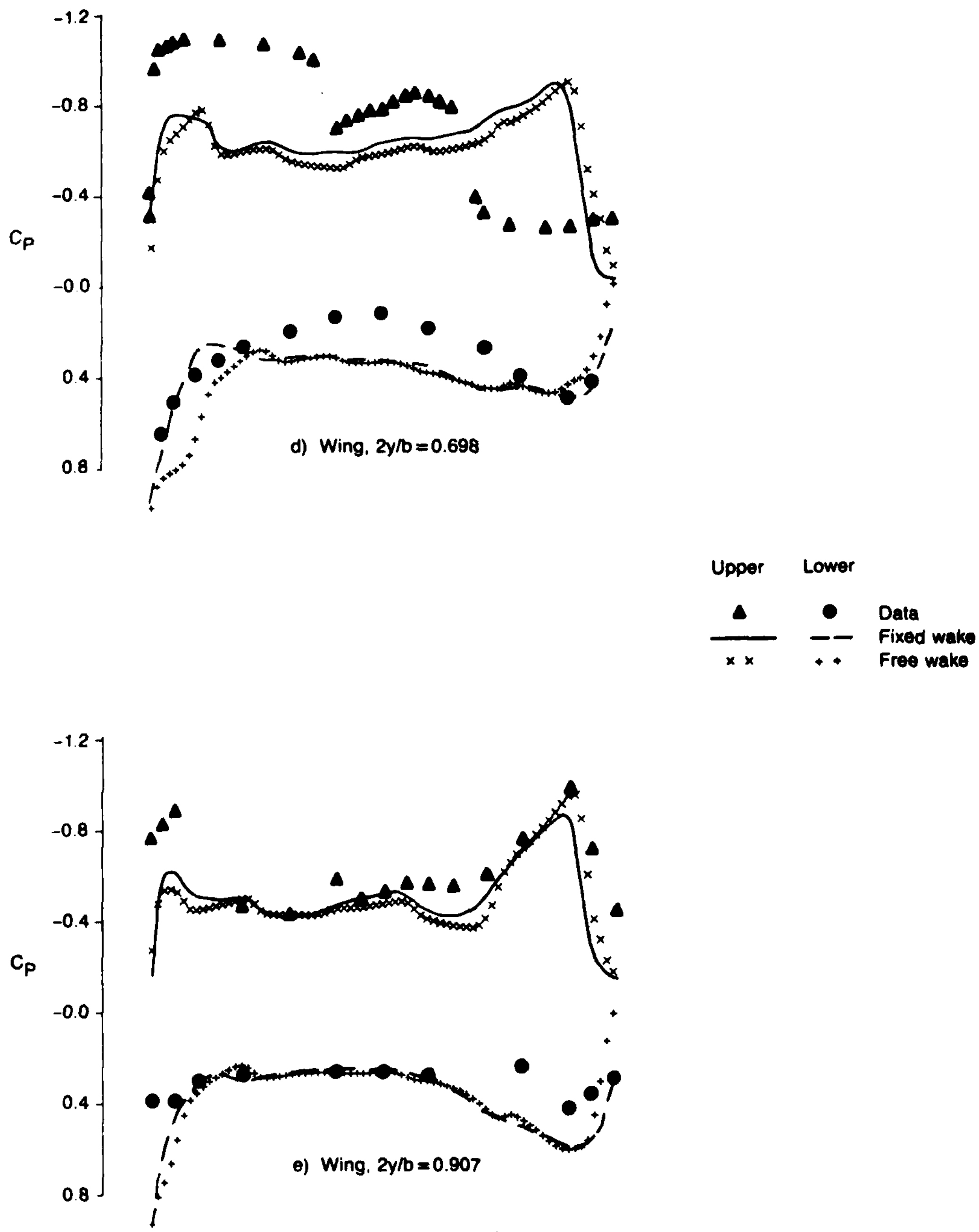

Figure 7. Data-analysis pressure comparison, X-29, Mach 0.9, α 7.6 (sheet 2 of 2).

location inboard, with very little effect outboard. This would be expected, considering that the wing tip is fairly well separated, both outboard and upstream, from the principal canard wake effects.

Analysis results for the CDAF configuration at Mach 0.9, 7.0 degrees angle-of-attack are compared with data (Ref 9) in Figure 8. The flow conditions are severe for a potential flow analysis, with local Mach numbers exceeding 1.7 at several locations. The canard and inboard wing pressures show good agreement with the data. The two outboard wing stations are not as well predicted. This may be because the local flow conditions are too severe for potential flow modeling, or because of flow separation which is beyond the modeling capability of the boundary layer analysis. The free wake analysis results in a more negative leading edge pressure peak at the two inboard stations. Relative to a wake shape that is fixed at the height of the canard surface, a "free" wake moves downward (for positive canard lift). The results shown in Figure 8 indicate that a more complex process occurs. Figure 9 shows the spanwise movement of the canard and wing vortex lines. There is a substantial redistribution of the vorticity in the canard wake. The edge of the canard wake moves inboard more than one grid plane, and two inboard canard vortex lines merge together just ahead of streamwise station 100.

Force and moment predictions for the CDAF configuration are presented in Figure 10. Three angles-of-attack, 6.0, 7.0 and 8.0 degrees, and three canard settings, 0, -5 and -10 degrees, were analyzed. The comparison with data shows good prediction of stability level and canard effectiveness. An overall shift in pitching moment of +0.06 has been added to the predictions. Several effects acting together are the most likely cause of this shift. The underprediction of the leading edge expansion would result in a more negative pitching moment prediction. In addition, the prediction of more negative pressures near the upper surface trailing edge and more positive pressures in the lower surface cove result in more negative pitching moment. Perhaps most significant is the lack of a detailed body solution. The body modeling is adequate to account for induced effects on the lifting surfaces, but is known to

9 Spurlin, C. J., "Test Report for AFWAL Optimal Transonic Configuration Fighter, Project No. P41T-G6, Test No. TF-570," April 1980.

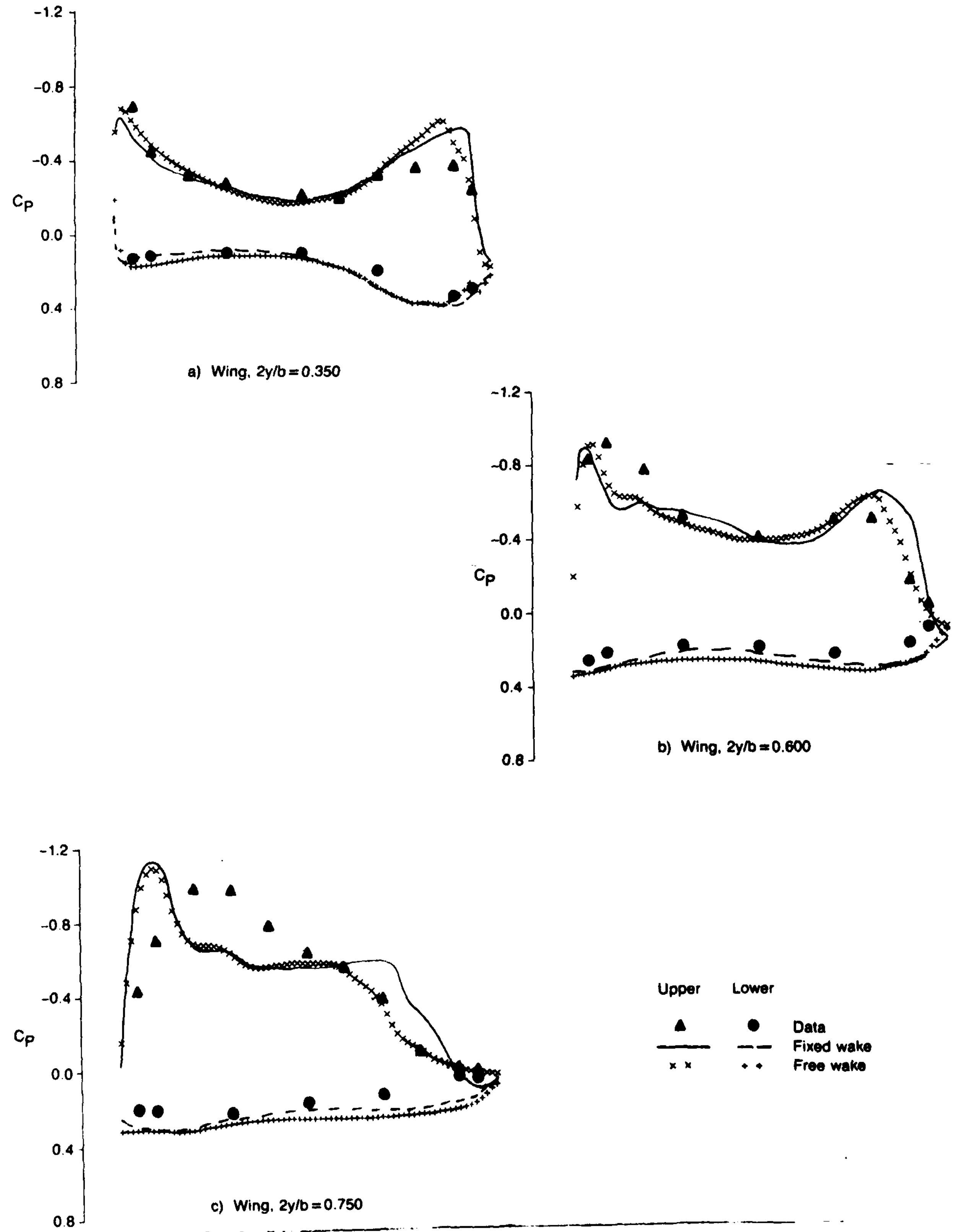

Figure 8. Data-analysis pressure comparison, CDAF, Mach 0.9, α 7.0 (sheet 1 of 2).

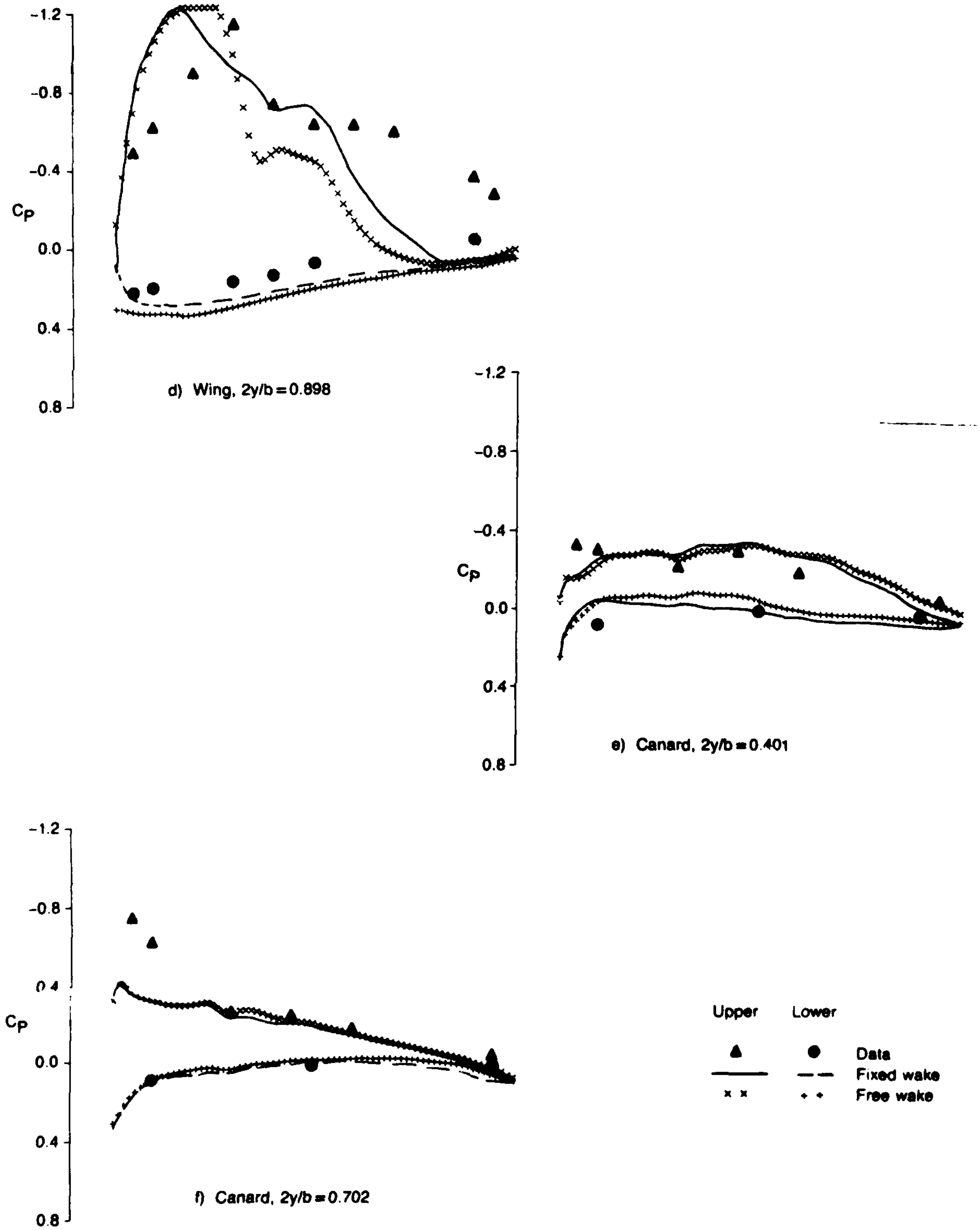

Figure 8. Data-analysis pressure comparison, CDAF, Mach 0.9, α 7.0 (sheet 2 of 2).

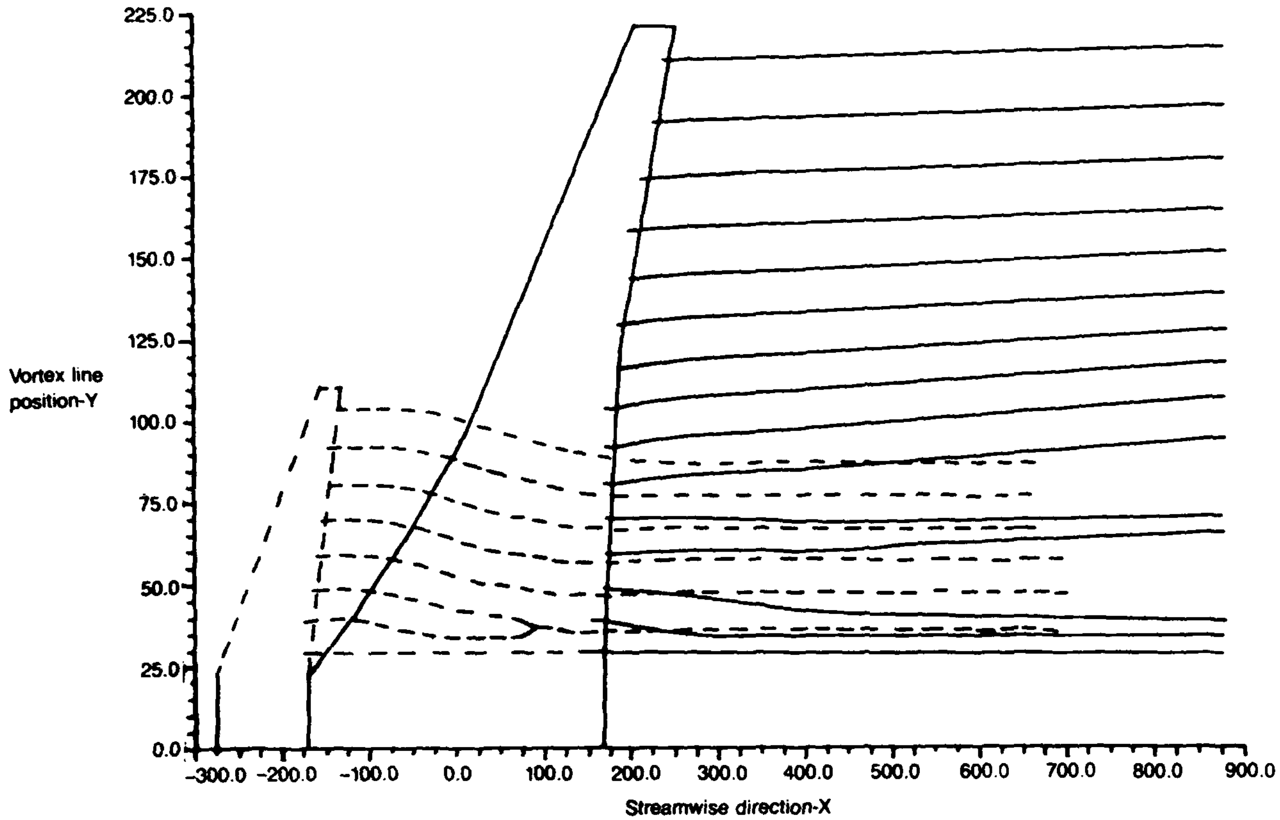

Figure 9. Vortex line spanwise movement, CDAF, Mach 0.9, α 7.0.

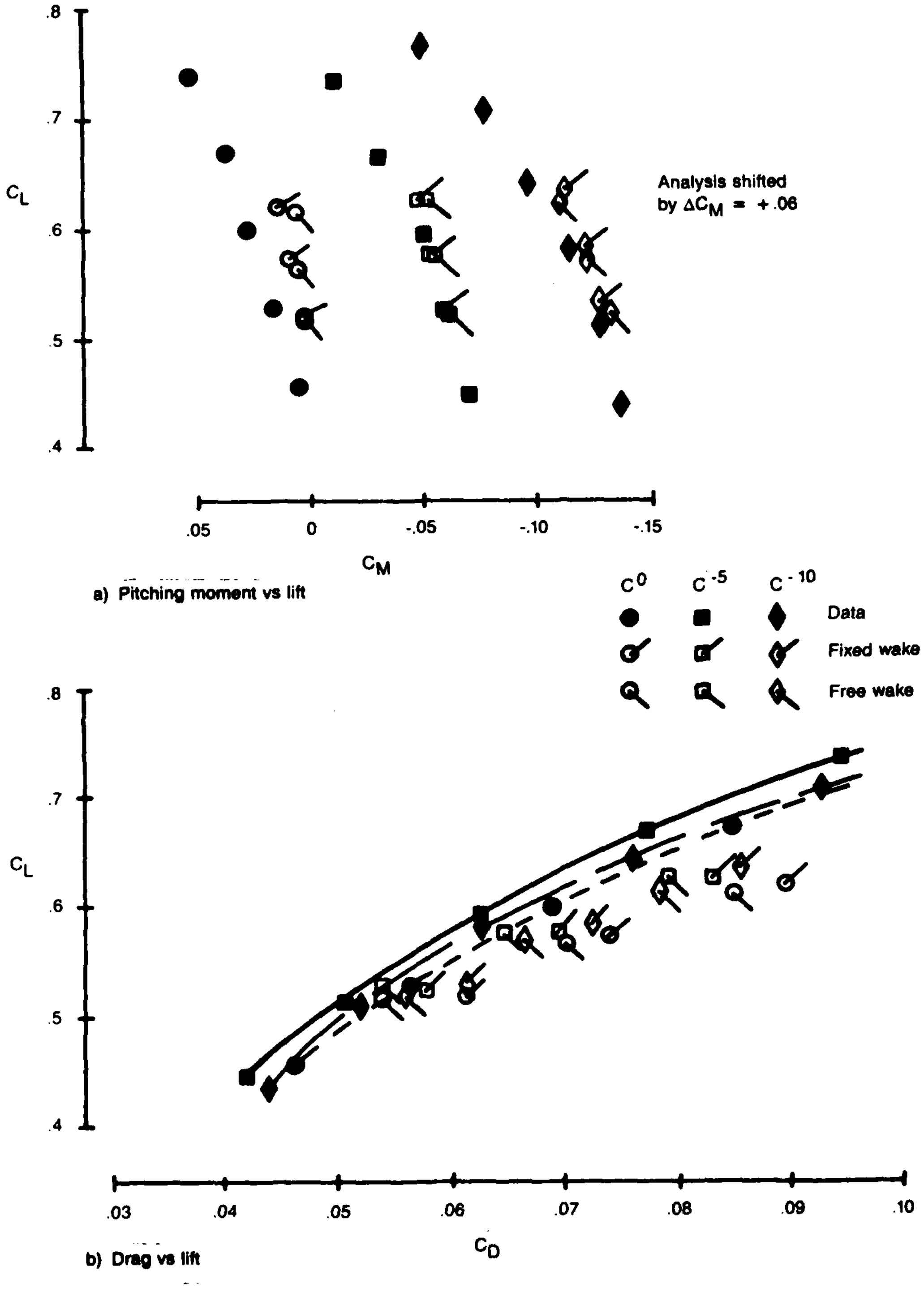

Figure 10. Force and moment prediction, CDAF, Mach 0.9

be inadequate near the fuselage nose. Thus, the predicted body contribution to pitching moment is unreliable. The free wake modeling results in a slightly more negative pitching moment and a more stable pitching moment slope.

The predicted drag is compared to wind tunnel data in Figure 10b. The predicted drag levels for the fixed wake analysis are all too high. As for the pitching moment prediction, the lack of an accurate body solution is probably part of the error. In general, a small disturbance analysis is not expected to predict the leading edge suction of the lifting surfaces. Thus, the increase in drag for an increase in lift will be overpredicted, as the results show. The free wake analysis results in lower predicted drag at all lift coefficients. At $C_L = 0.5$, the predicted drag values are very good, falling within the experimental uncertainty (Ref 1). As for the fixed wake analysis, the increase in drag for an increase in lift is overpredicted.

The C-5A represents a much milder case for potential flow analysis. Figure 11 compares data (Ref 10) and analysis results at Mach 0.75 and 2.0 degrees angle-of-attack. In general, the leading edge expansion on the wing is under-predicted, and the predicted outboard shock is too far aft. The predicted horizontal tail pressures show good agreement with the data. The inboard station on the horizontal tail is influenced by the "bullet" at the top of the vertical tail. The bullet is not modeled in the analysis. The effect of the free wake model is slight on both the wing and tail, slightly improving the agreement on the horizontal tail.

During the study, pressure data for a "Propulsive Wing-Canard" configuration became available (Ref 11). The configuration is shown in Figure 12, and the comparison of predicted and experimental pressures is shown in Figure 13. Generally good agreement is seen, with the data indicating trailing edge separation much more than the analysis.

10 Harris, M. K., Huie, W. E, "C-5A Aerodynamic Data for Airloads," Lockheed-Georgia Report LG74ER0162, November 1974.

11 Stewart, V. R., "Evaluation of a Propulsive Wing/Canard Concept at Subsonic and Supersonic Speeds," Naval Air Systems Command Report NR82H-85, Vol. 1 and 2, February 1983.

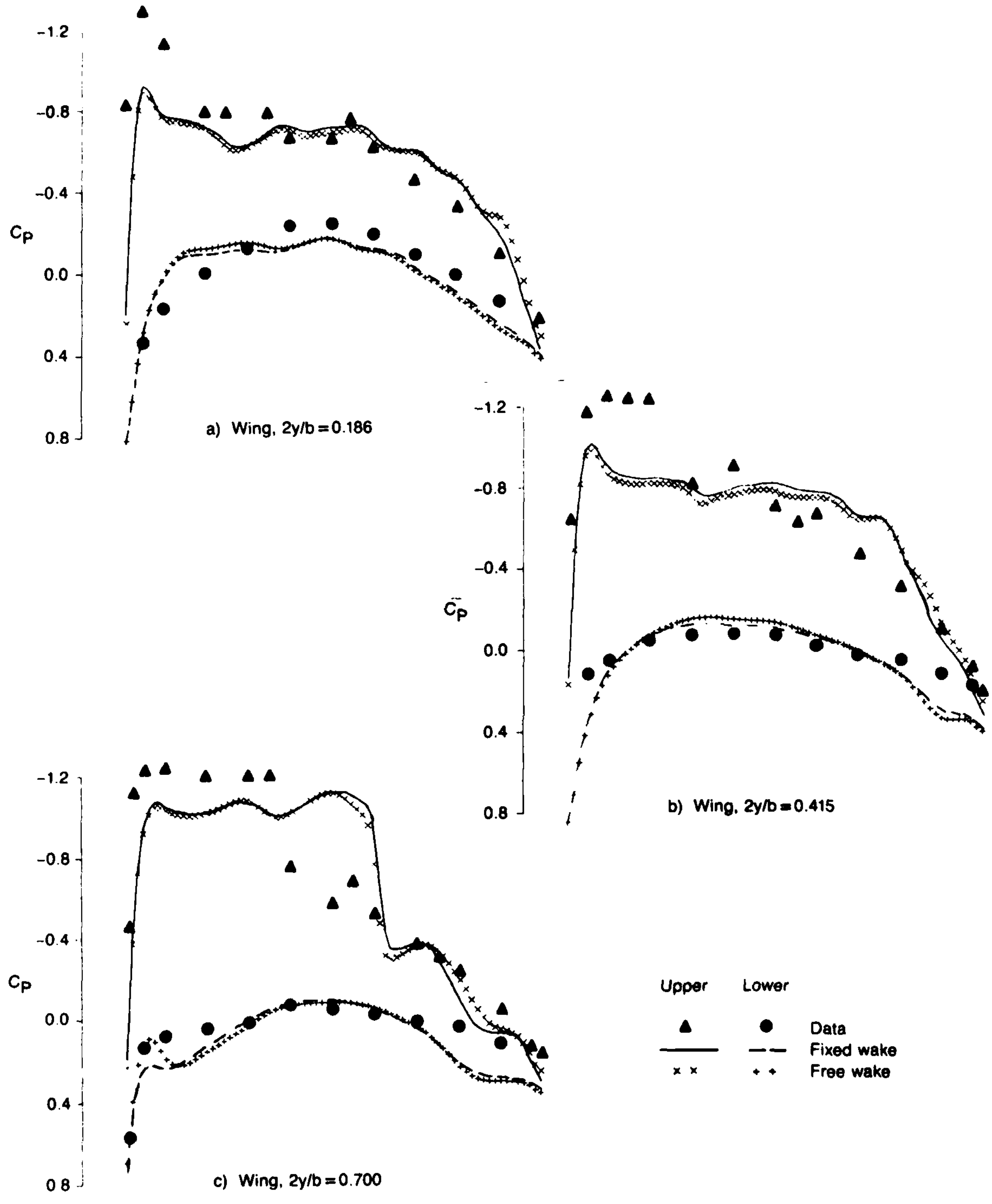

Figure 11. Data-analysis pressure comparison, C-54, Mach 0.75, α 2.0 (sheet 1 of 2).

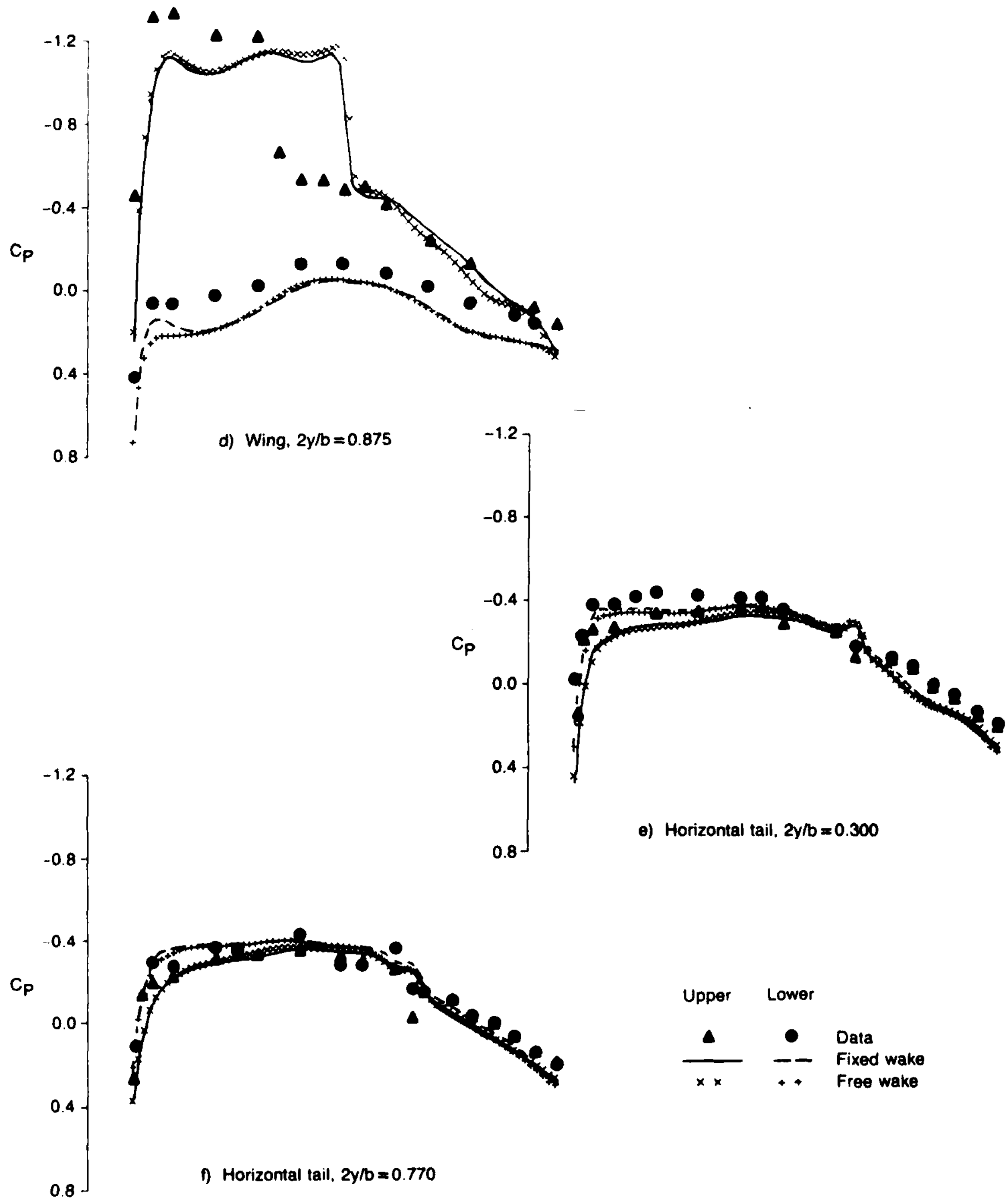

Figure 11. Data-analysis pressure comparison, C-54, Mach 0.75, α 2.0 (sheet 2 of 2).

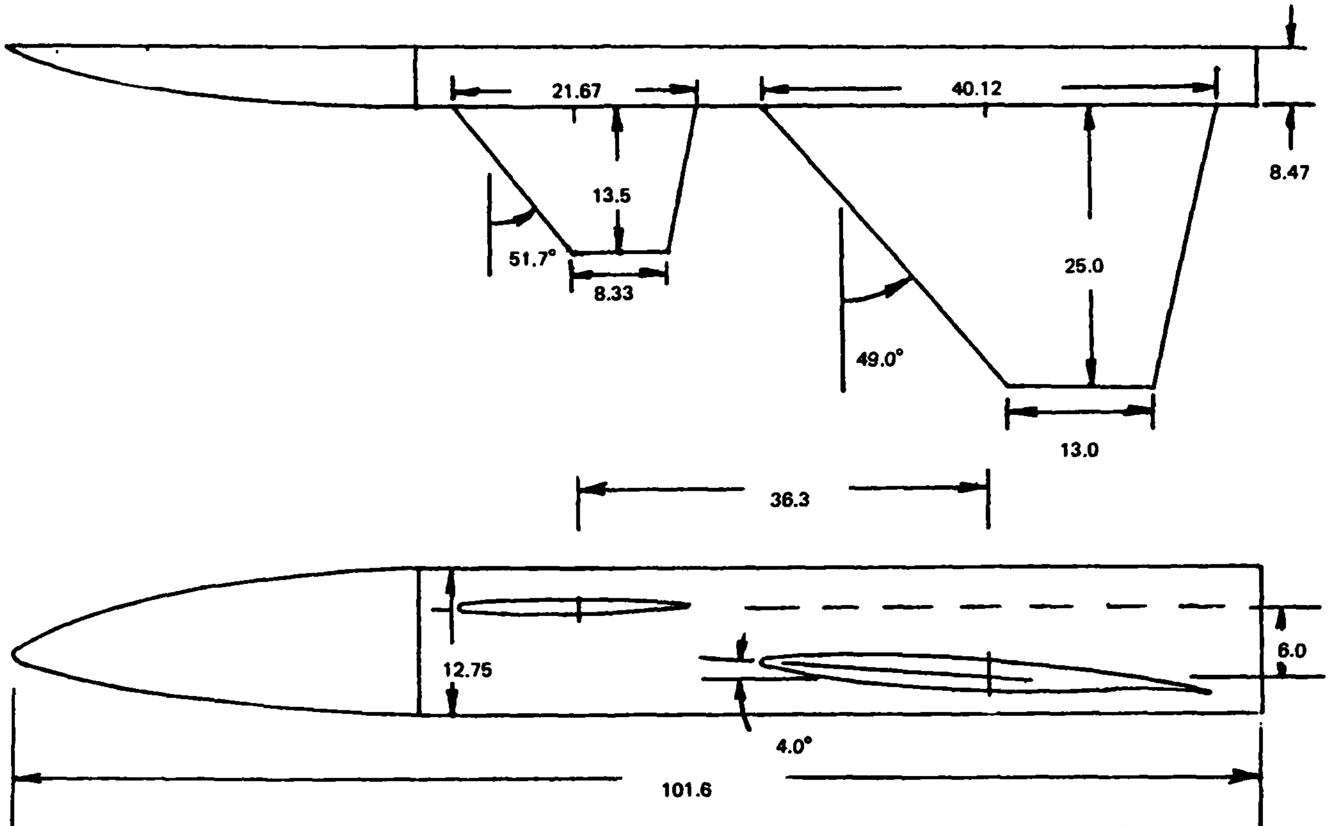

Note: Dimensions in inches except where noted.

Figure 12. Propulsive wing-canard configuration.

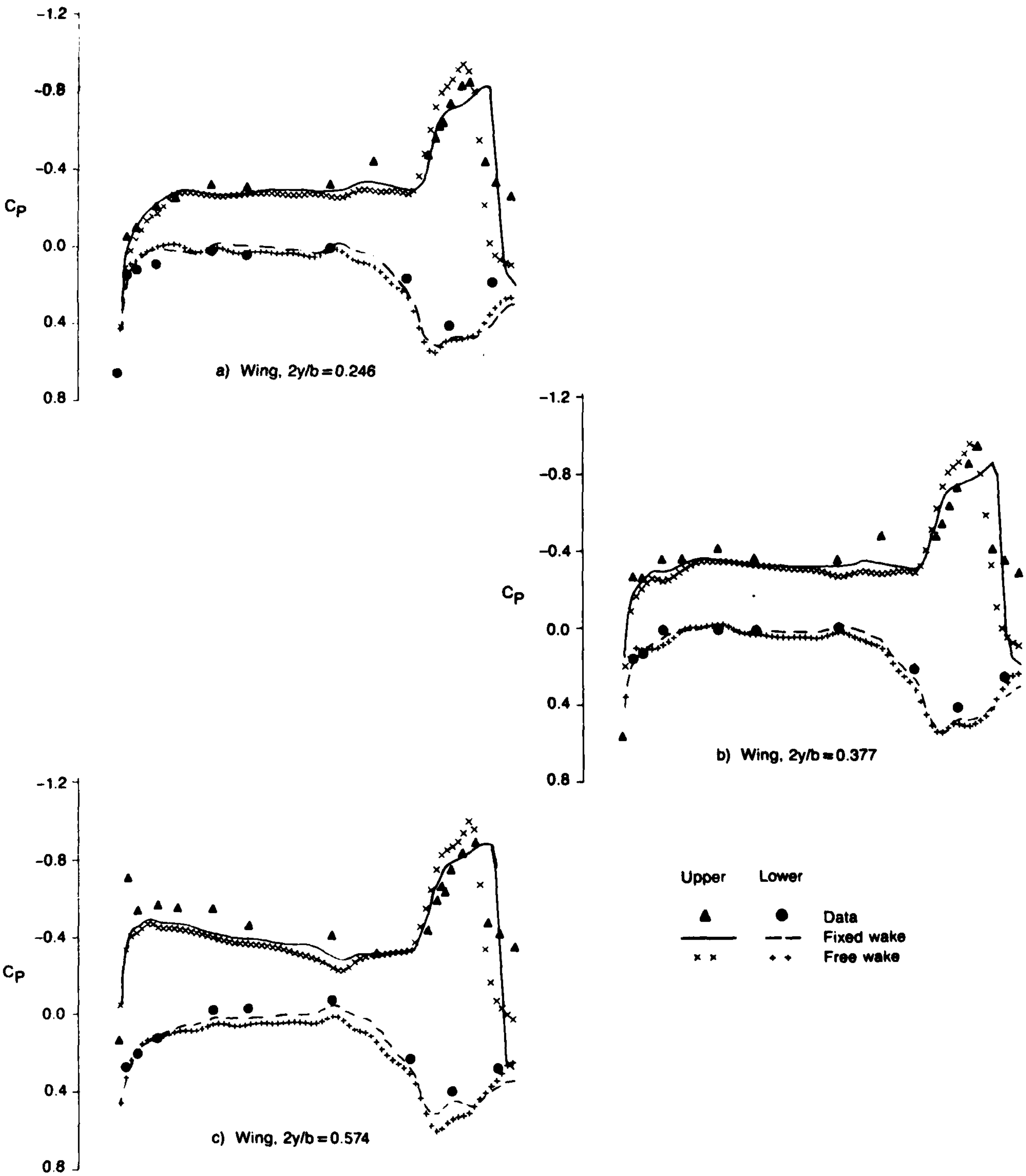

Figure 13. Data-analysis pressure comparisor., propulsive wing-canard, Mach 0.9, α 4.0 (sheet 1 of 2).

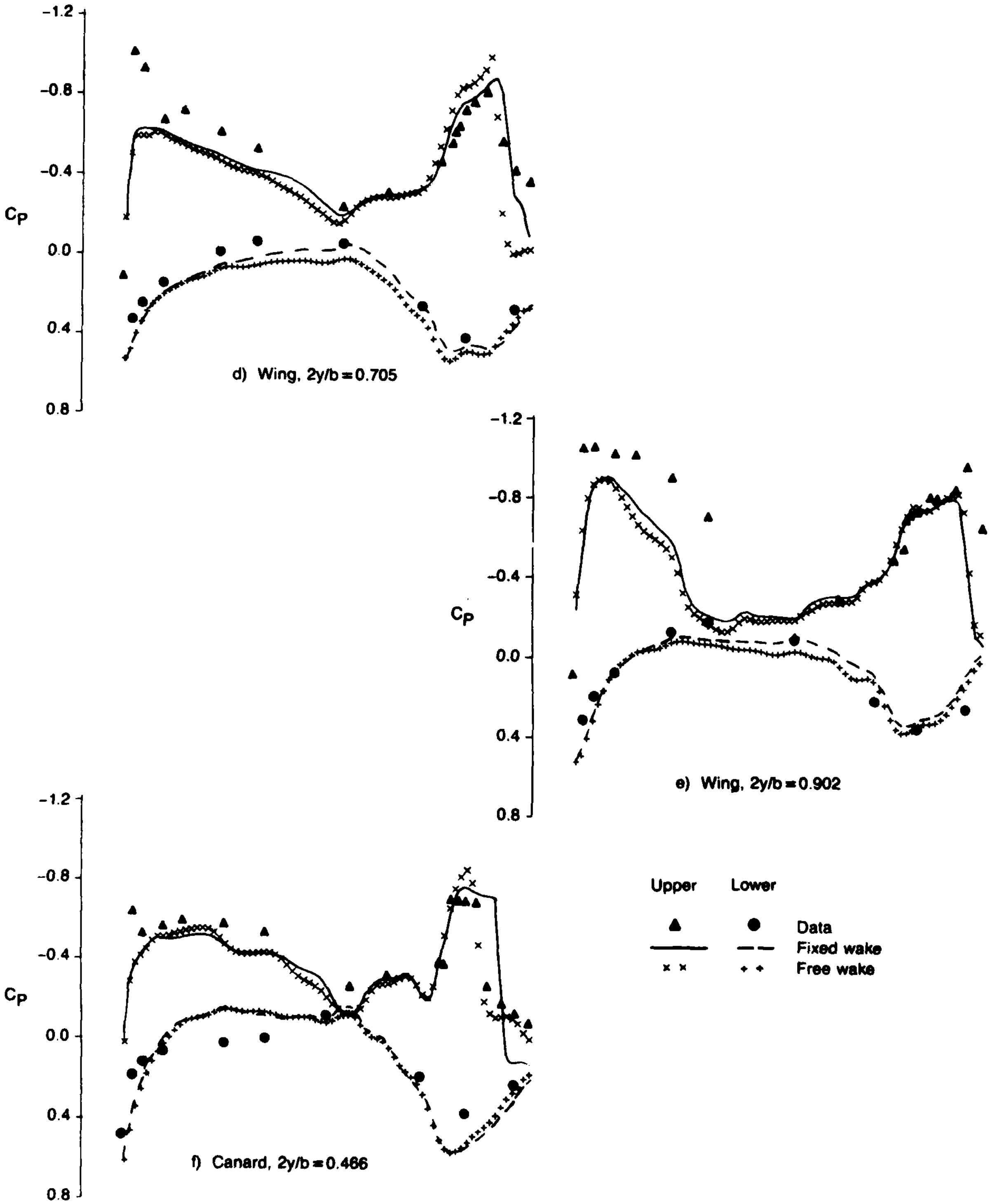

Figure 13. Data-analysis pressure comparison, propulsive wing-canard, Mach 0.9, α 4.0 (sheet 2 of 2).

4 - COPES/CONMIN OPTIMIZATION

The PANDORA wing-body-canard analysis code was coupled with the COPES and CONMIN routines of Vanderplaats (Ref 12, 13). The COPES code is a control program that connects the numerical optimization code CONMIN with the aerodynamic analysis code. The parts of the PANDORA code allowing the numerical optimization have been left intact in the CANTATA code.

The COPES and CONMIN routines were slightly modified in the PANDORA code. Changes were made in the main COPES routine and subroutine CNM06. The change to CNM06 is important. It provides subroutine ANALIZ with the index of the best result during an optimization search. In this way, the next search solution can be restarted from the best previous result. This more closely models the search strategy in CONMIN, resulting in more consistent information from the aerodynamic analysis. The changes in the COPES and CONMIN routines are identified in the code with comment cards.

The optimization algorithm within CONMIN is a modified Method of Feasible Directions (Ref 13). The gradient information for the algorithm is calculated by sequentially perturbing each design variable. Each design variable perturbation requires analysis by the flow solution routines. Thus, the computer time is proportional to the number of design variables. The gradient information establishes a search direction that should improve the design (decrease the objective function) while satisfying any constraints. The search direction is "explored" until a relative optimum is found or any constraints become violated. If the starting conditions violated any constraints, the search direction will be that which satifies the constraints with the least objective function increase. One to four flow solutions are required during the search.

12 Vanderplaats, G. N., "COPES--Control Program for Engineering Synthesis," to be published as a Naval Postgraduate School Memorandum.

13 Vanderplaats, G. N., "CONMIN--A Fortran Program for Constrained Function Minimization," NASA TM X-62282, August 1973.

Completion of the search constitutes one optimization iteration. The following discussion of COPES usage is excerpted from Ref 12. A more detailed description will be found in the reference. Reference 13 should be consulted if more details of the numerical optimization algorithm are desired.

If it is desired to run only a simple analysis using COPES, only three data cards are required for the COPES program: a TITLE card, a control parameter (NCALC = 1), and an END card. If the optimization or parametric analysis (sensitivity) capabilities of COPES are to be used, additional data must be read. This data will identify which parameters in the global common block, GLOBCM, are used. To set up the COPES data, the user must have a basic understanding of how the data in the global common block is accessed by COPES. This is outlined in the following section.

4.1 OPTIMIZATION DATA MANAGEMENT

In order to perform design operations, the COPES program must access the data in common block GLOBCM. This is done by defining the location in GLOBCM where a specified parameter resides. For example, consider the common block for a cantilevered beam design problem:

```
COMMON/GLOBCM/B,H,VOL,BSTRES,SHRSTR,DELTA,HB,E,AL
```

The volume of material, VOL, is the third parameter in the common block; that is, it resides in Location 3, referred to as the Global Location number. Similarly the bending stress, BSTRES, is in Global Location 4 and the beam width is in Global Location 1. Thus, the parameters are referred to by their respective location numbers in global common.

For convenience in preparing data for the COPES program, a simple "CATALOG" of parameters may be defined. For the cantilevered beam, this catalog would be:

GLOBAL LOCATION	FORTRAN NAME	DEFINITION
1	B	Beam width
2	H	Beam height
3	VOL	Volume of material
4	BSTRES	Maximum bending stress
5	SHRSTR	Maximum shear stress
6	DELTA	Deflection under the load
7	HB	Ratio, H/B
8	E	Young's modulus
9	AL	Length of beam

As another example, consider a global common block containing arrays:

GLOBAL LOCATION	FORTRAN NAME	DEFINITION
1	A	Area
2	Y(10)	Vector
12	Q	.
13	C(2,2)	.
17	H	etc.

The dimensions are given with the FORTRAN name as a reminder that the parameter is an array. In this case, the third parameter in the Y array is in Global Location 4. Remembering that arrays are stored column by column, the C(1,2) array location is in Global Location 15.

It will be seen that identifying parameters according to their location in GLOBCM provides a great deal of flexibility in using the COPES program for design.

In the following section, definitions of terms commonly used in automated design are given for easy reference.

4.2 OPTIMIZATION TERMINOLOGY

The COPES program currently provides six specific capabilities:

- Simple analysis - just as if COPES was not used

- Optimization - minimization or maximization of one calculated function with limits imposed on other functions
- Sensitivity analysis - the effect of changing one or more design variables on one or more calculated functions
- Two-variable functions space - analysis for all specified combinations of two design variables
- Optimum sensitivity - same as sensitivity analysis except, at each step, the design is optimized with respect to the remaining independent design variables
- Approximate optimization - optimization using approximation techniques. Usually more efficient than standard optimization for up to 10 design variables if multiple optimizations are to be performed.

In defining the data required to execute the COPES program, the following definitions are useful.

DESIGN VARIABLES - Those parameters which the optimization program is allowed to change in order to improve the design. Design variables appear only on the right hand side of equations in the analysis program. COPES considers two types of design variables, independent and dependent. If two or more variables are always required to have the same value or be in a constant ratio, one is the independent variable while the remaining are dependent variables. For example, if the height is required to be 10 times the width of the cantilevered beam, B would be the independent variable while H would be the dependent variable.

OBJECTIVE FUNCTION - The parameter to be minimized or maximized during optimization. Also the parameters calculated as functions of specified design variables during a sensitivity or two-variable function space study. Objective functions always occur on the left side of equations, unless the objective function is also a design variable (the beam height may be minimized as an objective function if it is also a design variable; in this way, the minimum height is found for which no constraints are violated). An objective function may be linear or non-linear, implicit or explicit, but must be a function of the design variables to be meaningful.

CONSTRAINT - Any parameter which must not exceed specified bounds for the design to be acceptable. Constraint functions always appear on the left side

of equations. Just as for objective functions, constraints may be linear or non-linear, implicit or explicit, but must be functions of the design variables.

CONSTRAINT SET - A group of constraints which appear consecutively in the global common block and which all have the same limits imposed. This is a convenience which allows several constraints to be identified with a minimum of data.

GLOBAL COMMON - Common block GLOBCM containing design information.

GLOBAL LOCATION - Location of a particular parameter in GLOBCM.

4.3 OPTIMIZATION INPUT DATA FORMAT

In order to execute the COPES program it is necessary to provide formatted data for COPES, followed by data for the ANALIZ program which is coupled to COPES. Section 4.1 defines the data which is required by COPES. The data is segmented into "BLOCKS" for convenience. All formats are alpha-numeric for TITLE, and END cards, F10 for real data and I10 for integer data.

The COPES data begins with a TITLE card and ends with an END card. This is followed by data to be read by the user-supplied subroutine ANALIZ.

Comment cards may be inserted anywhere in the COPES data stack prior to the END card, and are identified by a dollar sign ($) in column 1.

While the input description defines COPES data in formatted fields of ten, the data may actually be read in more conveniently by separating data by commas or one or more blanks. If more than one number is contained on an unformatted data card, a comma must appear somewhere on the card. If exponential numbers such as 2.5+10 are read on an unformatted card, there must be no embedded blanks. Unformatted cards may be intermingled with formatted cards. Real numbers on an unformatted card must have a decimal point. Some examples:

Unformatted data:

```
5,7,1.3,1.0+20,0,-5.1
5,7,1.3,1.0+20,,-5.1
5 7 1.3 1.0+20,, - 5.1
5      7  1.3, 1.0+20 0 -5.1
```

Equivalent formatted data:

col	10	20	30	40	50	60	70	80
	5	7	1.3	1.0+20	0	-5.1		

Unformatted data

2

2,3

2 3

Equivalent formatted data:

col	10	20	30
	2		
	2	3	

2 3

Note that this data contains no commas, so it is assumed to be formatted already.

Unformatted data:

1,2,3,4,5,6,7,8,9,10,11

col	10	20	30	40	50	60	70	80
	1	2	3	4	5	6	7	8
	9	10	11					

Note that two formatted data cards are created here.

Unformatted data:

1,2,3,4,5,6

7,8,9,10,11

Equivalent formatted data:

col	10	20	30	40	50	60	70	80
	1	2	3	4	5	6		
	7	8	9	10	11			

Note that the two examples above do not produce the same formatted data cards.

5 - INPUT DATA DESCRIPTION

This section describes the necessary solution/optimization parameters and geometry input needed to operate the CANTATA code. The information of Section 4, COPES/CONMIN Optimization, is important for using the optimization. Only the one-cycle analysis (NCALC = 1 in DATA BLOCK B) and optimization (NCALC = 2) COPES options have been thoroughly tested in this effort. The transonic analysis input is an extension of that from the base code (Ref 1). A set of Usage Notes (Subsection 5.3) appears at the end of the analysis input description to elaborate on the less familiar input parameters. Volume 2, Part 2 of Ref 1 contains important discussions of the optimization application that are not repeated here.

5.1 OPTIMIZATION INPUT DATA

<u>DATA BLOCK</u> <u>A</u>

DESCRIPTION: Title card.

FORMAT AND EXAMPLE

1	2	3	4	5	6	7	8	FORMAT
TITLE								20A4

CANTILEVERED BEAM DESIGN

FIELD	CONTENTS
1-8	Any 80 character title may be given on this card.

DATA BLOCK B

DESCRIPTION: Program Control Parameters.

FORMAT AND EXAMPLE

1	2	3	4	5	6	7	FORMAT
NCALC	NDV	NSV	N2VAR	NXAPRX	IPNPUT	IPDBG	7I10
2	2	3	5	2	0	0	

FIELD		CONTENTS
1	NCALC:	Calculation Control
	0 -	Read input and stop. Data of blocks A, B and V is required. Remaining data is optional.
	1 -	One cycle through program. The same as executing ANALIZ stand-along (i.e., no optimization). Data of blocks A, B and V is required. Remaining data is optional.
	2 -	Optimization. Data of blocks A-I and V is required. Remaining data is optional.
	3 -	Sensitivity analysis. Data of blocks A, B, P, Q and V is required. Remaining data is optional.
	4 -	Two variable function space. Data of blocks A, B, and R-V is required. Remaining data is optional.
	5 -	Optimum sensitivity. Data of blocks A-I, P, Q, and V is required. Remaining data is optional.
	6 -	Optimization using approximation techniques. Data of blocks A-O and V is required. Remaining data is optional.
2	NDV:	Number of design variables on which sensitivity analysis or optimization will be performed.
4	N2VAR:	Number of objective functions in a two variable function space study.
5	NXAPRX:	Number of X-variables for approximate analysis/optimization. $\geq$ NDV
6	IPNPUT:	Input print control
	0 -	Print card images of data plus formatted print of input data
	1 -	Formatted print only of input data
	2 -	No print of input data.

7 IPDBG: Debug print control

0 - Off

1 - On, ANALIZ called for output after each analysis.

DATA BLOCK C OMIT IF NDV = 0 IN BLOCK B

DESCRIPTION: Integer optimization control parameter.

FORMAT AND EXAMPLE

1	2	3	4	5	6	7	8	FORMAT
IPRINT	ITMAX	ICNDIR	NSCAL	ITRM	LINOBJ	NACMX1	NFDG	7I10
5	0	0	0	0	0	0	0	

FIELD		CONTENTS
1	IPRINT:	Print control used in the optimization program CONMIN. 0 - No print during optimization. 1 - Print initial and final optimization information. 2 - Print above plus objective function value and design variable values at each iteration. 3 - Print above plus constraint values, direction vector and move parameter at each iteration. 4 - Print above plus gradient information. 5 - Print above plus each proposed design vector, objective function and constraint values during the one-dimensional search.
2	ITMAX:	Maximum number of optimization iterations allowed. DEFAULT = 20.
3	ICNDIR:	Conjugate direction restart parameter. DEFAULT = NDV + 1.
4	NSCAL:	Scaling parameter. .GT.0 - Scale design variables to order of magnitudes one every NSCAL iterations. .LT.0 - Scale design variables according to user-input scaling values. Good value is ICNDIR, 1 is not.
5	ITRM:	Number of consecutive iterations which must satisfy relative or absolute convergence criterion before optimization process is terminated. DEFAULT = 3
6	LINOBJ:	Linear objective function identifier. If the optimization objective is known to be a linear function of the design variables, set LINOBJ = 1. DEFAULT = Nonlinear.
7	NACMX1:	One plus the maximum number of active constraints anticipated. DEFAULT = NDV + 2.

8 NFDG: Finite difference gradient identifier.

- 0 - All gradient information is computed by finite difference with CONMIN.
- 1 - All gradient information is computed analytically by the user-supplier code.
- 2 - Gradient of objective is computed analytically. Gradients of constraints are computed by finite difference within CONMIN.

REMARKS

- Currently NFDG must be zero in COPES
- IPRINT = 5 is recommended.

DATA BLOCK D OMIT IF NDV = 0 IN BLOCK B

DESCRIPTION: Floating point optimization program parameters.

FORMAT AND EXAMPLE

1	2	3	4	5	6	7	FORMAT
FDCH	FDCHM	CT	CTMIN	CTL	CTLMIN	THETA	7F10
0.0	0.0	0.0	0.0	0.0	0.0	0.0	
DELFUN	DABFUN	ALPHAX	ABOBJ1				
0.0	0.0	0.0	0.0				

NOTE: Two cards are read here.

FIELD		CONTENTS
1	FDCH:	Relative change in design variables in calculating finite difference gradients. DEFAULT = 0.01.
2	FDCHM:	Minimum absolute step in finite difference gradient calculations. DEFAULT = 0.001.
3	CT:	Constraint thickness parameter. DEFAULT = 0.05.
4	CTMIN:	Minimum absolute value of CT considered in the optimization process. DEFAULT = 0.004.
5	CTL:	Constraint thickness parameter for linear constraints. DEFAULT = -0.01.
6	CTLMIN:	Minimum absolute value of CTL considered in the optimization process. DEFAULT = 0.001.
7	THETA:	Mean value of push-off factor in the method of feasible directions. DEFAULT = 1.0.
1	DELFUN:	Minimum relative change in objective function to indicate convergence of the optimization process. DEFAULT = 0.001.
2	DABFUN:	Minimum absolute change in objective function to indicate convergence of the optimization process. DEFAULT = 0.001.
3	ALPHAX:	Maximum fractional change in any design variable for first estimate of the step in the one-dimensional search. DEFAULT = 0.1.
4	ABOBJ1:	Expected fractional change in the objective function for first estimate of the step in the one-dimensional search. DEFAULT = 0.1.

REMARKS

- The DEFAULT values for these parameters usually work well.

DATA BLOCK E OMIT IF NDV = 0 IN BLOCK B

DESCRIPTION: Total number of design variables, design objective identification and sign.

FORMAT AND EXAMPLE

1	2	3	FORMAT
NDVTOT	IOBJ	SGNOPT	2I10,F10
0	3	-1.0	

FIELD CONTENTS

1 NDVTOT: Total number of variables linked to the design variables. This option allows two or more parameters to be assigned to a single design variable. The value of each parameter is the value of the design variable times a multiplier, which may be different for each parameter. DEFAULT = NDV.

2 IOBJ: Global variable location associated with the objective function in optimization.

3 SGNOPT: Sign used to identify whether function is to be maximized or minimized. +1.0 indicates maximization. -1.0 indicates minimization. If SGNOPT is not unity in magnitude it scales the magnitude of the objective.

DATA BLOCK F OMIT IF NDV = 0 IN BLOCK B

DESCRIPTION: Design variable bounds, initial values and scaling factors.

FORMAT AND EXAMPLE

1	2	3	4	FORMAT
VLB	VUB	X	SCAL	4F10
.5	5.	0.0	0.0	

NOTE: Read one card for each of the NDV independent design variables. Values are in order for design variables NDSGN sequence (i.e., input sequence).

FIELD		CONTENTS
1	VLB:	Lower bound on the design variable. If VLB.LT.-1.0E+15, no lower bound.
2	VUB:	Upper bound on the design variable. If VUB.GT.1.0E+15, no upper bound.
3	X:	Initial value of the design variable. IF X is non-zero, this will supersede the value initialized by the user-supplied subroutine ANALIZ.
4	SCAL:	Design variable scale factor. Not used if NSCAL.GE.0 in BLOCK C.

DATA BLOCK G OMIT IF NDV = 0 IN BLOCK B

DESCRIPTION: Design variable identification.

FORMAT AND EXAMPLE

1	2	3	FORMAT
NDSGN	IDSGN	AMULT	2I10,F10
1	1	1.0	

NOTE: Read one card for each of the NDVTOT design variables.

FIELD		CONTENTS
1	NDSGN:	Design variable number associated with this variable.
2	IDSGN:	Global variable number associated with this variable.
3	AMULT:	Constant multiplier on this variable. The value of the variable will be the value of the design variable, NDSGN, times AMULT. DEFAULT = 1.0.

DATA BLOCK H OMIT IF NDV = 0 IN BLOCK B

DESCRIPTION: Number of constrained parameters.

FORMAT AND EXAMPLE

1	FORMAT
NCONS	I10
4	

FIELD		CONTENTS
1	NCONS:	Number of constraint sets in the optimization problem.

REMARKS

- If two or more adjacent parameters in the global common block have the same limits imposed, these are part of the same constraint set.

DATA BLOCK I OMIT IF NDV = 0 IN BLOCK B, OR NCONS = 0 IN BLOCK H

DESCRIPTION: Constraint identification and constraint bounds.

FORMAT AND EXAMPLE

1	2	3	4	FORMAT
ICON	JCON	LCON		3I10
4	0	0		
BL	SCAL1	BU	SCAL2	
-1.0+20	0.0	20000.	0.0	4F10

NOTE: Read two cards for each of the NCONS constraint sets.

FIELD		CONTENTS
1	ICON:	First global number corresponding to the constraint set.
2	JCON:	Last global number corresponding to the constraint set. DEFAULT = ICON.
3	LCON:	Linear constraint identifier for this constraint set. LCON = 1 indicates linear constraints. If in doubt, use nonlinear.
1	BL:	Lower bound on the constrained variables. If BL.LT.-1.0E+15, no lower bound.
2	SCAL1:	Normalization factor on lower bound. DEFAULT = MAX of (ABS(BL), 0.1).
3	BU:	Upper bound on the constrained variables. If BU.GT.1.0E+15, no upper bound.
4	SCAL2:	Normalization factor on upper bound. DEFAULT = MAX of (ABS(BU), 0.1).

REMARKS

- The normalization factor should usually be defaulted
- The constraint functions sent to CONMIN are of the form: (BL - VALUE)/SCAL1 .LE. 0.0 AND (VALUE - BU)/SCAL2 .LE. 0.0
- Each constrained parameter is converted to two constraints in CONMIN unless ABS(BL) or ABS(BU) exceeds 1.0E+15, in which case no constraint is created for that bound.

DATA BLOCK J OMIT IF NXAPRX = 0 IN BLOCK B

DESCRIPTION: Approximate analysis/optimization control parameters.

FORMAT AND EXAMPLE

1	2	3	4	5	6	7	8	FORMAT
NF	NXS	NXFS	NXA	INOM	ISCRX	IXCRXF	IPAPRX	8I10
5	1	1	1	0	0	0	1	
KMIN	KMAX	MPMAX	JNOM	INXLOC	INFLOC			6I10
0	0	0	0	0	0			

FIELD		CONTENTS
1	NF:	Number of functions to be approximated. DEFAULT = number of optimization objective and constraint functions.
2	NXS:	Number of X-vectors read as data.
3	NXFS:	Number of X-F pairs read as data.
4	NXA:	If non-zero, the design variables read by SUBROUTINE ANALIZ form an X-vector.
5	INOM:	Nominal X-vector about which to do Taylor expansion. DEFAULT = best available.
6	ISCRX:	File from which NXS X-vectors are read. DEFAULT = 5.
7	IXCRXF:	File from which NXFS X-F pairs of data are read. DEFAULT = 5.
8	IPAPRX:	Print control, 1 to 4. 4 is most.
1	KMIN:	Minimum number of approximation iterations.
2	KMAX:	Maximum number of approximation iterations.
3	NPMAX:	Maximum number of designs retained for Taylor series expansion.
4	JNOM:	Number of iterations after which the best design is picked as nominal.
5	INXLOC:	X-variable global location identifier. If INXLOC = 0, the Taylor series expansion is on the design variables listed in BLOCK G.
6	INFLOC:	Function global location identifier. If INFLOC = 0, the Objective and constraint functions identified in BLOCKS E and I are the functions on which the Taylor series expansion is performed.

REMARKS

- If ISCRX and/or ISCRXF file number is other than 5, the data read from that file is assumed to be binary data
- If NXS = NSFS = 0, NXA is defaulted to NXA = 1, even if it is read as zero. Also, a second vector of design variables is automatically defined by COPES to yield two independent designs to start the optimization.

DATA BLOCK K OMIT IF NDV = 0 IN BLOCK B, OR NXAPRX = 0 IN BLOCK B

DESCRIPTION: Bounds and multipliers for approximate optimization.

FORMAT AND EXAMPLE

1	2	3	4	5	6	7	8	FORMAT
DX1	DX2	DX3	DX4	DX5	...	...	...	8F10
.5	2.							
XFACT1	XFACT2							2F10
0.	0.							

NOTE: Two or more cards are read here.

FIELD		CONTENTS
1-8	DXI:	Allowable change (in magnitude) of the Ith design variable during each approximate optimization.
1	XFACT1:	Multiplier on DXI when the diagonal elements of the H matrix are available. DEFAULT = 1.5.
2	XFACT2:	Multiplier on DFXI when all elements of the H matrix are available. DEFAULT = 2.0.

DATA BLOCK L OMIT IF NXAPRX = 0 IN BLOCK B OR INXLOC = 0 IN BLOCK J

DESCRIPTION: *Global locations of approximating variables.*

FORMAT AND EXAMPLE

1	2	3	4	5	6	7	8	FORMAT
LOCX1	LOCX2	LOCX3	LOCX4	.....	.....	.....	.....	8I10
1	2							

NOTE: More than one card may be read here.

FIELD		CONTENTS
1-8	LOCI:	Global location of Ith approximating variable.

REMARKS

- If INXLOC = 0 in BLOCK J, this data is not read. In this case, the data is defaulted to be the global locations of the design variables (IDSGN values in BLOCK G).

DATA BLOCK M OMIT IF NXAPRX = 0 IN BLOCK B OR INFLOC = 0 IN BLOCK J

DESCRIPTION: Global locations of functions to be approximated.

FORMAT AND EXAMPLE

1	2	3	4	5	6	7	8	FORMAT
LOCF1	LOCF2	LOCF3	LOCF4	.....	.....	.....	.....	8I10
3	5	6	4					

NOTE: More than one card may be read here.

FIELD	CONTENTS
1-8	LOCI: Global location of Ith function to be approximated.

REMARKS

- If INXLOC = 0 in BLOCK J, this data is not read. In this case, the data is defaulted to be the global locations of the objective function (IOBJ in BLOCK E) followed by the global locations of the constrained parameters (ICON, JCON in BLOCK I).

DATA BLOCK N OMIT IF NXS = 0 IN BLOCK J

DESCRIPTION: X-vectors for approximate optimization.

FORMAT AND EXAMPLE

1	2	3	4	5	6	7	8	FORMAT
XI1	XI2	XI3	XI4	...	...	...	...	8F10
4.	15.							

NOTE: NXS Sets of data are read here.

NOTE: More than one card may be read for each set of data.

FIELD	CONTENTS
1-8	XIJ: Jth value of Ith X-vector, J = 1,NXAPRX.

DATA BLOCK O OMIT IF NXFS = 0 IN BLOCK J

DESCRIPTION: X-F pairs of information for approximate optimization.

FORMAT AND EXAMPLE

1	2	3	4	5	6	7	8	FORMAT
X1	X2	X3	X4	...	...	...	...	8F10
2.	18.							
Y1	Y2	Y3	Y4	Y5	...	...	...	
7200.	416.667	.914495	18418.419					

NOTE: NSFS sets of data are read here.

NOTE: More than one card may be required for XI or YI.

NOTE: NXAPRX values of X and NF values of Y are read for each set of data.

NOTE: Many significant digits are desirable.

FIELD		CONTENTS
1-8	XI:	Ith value of X, I = 1,NXAPRX.
1-8	YI:	Ith value of Y, I = 1,NF.

DATA BLOCK P OMIT IF NSV = 0 IN BLOCK B

DESCRIPTION: Sensitivity objectives (function values).

FORMAT AND EXAMPLE

1	2	3	4	5	6	7	8	FORMAT
NSOBJ	IPSENS							2I10
5	0							
NSN1	NSN2	NSN3	NSN4	NSN5	...	...	...	8I10
3	4	5	6	7				

NOTE: Two or more cards are read here.

FIELD		CONTENTS
1	NSOBJ:	Number of separate objective functions to be calculated as functions of the sensitivity variables.
2	IPSENS:	Print control. If IPSENS.GT.0, detailed print will be called at each step in the sensitivity analysis. DEFAULT = No print.
1-8	NSNI:	Global variable number associated with the sensitivity objective functions.

REMARKS

- More than eight sensitivity objectives are allowed. Add data cards as required to contain data.

DATA BLOCK Q OMIT IF NSV = 0 IN BLOCK B

DESCRIPTION: Sensitivity variables.

FORMAT AND EXAMPLE

1	2	3	4	5	6	7	8	FORMAT
ISENS	NSENS							2I10
9	4							
SNS1	SNS2	SNS3	SNS4	....	....	....	....	8F10
200.	100.	150.	250.					

NOTE: Read one set of data for each of the NSV sensitivity variables.

NOTE: Two or more cards are read for each set of data.

FIELD		CONTENTS
1	ISENS:	Global variable number associated with the sensitivity variable.
2	NSENS:	Number of values of this sensitivity variable to be read on the next card.
1-8	SENSI:	Values of the sensitivity variable. I = 1,NSENS. I = 1 correspond to the nominal value.

REMARKS

- More than eight values of the sensitivity variable are allowed. Add data cards as required to contain the data.

DATA BLOCK R OMIT IF N2VAR = 0 IN BLOCK B

DESCRIPTION: Two variable function space control parameters.

FORMAT AND EXAMPLE

1	2	3	4	5	FORMAT
N2VX	M2VX	N2VY	M2VY	IP2VAR	5I10
1	4	2	5	0	

FIELD		CONTENTS
1	N2VX:	Global location of the X-variable in the two variable function space.
2	M2VX:	Number of values of X to be considered.
3	N2VY:	Global location of the Y-variable in the two variable function space.
4	M2VY:	Number of values of Y to be considered.
5	IP2VAR:	Print control. If IP2VAR.GT.0, detailed print will be called at each step (each X-Y combination). DEFAULT = No print.

DATA BLOCK S OMIT IF N2VAR = 0 IN BLOCK B

DESCRIPTION: Objective functions of the two variable function space study.

FORMAT AND EXAMPLE

1	2	3	4	5	6	7	8	FORMAT
NZ1	NZ2	NZ3	NZ4	NZ5	...	...	...	8I10
3	4	5	6	7				

FIELD		CONTENTS
1-8	NZ1:	Global location corresponding to the Ith function of X and Y to be calculated. N2VAR values are read here.

REMARKS

- More than eight objective functions are allowed. Add data cards as required to contain the data.

DATA BLOCK T OMIT IF N2VAR = 0 IN BLOCK B

DESCRIPTION: Values of the X-variable in a two variable function space study.

FORMAT AND EXAMPLE

1	2	3	4	5	6	7	8	FORMAT
X1	X2	X3	X4	...	...	...	...	8F10
0.5	1.0	1.5	2.0					

FIELD		CONTENTS
1-8	XI:	Values of the X-variable in the two variable function space. M2VX values are read here.

REMARKS

- More than eight values are allowed. Add data cards as required to contain the data.

DATA BLOCK U OMIT IF N2VAR = 0 IN BLOCK B

DESCRIPTION: Values of the Y-variable in a two variable function space study.

FORMAT AND EXAMPLE

1	2	3	4	5	6	7	8	FORMAT
Y1	Y2	Y3	Y4	Y5	...	...	...	8F10
4.0	8.0	12.0	16.0	20.0				

FIELD		CONTENTS
1-8	YI:	Values of the Y-variable in the two variable function space. N2VY values are read here.

REMARKS

- More than eight values are allowed. Add data cards as required to contain the data.

DATA BLOCK V

DESCRIPTION: COPES data 'END' card.

FORMAT AND EXAMPLE

	1	FORMAT
	END	3A1
END		

FIELD	CONTENTS
1	The word 'END' in columns 1-3

REMARKS

- This card MUST appear at the end of the COPES data
- This ends the COPES input data
- Data for the user-supplied routine, ANALIZ, follows this.

5.2 TRANSONIC ANALYSIS INPUT DATA

NOTE: Excluding literal cards, all input data cards are 7F10. format.

CARD NUMBER	CARD COLUMN	VARIABLE NAME	DESCRIPTION
Card 1-A	1-80	TTLE	Configuration or run title to identify graphic and printed output.
Card 2-A	1-10	CASE	= 1. Isolated Body, used for input check of complex body definition. No flow solution. (Omit cards 3-A, 4-A and all cards -C, -W). = 2. Isolated Wing (omit all cards -C, -B). = 3. Wing-Body (omit cards -C). = 4. Isolated wing-canard (omit all cards -B). = 5. Wing-Body-Canard (omit cards -V). = 6. Wing-T-Tail. = 7. Wing-Body-T-Tail.
	11-20	AMACH	Mach Number (AMACH $\leq$ 1.0).
	21-30	AOA	Angle-of-Attack (degrees).
	31-40	WPO	$\leq$ -3. Same as WPO = -2. plus omit grid and body information output. $\leq$ -2. Same as WPO = -1. plus omit body C_p output. $\leq$ -1. Same as WPO = 0. plus omit Mach chart output. $\leq$ 0. No crude grid output. $\geq$ 1. Crude grid output for diagnostic purposes. $\geq$ 2. Same as WPO = 1. plus boundary layer information. $\geq$ 3. Same as WPO = 2. plus print C_p values off wing and canard. $\geq$ 4. Same as WPO = 3. plus print fine grid boundary conditions.

CARD NUMBER	CARD COLUMN	VARIABLE NAME	DESCRIPTION
Card 2-A (contd)			$\geq$ 5. Same as WPO = 4. plus print solution convergence information for every spanwise plane.
	41-50	AXIT	Number of initial crude grid iterations.
	51-60	AXITF	Number of crude/fine grid iteration cycles.
	61-70	VISMOD	= 1. No viscous effects. = 2. Viscous effects computed at end of inviscid analysis. = 3. Inviscid/viscous interaction.
Card 3-A	1-10	FSAVE	= 1. Save the flow solution on Unit 99. ≠ 1. Do not save the flow solution.
	11-20	FSTRT	= 1. Restart the flow solution from Unit 98. ≠ 1. Do not restart the flow solution. NOTE: See Usage Note 1.
	21-30	CNVTST	Convergence test based on average flow solution correction (CCAV). Default is 1.0E-06.
	31-40	FCASM2	= 1. Construct wing-canard or wing-tail grid, but run canard-off or tail-off solution. Will read canard or tail input (CASE = 4. through 7. on Card 2-A), construct grids and then do wing alone or wing-body solution. ≠ 1. Do not "turn off" canard or tail.
	41-50	PCTLE	Crude grid leading edge spacing tolerance. Default is 0.01, minimum allowed is 0.005. NOTE: See Usage Note 2.
	51-60	FCGRD	= 1. Places the canard surface in the vertical mid-location of the canard fine grid system. Appropriate for lightly or negatively loaded canards.

CARD NUMBER	CARD COLUMN	VARIABLE NAME	DESCRIPTION
Card 3-A (contd)			$\neq$ 1. Places the canard surface at the lower quarter vertical location in the canard fine grid system.
	61-70	FTWAKE	= 0. No wake deflection (FTWAKE defaults to 10000).
			$\geq$ 1. Wake deflection updated every FTWAKE iterations. Recommended value is 8.
Card 4-A	1-10	SREF	Reference area, if 0., code will calculate.
	11-20	AMAC	Mean aerodynamic chord, if 0., code will calculate.
	21-30	ALAM	Reference taper ratio, if 0., code will calculate.
	31-40	XMOM	X-position for pitching moment reference.
	41-50	ZMOM	Z-position for pitching moment reference.
	51-60	RE	Reynolds Number x 10^{-6}, based on AMAC. DEFAULT = 10.
	61-70	FYINT	= 0. Nondimensional ordinate spanwise interpolation.
			$\neq$ 1. Physical ordinate spanwise interpolation.
			NOTE: See Usage Note 3.

NOTE: Omit Card 1-C for CASE $<$ 4.

Card 1-C	1-10	ASECT	Number of streamwise sections defining the canard planform (2. $\leq$ ASECT $\leq$ 20.). ASECT for canard plus ASECT for wing must not exceed 20.
	11-20	ANIN	Number of ordinates defining each canard section (ANIN $\leq$ 60).
	21-30	ANOSW	= 0. Sharp nose canard section.
			= 1. Blunt nose canard section.
	31-40	ZWINGC	Z-position of canard (waterline).

CARD NUMBER	CARD COLUMN	VARIABLE NAME	DESCRIPTION
Card 1-C (contd)	41-50	XTRNC	Transition location for canard, streamwise. > 0. fraction of chord. < 0. physical distance from leading edge. = 0. default to fixed chord fraction of 0.05. NOTE: See Usage Note 4.
	51-60	CINSDS	Canard incidence, degrees, incorporated as added twist at each input station.
	61-70	SHIFTC	Grid shift for CASE = 4 or CASE = 5. NOTE: See Usage Note 5.
Card 1-W	1-10	ASECT	Number of streamwise sections defining the wing planform (2. $\leq$ ASECT $\leq$ 20.). ASECT for canard plus ASECT for wing must not exceed 20.
	11-20	ANIN	Number of ordinates defining each wing section (ANIN $\leq$ 60.).
	21-30	ANOSW	= 0. Sharp nose wing sections. = 1. Blunt nose wing sections.
	31-40	ZWING	Z-position of wing (waterline).
	41-50	XTRNW	Transition location for wing, streamwise. Same usage as for XTRNC (See Card 1-C and Usage Note 4.).
	51-60	WINSDS	Wing incidence, degrees, incorporated as added twist at each input station.
	61-70	SHIFTW	Grid shift for CASE < 4. NOTE: See Usage Note 5.

NOTE: Omit card 1-V for CASE < 6.

CARD NUMBER	CARD COLUMN	VARIABLE NAME	DESCRIPTION
Card 1-V	1-10	ASECT	Number of streamwise sections defining the vertical stabilizer (2. $\leq$ ASECT $\leq$ 5.).
	11-20	ANIN	Number of ordinates defining each input section (ANIN $\leq$ 60.).

CARD NUMBER	CARD COLUMN	VARIABLE NAME	DESCRIPTION
Card 1-V (contd)	21-30	ANOSW	= 0. Sharp nose sections = 1. Blunt nose sections.
	31-40	SHIFTT	Grid shift for CASE > 5. NOTE: See Usage Note 5.

NOTE: Omit Card Set 2-C through 5-C for CASE < 4. Card Set 2-C through 5-C is repeated ASECT (for canard) times.

CARD NUMBER	CARD COLUMN	VARIABLE NAME	DESCRIPTION
Card 2-C	1-10	XPL	Canard section leading edge (X-value).
	11-20	YP	Canard section span position (Y-value). First Y-Value must be 0.0 (symmetry plane), even for wing-body case.
	21-30	XPT	Canard section trailing edge (X-value).
	31-40	TWIST	Canard section local incidence (twist angle), degrees, added to input section.
	41-50	AKODE	= 0. Section ordinates identical to preceding section (omit cards 3-C through 5-C). = 1. New section definition expected on cards 4-C and 5-C.
Card 3-C	1-70	XINWC	Canard section x/c coordinates (cards 3-C defined only for first canard section, ANIN values).
Card 4-C	1-70	YINU	Canard section upper surface y/c coordinates (ANIN values).
Card 5-C	1-70	YINL	Canard section lower surface y/c coordinates (ANIN values).

NOTE: Card Set 2-W through 5-W is repeated ASECT (for wing) times.

CARD NUMBER	CARD COLUMN	VARIABLE NAME	DESCRIPTION
Card 2-W	1-10	XPL	Wing section leading edge (X value).
	11-20	YP	Wing section span position (Y-value). First Y-value must be 0.0 (symmetry plane), even for wing-body case.
	21-30	XPT	Wing section trailing edge (X-value).
	31-40	TWIST	Wing section local incidence (twist angle), degrees, added to input section.

CARD NUMBER	CARD COLUMN	VARIABLE NAME	DESCRIPTION
Card 2-W (contd)	41-50	AKODE	= 0. Section ordinates identical to preceding section (omit cards 3-W through 5-W). = 1. New section definition expected on cards 4-W and 5-W.
Card 3-W	1-70	XINW	Wing section x/c coordinates (cards 3-W defined only for first wing section, ANIN values expected).
Card 4-W	1-70	YINU	Wing section upper surface y/c coordinates (ANIN values).
Card 5-W	1-70	YINL	Wing section lower surface y/c coordinates (ANIN values).

NOTE: Omit Card Set 2-V through 4-V for Case < 6. Card Set 2-V through 4-V is repeated ASECT (for vertical stabilizer) times.

CARD NUMBER	CARD COLUMN	VARIABLE NAME	DESCRIPTION
Card 2-V	1-10	XPLV	Vertical stabilizer section leading edge (X-value).
	11-20	ZPV	Vertical stabilizer section Waterline (Z-value).
	21-30	XPTV	Vertical stabilizer section trailing edge (X-value).
	31-40	AKODE	= 0. Section ordinates identical to preceding section (omit cards 3-V and 4-V). = 1. New section definition expected on card 4-V.
Card(s) 3-V	1-70	XINV	Vertical stabilizer section x/c coordinates (Card(s) 3-V defined only for first input section, ANIN values).
Card(s) 4-V	1-70	YINV	Vertical stabilizer y/c coordinates (ANIN values). Code allows symmetrical sections only.

CARD NUMBER	CARD COLUMN	VARIABLE NAME	DESCRIPTION
NOTE: Omit card set 1-B through 13-B for CASE = 2, CASE = 4, or CASE = 6.			
Card 1-B	1-10	BKOD	= 1. Infinite cylinder (only RADIUS need be input).
			=-1. Same as BKOD = 1. No embedded body grid. Crude grid body representation only.
			= 2. Simple axisymmetric body definition requested (input XBIN, RIN on card(s) 2-B and 3-B.
			=-2. Same as BKOD = 2. No embedded body grid. Crude grid body representation only.
			= 3. Complex body definition requested (input Quick-Geometry model on card(s) 4-B through 13-B). Detailed model interrogation for checking input.
			=-3. Same as BKOD = 3. No embedded body grid. Crude grid body representation only.
NOTE: BKOD > 0. is available for body input checkout only. Flow solution is available for BKOD < 0. only.			
			NOTE: See Usage Note 6.
	11-20	BNOSE	Body nose (X-value) used for BKOD $\neq$ 1.
	21-30	BTAIL	Body tail (X-value) used for BKOD $\neq$ 1.
Card 1-B	31-40	BNIN	Number of axisymmetric body coordinates to be input. BNIN $\leq$ 60. (for BKOD = ±2. only).

CARD NUMBER	CARD COLUMN	VARIABLE NAME	DESCRIPTION
Card 1-B	41-50	RADIUS	Cylinder radius for BKOD = ±1. only.
(contd)	51-60	ANOSB	= 0. Sharp nose body. = 1. Blunt nose body. Used for BKOD = ±2. only.

NOTE: Omit card sets 2-B and 3-B for BKOD = ±1. or BKOD = ±3.

CARD NUMBER	CARD COLUMN	VARIABLE NAME	DESCRIPTION
Card(s) 2-B	1-70	XINB	Axisymmetric body X-coordinates (BNIN values).
Card(s) 3-B	1-70	RIN	Axisymmetric body radii (BNIN values).

NOTE: Omit card sets 4-B through 13-B for BKOD = ±1. or BKOD = ±2.

CARD NUMBER	CARD COLUMN	VARIABLE NAME	DESCRIPTION
Card 4-B	1-70	VTITLE	Quick-Geometry model title.
Card 5-B	1-10	ACSM	Number of distinct cross-section models (ACSM card sets 6-B and 7-B will follow).
Card 6-B	1-10	ADUM	Running count of current cross-section model (1-ACSM).
	11-20	AARC	Number of arcs in current cross-section model (AARC Card(s) 7-B will follow).
	21-60	CTITLE	Title or descriptor of current cross-section model.
Card 7-B	1-8	ARCNAM	Arc or component name.
	11-14	ASHAPE	Arc or component shape.
	21-28	PNTNAM(1)	Control point name for beginning of this arc.
	31-38	PNTNAM(2)	Control point name for termination of this arc.
	41-48	PNTNAM(3)	Slope control point name for this arc, if required.
Card 8-B	1-10	ANTCSM	Number of cross-section models to define entire body (ANTCSM card(s) 9-B will follow).

CARD NUMBER	CARD COLUMN	VARIABLE NAME	DESCRIPTION
Card 9-B	1-10	ADUM	Running count of current cross-section model (1-ANTCSM).
	11-20	AMODEL	Index corresponding to already defined cross-section models (between 1 and ACSM).
	21-30	XCSMS1	Starting X-station for current cross-section model.
	31-40	XCSMS2	Ending X-station for current cross-section model.
Card 10-B	1-10	BLINE	Number of body line models to be defined by segments (BLINE card set 11-B and 12-B follow).
	11-20	ALIAS	Number of body line models to be aliased. (Input ALIAS card(s) 13-B below).
Card 11-B	1-10	BLSEG	Number of segment(s) defining body line model.
	11	BYORZ	The letter Y or Z indicates which data definition is to follow.
	12-19	BNAME	Body line name to be defined.
Card 12-B	1-4	SSHAPE	Segment shape.
	11-20	D(1)	X-station for beginning of segment.
	21-30	D(2)	Y or Z value corresponding to D(1).
	31-40	D(3)	X-station for termination of segment.
	41-50	D(4)	Y or Z value corresponding to D(3).
	51-60	D(5)	X-station for segment slope control point.
	61-70	D(6)	Y or Z value corresponding to D(5).
Card 13-B	11	BYORZ	The letter Y or Z indicates which data definition is to follow.
	12-19	BNAME	Body line name to be defined.
	21	AYORZ	The letter Y or Z indicates which definition is to be used for aliasing.
	22-29	ANAME	Body line name to which BNAME is aliased.

5.3 USAGE NOTES

Note 1. Saved Solution

When an analysis consists of both crude only and then crude/fine iterations, a saved solution is written on unit 99 immediately before the crude/ fine iterations begin. At the end of the crude/fine iterations, the previous saved solution is overwritten with the most recent results. In this way, an abnormal termination of the crude/fine iterations will have the crude iteration results saved on unit 99. With an abnormal termination, appropriate job control cards may be needed to "permanently" save the unit 99 data.

Note 2. PCTLE Parameter

The code will shift the input geometry to find a streamwise location in the crude grid where the first points at each span station on the wing and canard is not "too close" to the leading edge. (Riegel's rule is not used for the boundary conditions.) The PCTLE parameter is the required minimum distance from the leading edge. See also Usage Note 5, Grid Shift Parameters.

Note 3. FYINT Parameter

The input wing and canard section ordinates (YINU AND YINL) are linearly interpolated from the input span stations to the analysis span stations. The method of interpolation is controlled by the parameter FYINT. If FYINT = 0. nondimensional spanwise interpolation of the ordinates is used:

$$(z/c)_Y = (z/c)_{Y1}(1.-R) + (z/c)_{Y2}(R)$$

If FYINT = 1. physical spanwise interpolation of the ordinates is used:

$$(z/c)_Y = (z/c)_{Y1}(1.-R)(c_{Y1}/c_Y) + (z/c)_{Y2}(R)(c_{Y2}/c_Y)$$

where

c = local chord   Y = interpolated span station

R = (Y-Y1)/(Y2-Y1)   Y1,Y2 = input span stations

z/c = nondimensional section ordinate

The first formula is the more usual analysis code interpolation, while the second formula corresponds to manufacturing lofting methods. The difference between the two formulas becomes greater for more highly tapered wings and fewer input span stations.

Note 4. Boundary Layer Transition

The fraction of chord designation results in transition specified at the same percentage chord location at all span stations. Thus, the physical distance from the leading edge decreases as the local chord length decreases. The physical distance designation results in transition specified at the same fixed distance from the leading edge. Thus, the percentage chord from the leading edge increases as the local chord length decreases.

Note 5. Grid Shift Parameters

Variables SHIFTC, SHIFTW and SHIFTT can be used to set the initial streamwise placement of the configuration. (The grid is fixed in location and the input geometry is shifted.) The code will determinate the appropriate shift with a search procedure. After the first analysis run, the resulting shift parameter can be input to eliminate the search in subsequent runs. The shift parameter can also be used to evaluate different grid placements. If the grid placement search should fail, the shift parameter can be used to start the search at different locations, possibly finding a satisfactory grid placement.

Note 6. Body/Fuselage Geometry Model

The present method allows complex three-dimensional geometries to be input, processed and converted into a suitable array of boundary conditions for analysis. Although the input or modeling of complex body shapes is extremely error prone and certain applications might not warrant this level of effort, it is necessary in aircraft application when fuselage contours (e.g., canopies, fairings) are required. The code does not provide an embedded fine grid body analysis. The embedded body grid option is provided to allow a detailed body input definition checkout.

This will be most useful if the graphical output is available. The following discussion is excerpted from Ref 2. Additional information and examples will be found in the reference.

The complex fuselage modeling system has been named "Quick-Geometry" by its developers, Vachris and Yaeger (Ref 3). A detailed User's Guide for the Quick-Geometry system can be found in the appendix of Ref 14. This system was originally developed for the geometric modeling of wing-body shapes. Since only fuselage shapes are of concern here, many of the more sophisticated options including fillets and patches will not be described in the paragraphs which follow. In addition, if Ref 3 and 14 are being used to augment the modeling description provided herein, it should be noted that the input format has been modified to be more consistent with that of the basic transonic wing-body code.

The geometry package requires that certain body line and cross-section lines be defined. The body lines and cross-section lines may be likened to the stringers and bulkheads, respectively, used in fuselage construction. These line models are defined by a combination of simple curves (i.e., lines, ellipses, cubics). They are taken together to provide a continuous analytical model of the surface geometry. Slopes and normals are developed analytically. Either discontinuous intersections or smooth fairings can be modeled and enforced.

Two different coordinate systems are employed. Geometry definition is performed in a Cartesian coordinate system (X,Y,Z), while interrogation of the model for body boundary conditions is performed in cylindrical coordinates (X,R,θ). This results in the use of a plane of symmetry map axis, the height of which usually corresponds to the position of the max-half-breadth line. It is required that the configuration radius at any cross-sectional cut be a single valued function of the angle θ. These definition lines and coordinate systems are illustrated in Figure 14.

14 Marconi, F. and Yaeger, L., "Development of A Computer Code for Calculating the Steady Super/Hypersonic Inviscid Flow Around Real Configurations," NASA CR-2676 (Vol. II), May 1976.

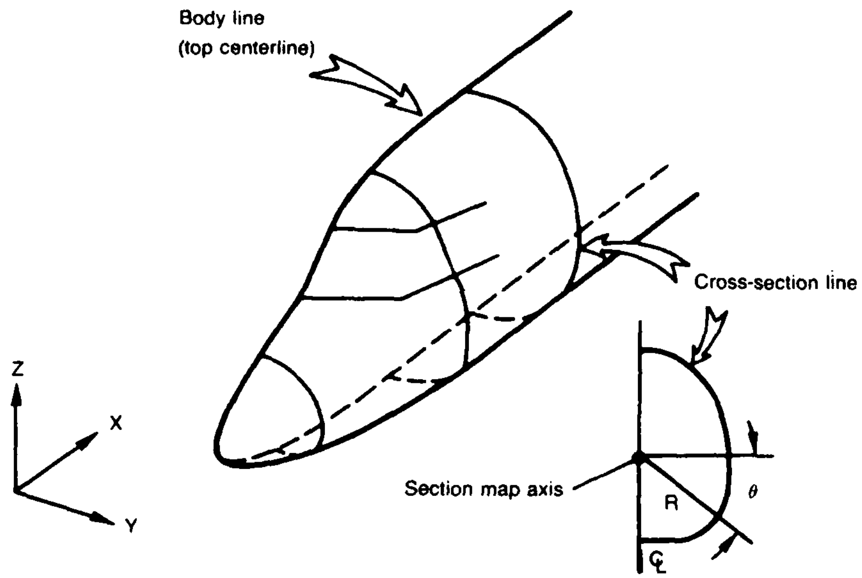

Figure 14. Quick geometry model lines and coordinate systems (from Ref 2).

A minimum of four body lines are required for the simplest fuselage. These are: top centerline, bottom centerline, max-half-breadth line, and the map axis. Each body line must be defined by both its Y and Z values over the full range of X (between fuselage nose and tail). Similarly, a minimum of two cross-section line segments are required for each different cross-section line model. These are body upper, and body lower.

Both body lines and cross-section lines are specified by defining key arc or segment shapes and their accompanying limiters. The segment shape boundary conditions used to determine the coefficients of the slope equation are the origin point, termination point, and slope control point. The slope control point lies at the intersection of the line which is tangent to the segment shape at the origin point and the line which is tangent to the segment shape at the termination point (see Figure 15). The slope control point is a very convenient way of specifying slope conditions. In particular, it allows for the simultaneous specification of slope conditions at both ends of the segment.

Figure 15 is a schematic illustrating the component build-up of a particular body line and cross-section line model. Naturally, LINE segments do not require a slope control point. In this case, the portion of the body top centerline illustrated requires four body line segments and the cross-section is constructed with two arcs (two is the minimum number allowed).

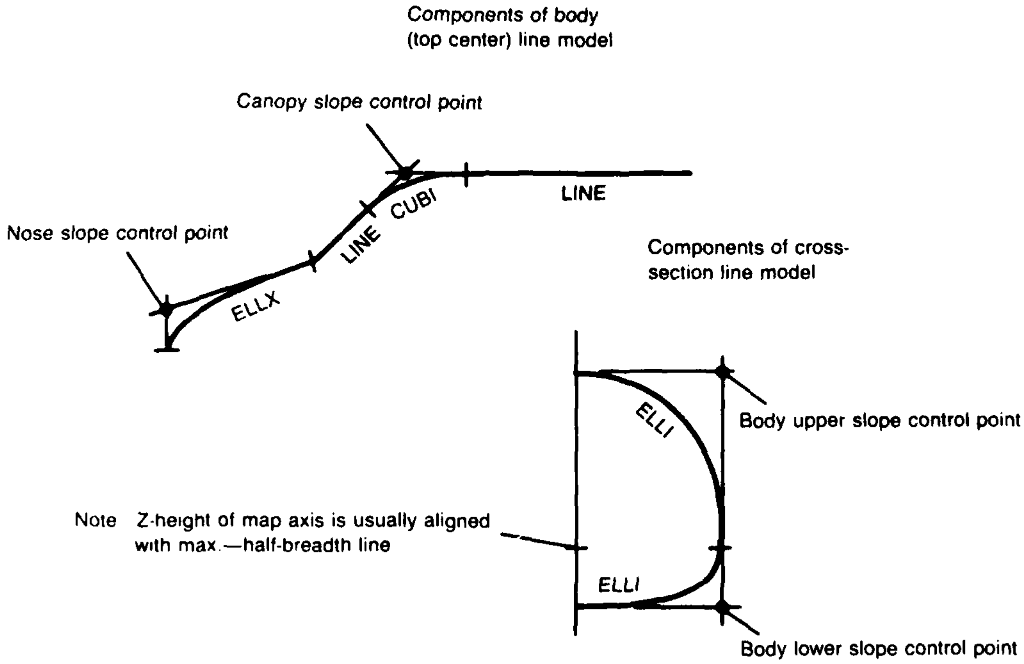

Figure 15. Quick geometry body and cross-section line models (from Ref 2).

The arc shapes used for defining a cross-section line model are listed in Table 1. They are input in an order which starts at the body bottom centerline and proceeds to the body top center line. The segment shapes used for defining a body line model are listed in Table 2.

Cross-section arcs are input in their order of appearance. However, body line segments are defined along with an index which establishes their order in the X direction. In addition, body lines may be aliased to other body lines. This allows two body line models to have identical mathematical representations without repeating the body line segment input. For example, the Z value of the map axis (ZMAP) is typically the Z value of the maximum half-breadth (ZMHB). The two are made identical by aliasing the two body line model names ZMAP and ZMHB.

TABLE 1. CROSS-SECTION ARC SHAPES

SHAPE	KEYWORD	EQUATION
LINE	LINE	$Ay + Bz + C = 0$
ELLIPSE (CONCAVE TO ORIGIN)	ELLI	$\frac{(y - y_0)^2}{A^2} + \frac{(z - z_0)^2}{B^2} = 0$
ELLIPSE (CONVEX TO ORIGIN)	ELLO	SAME AS ELLI.

TABLE 2. BODY LINE SEGMENTS

SHAPE	KEYWORD	EQUATION
LINE	LINE	$Ax + By = 0$
X-PARABOLA	XPAR	$Ax + By + y^2 = 0$
Y-PARABOLA	YPAR	$Ax + By + x^2 = 0$
X-ELLIPSE	ELLX	$Ax + By + Cx^2 + y^2 = 0$
Y-ELLIPSE	ELLY	$Ax + By + Cy^2 + x^2 = 0$
CUBIC	CUBI	$Ax + By + Cx^2 + x^3 = 0$

It should be noted that cross-sections are defined only in terms of named component arcs (arc shape table) and named control points. On the other hand, body lines are defined mathematically by coordinates over the length of the configuration for which they are required. At a given X station, the body lines are interrogated to give the key control points required to construct the cross-sectional arcs.

6 - CODE OPERATION

The program reads data from unit 5 and writes output on unit 6. Units 20 and 40 are used as scratch files in the COPES routines. The scratch file numbers may be changed by changing two cards at the beginning of the COPES program. The analysis code stores data on unit numbers 1, 4, 8, 15, 85, 90, 94, 98 and 99. Unit 15 is used by the Ames plotting software for graphical output. It has been left available to facilitate incorporation of graphic capability by other users.

The computer code is written in FORTRAN, employing the CRAY segmentation loader. Storage requirements on a CRAY X-MP are 806,000 words of memory. Typical CPU time for a wing-body-canard analysis with viscous effects is four minutes. The CPU time for an optimization run will vary according to the complexity of the optimization problem, as discussed in Section 4, COPES/COMIN OPTIMIZATION.

The segmentation structure is described in Table 3. The Job Control Language (JCL) for operation on the Ames CRAY is shown in Figure 16. The job

TABLE 3. SEGMENTATION STRUCTURE

SEGMENT	CONTENTS
A	COPES CONTROL PROGRAM, SUBROUTINES NEEDED THROUGHOUT THE CODE
B	CONMIN OPTIMIZATION ROUTINES
C	TRANSONIC ANALYSIS CONTROL PROGRAM, WITH OPTIMIZATION INTERFACE
D	INPUT CONTROL PROGRAM, QUICK GEOMETRY LOOK-UP ROUTINES INPUT PROCESSING INPUT GEOMETRY PLOTTING, BODY AREA CALCULATIONS
E	POTENTIAL FLOW SOLUTION AND OUTPUT
F	PLOTTING
G	BOUNDARY LAYER CALCULATION
H	INDUCED DRAG CALCULATION
I	FREE WAKE CALCULATION

```
JOB,JN=SAMPLE,T=660,MFL=850000.
-----      ACCOUNT CARD      -----
*
COPYF,I=$IN,O=SEGDIR.
REWIND,DN=SEGDIR.
*
ACCESS,DN=CANPL,PDN=CANPL10,ID=CANTATA,OWN=RFAPXA.
UPDATE,P=CANPL,C=COMPILE,IN,ID,ED,UM.
*
CFT,I=COMPILE,OFF=P,ON=A,L=0,OPT=FULLIFCON.
RELEASE,DN=CANPL:COMPILE.
*
ACCESS,DN=CANLIB,PDN=CANLB10,ID=CANTATA,OWN=RFAPXA.
SEGLDR,DW=72,I=SEGDIR.
RELEASE,DN=$BLD:SEGDIR.
*
CANTATA.
/EOF
PRESET=INDEF
MAP=PART
REDEF=IGNORE
ABS=CANTATA
LIB=CANLIB
TREE
 A(B,G)
 B(C,D,E)
 D(H,I,J)
ENDTREE
SEGMENT=A;SAVE=ON
 MODULES=COPES
ENDSEG
SEGMENT=B;SAVE=ON
 MODULES=ANALIZ
ENDSEG
SEGMENT=C
 MODULES=OVL10,MLSIN
ENDSEG
SEGMENT=D;SAVE=ON
 MODULES=MLSNLS
ENDSEG
SEGMENT=E;SAVE=ON
 MODULES=PLTSEG
ENDSEG
SEGMENT=G
MODULES=OPT,CONMIN
ENDSEG
SEGMENT=H
 MODULES=STRIPK
ENDSEG
SEGMENT=I
 MODULES=LIDRAG
ENDSEG
SEGMENT=J;SAVE=ON
 MODULES=WAKEC
ENDSEG
/EOF
*COMPILE COPES,BLKDAT
-----      ADDITIONAL UPDATES AS APPROPRIATE      -----
/EOF
-----      INPUT DATA      -----
```

Figure 16. Job Control Language.

card and account card will vary with the individual user. To save CPU time for compilation, a binary file of the code is stored as a permanent file. Thus, the JCL uses an UPDATE command followed by CFT to change, compile and replace only those routines being modified for a particular run. The numerical optimization will require changes to the subroutines OGEOM, MOD and ANALIZ. For simple analysis, no changes need be made, except perhaps to BLOCK DATA to change some defaults. The UPDATE step always requires some input. The *COMPILE COPES,BLKDAT card in Figure 16 is shown as an example that satisfies this requirement.

Not shown in the JCL are the cards for saving and restarting the flow solution with FORTRAN files 98 and 99. The Applied Computational Fluids Branch at Ames can provide the necessary authorization and information.

If the code is converted for use on IBM type computers, several Quick-Geometry variables need special treatment. These variables and the subroutines in which they appear are listed in Table 4. The REAL*8 declaration is needed to have sufficient word length for line model labeling and increase the accuracy of the body model calculations. The CRAY compiler option OFF=P is used to allow the REAL*8 declarations to remain in the code and have no effect. CRAY compiler directives are used in several places. These begin

TABLE 4. REAL *8 VARIABLES FOR IBM USAGE OF QUICK-GEOMETRY

SUBROUTINE NAME	VARIABLE NAME
CURVES	A, B, C, Y, T, X, FACT, RFACT, S
MODTV	SUM, ONE
VDOTV	C, ONE
QWIKDE	CPNTNM, COMPNM
BLMCHK	CPNTNM, COMPNM, ANAME, BNAME, BLMNAM, EQUNB, EQUNA
BLMDEF	CPNTNM, COMPNM, ANAME, BNAME, BLMNAM, BLANK2
CSMCHK	CPNTNM, COMPNM, ARCNAM, PNTNAM, BLANK2, ZMAPNM, ARCNM
CSMDEF	CPNTNM, COMPNM, ARCNAM, PNTNAM, BLANK2, ZMAPNM, ARCNM, AMAPAX
GEMOUT	CPNTNM, COMPNM, ARCNM, PNTNAM, BLANK2, AMAPNM, ARCNM
DSETUP	ALABLE, BLABLE

with a letter C in the first column, so that they will be interpreted as comment cards on other computers. Two CRAY library functions, ISMAX and ISAMAX are used in the code. The ISMAX function returns the index of the vector element with the largest value. The ISAMAX function returns the index of the vector element with the largest absolute value. Their FORTRAN equivalents are easily incorporated. The overall scalar-to-vector CPU time ratio is 2.6.

The program output listing of the input data for a sample analysis run is shown in Figure 17. In front of this input were the COPES control cards:

```
TITLE
1,
END
```

with no delimiters in between. The input example uses NACA 0010 wing sections. Following the input data listing is a data read echo showing the information the program has read from the input cards (Figure 18). Portions of the grid generation output are shown in Figures 19 and 20.

In this example, the flowfield solution begins with nine crude grid iterations, and then continues with nine fine grid/crude grid iterations. The program output for this is shown in Figure 21. When the flow solution is completed, detailed flow information is output at each analysis station on the wing and canard. An example for station 11 is shown in Figure 22.

Force and moment output for the wing, canard and body is shown in Figure 23. Figure 24 shows the final wing-body-canard spanload output. All of the results shown in Figure 18 through 24 were for the analysis input data of Figure 17.

```
CANTATA --- CANARD TAIL TRANSONIC AERODYNAMICS

DEVELOPED AT GRUMMAN AEROSPACE CORPORATION,BETHPAGE, NEW YORK
FOR AIR FORCE FLIGHT DYNAMICS LABORATORY, WPAFB, OHIO
J. R. SIRBAUGH, CONTRACT MONITOR, FIMM

              INPUT DATA LISTING

12345678901234567890123456789012345678901234567890123456789012345678901234567890
FORWARD SWEPT SAMPLE CASE
5.0       0.7       8.0       0.000     9.0       9.0       1.0
0.0       0.0       0.0       0.0       0.0       0.0       8.0
0.0       0.0       0.0       44.00     -2.00     0.0       1.0
3.0       18.       1.0       4.00      .05       -2.0
5.0       18.       1.0       -4.00     .05       1.0
27.0      0.0       43.0      0.0       1.0
0.00      1.25      2.50      5.00      7.50      10.0      15.0
20.0      25.0      30.0      40.0      50.0      60.0      70.0
80.0      90.0      95.0      100.
0.000     1.578     2.178     2.962     3.500     3.902     4.455
4.782     4.952     5.002     4.837     4.412     3.803     3.053
2.187     1.207     0.672     0.105
-0.000    -1.578    -2.178    -2.962    -3.500    -3.902     -4.455
-4.782    -4.952    -5.002    -4.837    -4.412    -3.803    -3.053
-2.187    -1.207    -0.672    -0.105
27.       5.5       43.0      0.0       0.
33.0      18.0      38.0      0.0       0.
54.0      0.        103.0     0.0       1.0
0.00      1.25      2.50      5.00      7.50      10.0      15.0
20.0      25.0      30.0      40.0      50.0      60.0      70.0
80.0      90.0      95.0      100.
0.000     1.578     2.178     2.962     3.500     3.902     4.455
4.782     4.952     5.002     4.837     4.412     3.803     3.053
2.187     1.207     0.672     0.105
-0.000    -1.578    -2.178    -2.962    -3.500    -3.902     -4.455
-4.782    -4.952    -5.002    -4.837    -4.412    -3.803    -3.053
-2.187    -1.207    -0.672    -0.105
54.0      5.5       103.0     0.0       0.0
57.0      12.0      80.00     0.0       0.
58.0      14.0      78.0      0.0       0.
38.0      36.0      48.0      0.0       0.
-3.0      0.        126.0
 QUICK-BODY FUSELAGE
2.0
1.0       3.0       AFTBOX
ABOT      LINE      BDYBCL    BDYMHB
ASIDE     LINE      BDYMHB    SIDHI
ATOP      LINE      SIDHI     BDYTCL
2.0       5.0       MIDFUS
MBOT      LINE      BDYBCL    BOTCRN
MLOCR     ELLI      BOTCRN    BDYMHB    LOSLCP
MSIDE     LINE      BDYMHB    SIDHI
MHICR     ELLI      SIDHI     TOPCRN    HISLCP
MTOP      LINE      TOPCRN    BDYTCL
2.0
1.0       2.0       0.0       27.73
2.0       1.0       27.73     126.0
13.0      6.0
```

Figure 17. Analysis code input data listing (sheet 1 of 2).

```
1.0       YCENTER
LINE      0.0       0.0       126.0     0.0
2.0       ZBDYBCL
ELLX      0.0       -2.2      27.73     -6.0      16.75     -6.0
LINE      27.73     -6.0      126.0     -6.0
2.0       ZBDYTCL
ELLX      0.0       -2.2      27.73     6.75      15.12     6.75
LINE      27.73     6.75      126.0     6.75
4.0       ZBDYMHB
LINE      0.0       -2.2      8.31      -.6
CUBI      8.31      -.6       16.31     -2.0      11.9      0.14
LINE      16.31     -2.0      27.73     -6.0
LINE      27.73     -6.0      126.0     -6.0
2.        YBDYMHB
CUBI      0.0       0.0       27.73     5.5       12.7      5.5
LINE      27.73     5.5       126.0     5.5
1.0       YBOTCRN
LINE      0.0       0.0       27.73     5.5
1.0       YTOPCRN
LINE      0.0       0.0       27.73     5.5
2.0       YSIDHI
CUBI      0.0       0.0       27.73     5.50      12.7      5.50
LINE      27.73     5.5       126.0     5.5
3.0       ZSIDHI
LINE      0.0       -2.2      8.31      0.0
CUBI      8.31      0.0       27.73     6.75      15.12     4.86
LINE      27.73     6.75      126.0     6.75
1.0       ZBOTCRN
ELLX      0.0       -2.2      27.73     -6.0      16.75     -6.0
1.0       YLOSLCP
CUBI      0.0       0.0       27.73     5.5       12.7      5.5
4.0       ZMAPAXIS
LINE      0.0       -2.2      3.4       -1.6
LINE      3.4       -1.6      8.31      0.0
LINE      8.31      0.0       27.73     0.0
LINE      27.73     0.0       126.0     0.0
1.0       ZTOPCRN
ELLX      0.0       -2.2      27.73     6.75      15.12     6.75
          YBDYBCL   YCENTER
          YBDYTCL   YCENTER
          YMAPAXIS  YCENTER
          ZLOSLCP   ZBOTCRN
          YHISLCP   YLOSLCP
          ZHISLCP   ZTOPCRN
1234567890123456789012345678901234567890123456789012345678901234567890
```

Figure 17. Analysis code input data listing (sheet 2 of 2).

```
DATA READ ECHO      (DEFAULTS AND INTEGER CONVERSION INCLUDED)

INPUT CARD 1-A      FORWARD SWEPT SAMPLE CASE

INPUT CARD 2-A      CASE=  5  AMACH=0.700  AOA= 8.000  WPO=  0  AXIT=   9  AXITF=   9  VISMOD=  1

INPUT CARD 3-A      FSAVE=  0  FSTRT=  0  CNVTST= 1.000E-06  NCASM2=  0  PCTLE=    0.010  FCGRD=  0  FTWAKE=     8

INPUT CARD 4-A      SREF=       0.000  AMAC=   0.000  ALAM= 0.000     (PROGRAM WILL CALCULATE VALUES IF ZERO)
                     XMOM=  44.000  ZMOM=  -2.000  RE=   1.000E+07  FYINT=  1

INPUT CARD 1-C      ASECT=  3  ANIN= 18  ANOSW=  1  ZWINGC=     4.000  XTRNC=  0.050  CINSDS=  -2.000  SHIFTC=     0.000

INPUT CARD 1-W      ASECT=  5  ANIN= 18  ANOSW=  1  ZWING=    -4.000  XTRNW=  0.050  WINSDS=   1.000  SHIFTW=     0.000

INPUT CARD  1  OF CARD SET 2-C     XPL=    27.000  YP=     0.000  XPT=    43.000  TWIST=   0.000  AKODE=  1

INPUT CARD  2  OF CARD SET 2-C     XPL=    27.000  YP=     5.500  XPT=    43.000  TWIST=   0.000  AKODE=  0

INPUT CARD  3  OF CARD SET 2-C     XPL=    33.000  YP=    18.000  XPT=    38.000  TWIST=   0.000  AKODE=  0

INPUT CARD  1  OF CARD SET 2-W     XPL=    54.000  YP=     0.000  XPT=   103.000  TWIST=   0.000  AKODE=  1

INPUT CARD  2  OF CARD SET 2-W     XPL=    54.000  YP=     5.500  XPT=   103.000  TWIST=   0.000  AKODE=  0

INPUT CARD  3  OF CARD SET 2-W     XPL=    57.000  YP=    12.000  XPT=    80.000  TWIST=   0.000  AKODE=  0

INPUT CARD  4  OF CARD SET 2-W     XPL=    58.000  YP=    14.000  XPT=    78.000  TWIST=   0.000  AKODE=  0

INPUT CARD  5  OF CARD SET 2-W     XPL=    38.000  YP=    36.000  XPT=    48.000  TWIST=   0.000  AKODE=  0

INPUT CARD 1-B      BKOD= -3  BNOSE=     0.000  BTAIL=    126.000  BNIN=  0  RADIUS=    0.000  ANOSB=  0
```

Figure 18. Analysis code data read echo.

CRUDE GRID

64 X GRID POINTS 26 Y GRID POINTS 31 Z GRID POINTS

	COMPUTATIONAL DOMAIN	PHYSICAL DOMAIN
GRID POINT	XI	X
1	-2.55471	UPSTREAM INFINITY
2	-2.47361	-257.13690
3	-2.39251	-181.15935
4	-2.31140	-133.83617
5	-2.23030	-105.09423
6	-2.14920	-87.00033
7	-2.06810	-74.59696
8	-1.98700	-65.35651
9	-1.90589	-58.13740
10	-1.82479	-52.39827
11	-1.74369	-47.82269
12	-1.66259	-44.18596
13	-1.58149	-41.31113
14	-1.50038	-39.05155
15	-1.41928	-37.28227
16	-1.33818	-35.89526
17	-1.25708	-34.79652
18	-1.17598	-33.90411
19	-1.09488	-33.14677
20	-1.01377	-32.46290
21	-0.93267	-31.79964
22	-0.85157	-31.11221
23	-0.77047	-30.36320
24	-0.68937	-29.52205
25	-0.60826	-28.56450
26	-0.52716	-27.47203
27	-0.44606	-26.23143
28	-0.36496	-24.83427
29	-0.28386	-23.27646
30	-0.20275	-21.55779
31	-0.12165	-19.68146
32	-0.04055	-17.65365
33	0.04055	-15.48305
34	0.12165	-13.18041
35	0.20275	-10.75813
36	0.28386	-8.22978
37	0.36496	-5.60966
38	0.44606	-2.91234
39	0.52716	-0.15223
40	0.60826	2.65690
41	0.68937	5.50238
42	0.77047	8.37314
43	0.85157	11.26016
44	0.93267	14.15702
45	1.01377	17.06042
46	1.09488	19.97078
47	1.17598	22.89287
48	1.25708	25.83654
49	1.33818	28.81754
50	1.41928	31.85864
51	1.50038	34.99098
52	1.58149	38.25600

Figure 19. Crude grid generation output (sheet 1 of 3).

53	1.66259	41.70839
54	1.74369	45.42085
55	1.82479	49.49263
56	1.90589	54.06708
57	1.98700	59.37556
58	2.06810	65.87067
59	2.14920	74.60155
60	2.23030	87.99974
61	2.31140	110.92332
62	2.39251	151.20338
63	2.47361	218.80936
64	2.55471	DOWNSTREAM INFINITY

Y GRID POINT	ETA	Y
1	0.00000	0.00000
2	0.04000	1.57476
3	0.08000	3.15656
4	0.12000	4.75254
5	0.16000	6.37005
6	0.20000	8.01678
7	0.24000	9.70088
8	0.28000	11.43115
9	0.32000	13.21718
10	0.36000	15.06968
11	0.40000	17.00074
12	0.44000	19.02429
13	0.48000	21.15668
14	0.52000	23.41745
15	0.56000	25.83057
16	0.60000	28.42606
17	0.64000	31.24265
18	0.68000	34.33190
19	0.72000	37.76511
20	0.76000	41.64561
21	0.80000	46.13233
22	0.84000	51.49001
23	0.88000	58.21300
24	0.92000	67.40845
25	0.96000	82.60454
26	1.00000	+ Y INFINITY

Z GRID POINT	ZETA	Z
1	-1.00000	-702.57039
2	-0.93333	-270.37288
3	-0.86667	-135.11210
4	-0.80000	-73.88891
5	-0.73333	-42.04400
6	-0.66667	-24.60838
7	-0.60000	-15.07436
8	-0.53333	-10.07788
9	-0.46667	-7.61124
10	-0.40000	-6.28571
11	-0.33333	-5.14286
12	-0.26667	-4.00000
13	-0.20000	-2.85714
14	-0.13333	-1.71429
15	-0.06667	-0.57143
16	0.00000	0.57143
17	0.06667	1.71429
18	0.13333	2.85714
19	0.20000	4.00000

Figure 19. Crude grid generation output (sheet 2 of 3).

20	0.26667	5.14286
21	0.33333	6.28571
22	0.40000	7.54570
23	0.46667	9.53220
24	0.53333	13.09980
25	0.60000	19.41047
26	0.66667	30.25351
27	0.73333	48.72232
28	0.80000	80.88514
29	0.86667	140.77957
30	0.93333	270.37288
31	1.00000	679.25954

Figure 19. Crude grid generation output (sheet 3 of 3).

PHYSICAL DOMAIN - X GRID POINTS

SPAN STATION	4	Y= 4.753							
-29.63633	-28.96046	-28.28460	-27.60874	-26.93288	-26.25701	-25.58115	-24.90529	-24.22943	-23.55357
-22.87770	-22.20184	-21.52598	-20.85012	-20.17426	-19.49839	-18.82253	-18.14667	-17.47081	-16.79495
-16.11908	-15.44322	-14.76736	-14.09150	-13.41564	-12.73977	-12.06391	-11.38805	-10.71219	-10.03633
-9.36046	-8.68460	-8.00874	-7.33288	-6.65701	-5.98115	-5.30529	-4.62943	-3.95357	-3.27770
-2.60184	-1.92598	-1.25012	-0.57426	0.10161	0.77747	1.45333	2.12919	2.80505	3.48092
4.15678	4.83264	5.50850	6.18436	6.86023	7.53609	8.21195	8.88781	9.56367	10.23954
10.91540	11.59126	12.26712	12.94299	13.61885	14.29471	14.97057	15.64643	16.32230	16.99816
17.67402	18.34988	19.02574	19.70161	20.37747	21.05333	21.72919	22.40505	23.08092	23.75678
24.43264	25.10850	25.78436	26.46023	27.13609	27.81195	28.48781	29.16367	29.83954	30.51540
31.19126	31.86712	32.54299	33.21885	33.89471	34.57057	35.24643	35.92230	36.59816	37.27402
37.94988	38.62574	39.30161	39.97747	40.65333	41.32919	42.00505	42.68092	43.35678	44.03264
44.70850	45.38436	46.06023	46.73609	47.41195	48.08781	48.76367	49.43954	50.11540	50.79126
51.46712	52.14299	52.81885	53.49471	54.17057	54.84643	55.52230	56.19816	56.87402	57.54988
58.22574	58.90161	59.57747							

SPAN STATION	5	Y= 6.370							
-27.96269	-27.33483	-26.70697	-26.07912	-25.45126	-24.82340	-24.19554	-23.56768	-22.93982	-22.31196
-21.68410	-21.05624	-20.42838	-19.80052	-19.17266	-18.54480	-17.91694	-17.28908	-16.66122	-16.03337
-15.40551	-14.77765	-14.14979	-13.52193	-12.89407	-12.26621	-11.63835	-11.01049	-10.38263	-9.75477
-9.12691	-8.49905	-7.87119	-7.24333	-6.61547	-5.98761	-5.35976	-4.73190	-4.10404	-3.47618
-2.84832	-2.22046	-1.59260	-0.96474	-0.33688	0.29098	0.91884	1.54670	2.17456	2.80242
3.43028	4.05814	4.68599	5.31385	5.94171	6.56957	7.19743	7.82529	8.45315	9.08101
9.70887	10.33673	10.96459	11.59245	12.22031	12.84817	13.47603	14.10389	14.73175	15.35960
15.98746	16.61532	17.24318	17.87104	18.49890	19.12676	19.75462	20.38248	21.01034	21.63820
22.26606	22.89392	23.52178	24.14964	24.77750	25.40535	26.03321	26.66107	27.28893	27.91679
28.54465	29.17251	29.80037	30.42823	31.05609	31.68395	32.31181	32.93967	33.56753	34.19539
34.82325	35.45111	36.07896	36.70682	37.33468	37.96254	38.59040	39.21826	39.84612	40.47398
41.10184	41.72970	42.35756	42.98542	43.61328	44.24114	44.86900	45.49686	46.12471	46.75257
47.38043	48.00829	48.63615	49.26401	49.89187	50.51973	51.14759	51.77545	52.40331	53.03117
53.65903	54.28689	54.91475							

SPAN STATION	6	Y= 8.017							
-24.79503	-24.25802	-23.72102	-23.18401	-22.64701	-22.11000	-21.57300	-21.03599	-20.49899	-19.96198
-19.42498	-18.88797	-18.35097	-17.81396	-17.27696	-16.73995	-16.20295	-15.66594	-15.12893	-14.59193
-14.05492	-13.51792	-12.98091	-12.44391	-11.90690	-11.36990	-10.83289	-10.29589	-9.75888	-9.22188
-8.68487	-8.14787	-7.61086	-7.07386	-6.53685	-5.99985	-5.46284	-4.92583	-4.38883	-3.85182
-3.31482	-2.77781	-2.24081	-1.70380	-1.16680	-0.62979	-0.09279	0.44422	0.98122	1.51823
2.05523	2.59224	3.12924	3.66625	4.20326	4.74026	5.27727	5.81427	6.35128	6.88828
7.42529	7.96229	8.49930	9.03630	9.57331	10.11031	10.64732	11.18432	11.72133	12.25833
12.79534	13.33234	13.86935	14.40636	14.94336	15.48037	16.01737	16.55438	17.09138	17.62839
18.16539	18.70240	19.23940	19.77641	20.31341	20.85042	21.38742	21.92443	22.46143	22.99844
23.53545	24.07245	24.60946	25.14646	25.68347	26.22047	26.75748	27.29448	27.83149	28.36849
28.90550	29.44250	29.97951	30.51651	31.05352	31.59052	32.12753	32.66453	33.20154	33.73855
34.27555	34.81256	35.34956	35.88657	36.42357	36.96058	37.49758	38.03459	38.57159	39.10860
39.64560	40.18261	40.71961	41.25662	41.79362	42.33063	42.86764	43.40464	43.94165	44.47865
45.01566	45.55266	46.08967							

a) Aft surface (wing).

Figure 20. Excerpt of fine grid generation output (sheet 1 of 2).

SPAN STATION 4 Y= 4.753

-44.57426	-44.35357	-44.13288	-43.91219	-43.69150	-43.47081	-43.25012	-43.02943	-42.80874	-42.58805
-42.36736	-42.14667	-41.92598	-41.70529	-41.48460	-41.26391	-41.04322	-40.82253	-40.60184	-40.38115
-40.16046	-39.93977	-39.71908	-39.49839	-39.27770	-39.05701	-38.83633	-38.61564	-38.39495	-38.17426
-37.95357	-37.73288	-37.51219	-37.29150	-37.07081	-36.85012	-36.62943	-36.40874	-36.18805	-35.96736
-35.74667	-35.52598	-35.30529	-35.08460	-34.86391	-34.64322	-34.42253	-34.20184	-33.98115	-33.76046
-33.53977	-33.31908	-33.09839	-32.87770	-32.65701	-32.43633	-32.21564	-31.99495	-31.77426	-31.55357
-31.33288	-31.11219	-30.89150	-30.67081	-30.45012	-30.22943	-30.00874	-29.78805	-29.56736	-29.34667
-29.12598	-28.90529	-28.68460	-28.46391	-28.24322	-28.02253	-27.80184	-27.58115	-27.36046	-27.13977
-26.91908	-26.69839	-26.47770	-26.25701	-26.03633	-25.81564	-25.59495	-25.37426	-25.15357	-24.93288
-24.71219	-24.49150	-24.27081	-24.05012	-23.82943	-23.60874	-23.38805	-23.16736	-22.94667	-22.72598
-22.50529	-22.28460	-22.06391	-21.84322	-21.62253	-21.40184	-21.18115	-20.96046	-20.73977	-20.51908
-20.29839	-20.07770	-19.85701	-19.63633	-19.41564	-19.19495	-18.97426	-18.75357	-18.53288	-18.31219
-18.09150	-17.87081	-17.65012	-17.42943	-17.20874	-16.98805	-16.76736	-16.54667	-16.32598	-16.10529
-15.88460	-15.66391	-15.44322							

SPAN STATION 5 Y= 6.370

-43.87678	-43.66665	-43.45652	-43.24639	-43.03626	-42.82613	-42.61600	-42.40587	-42.19574	-41.98562
-41.77549	-41.56536	-41.35523	-41.14510	-40.93497	-40.72484	-40.51471	-40.30458	-40.09445	-39.88433
-39.67420	-39.46407	-39.25394	-39.04381	-38.83368	-38.62355	-38.41342	-38.20329	-37.99316	-37.78303
-37.57291	-37.36278	-37.15265	-36.94252	-36.73239	-36.52226	-36.31213	-36.10200	-35.89187	-35.68174
-35.47161	-35.26149	-35.05136	-34.84123	-34.63110	-34.42097	-34.21084	-34.00071	-33.79058	-33.58045
-33.37032	-33.16020	-32.95007	-32.73994	-32.52981	-32.31968	-32.10955	-31.89942	-31.68929	-31.47916
-31.26903	-31.05890	-30.84878	-30.63865	-30.42852	-30.21839	-30.00826	-29.79813	-29.58800	-29.37787
-29.16774	-28.95761	-28.74748	-28.53736	-28.32723	-28.11710	-27.90697	-27.69684	-27.48671	-27.27658
-27.06645	-26.85632	-26.64619	-26.43606	-26.22594	-26.01581	-25.80568	-25.59555	-25.38542	-25.17529
-24.96516	-24.75503	-24.54490	-24.33477	-24.12465	-23.91452	-23.70439	-23.49426	-23.28413	-23.07400
-22.86387	-22.65374	-22.44361	-22.23348	-22.02335	-21.81323	-21.60310	-21.39297	-21.18284	-20.97271
-20.76258	-20.55245	-20.34232	-20.13219	-19.92206	-19.71193	-19.50181	-19.29168	-19.08155	-18.87142
-18.66129	-18.45116	-18.24103	-18.03090	-17.82077	-17.61064	-17.40052	-17.19039	-16.98026	-16.77013
-16.56000	-16.34987	-16.13974							

SPAN STATION 6 Y= 8.017

-42.55667	-42.36653	-42.17638	-41.98624	-41.79610	-41.60596	-41.41582	-41.22568	-41.03554	-40.84540
-40.65526	-40.46511	-40.27497	-40.08483	-39.89469	-39.70455	-39.51441	-39.32427	-39.13413	-38.94399
-38.75384	-38.56370	-38.37356	-38.18342	-37.99328	-37.80314	-37.61300	-37.42286	-37.23271	-37.04257
-36.85243	-36.66229	-36.47215	-36.28201	-36.09187	-35.90173	-35.71159	-35.52144	-35.33130	-35.14116
-34.95102	-34.76088	-34.57074	-34.38060	-34.19046	-34.00031	-33.81017	-33.62003	-33.42989	-33.23975
-33.04961	-32.85947	-32.66933	-32.47919	-32.28904	-32.09890	-31.90876	-31.71862	-31.52848	-31.33834
-31.14820	-30.95806	-30.76792	-30.57777	-30.38763	-30.19749	-30.00735	-29.81721	-29.62707	-29.43693
-29.24679	-29.05664	-28.86650	-28.67636	-28.48622	-28.29608	-28.10594	-27.91580	-27.72566	-27.53552
-27.34537	-27.15523	-26.96509	-26.77495	-26.58481	-26.39467	-26.20453	-26.01439	-25.82424	-25.63410
-25.44396	-25.25382	-25.06368	-24.87354	-24.68340	-24.49326	-24.30312	-24.11297	-23.92283	-23.73269
-23.54255	-23.35241	-23.16227	-22.97213	-22.78199	-22.59185	-22.40170	-22.21156	-22.02142	-21.83128
-21.64114	-21.45100	-21.26086	-21.07072	-20.88057	-20.69043	-20.50029	-20.31015	-20.12001	-19.92987
-19.73973	-19.54959	-19.35945	-19.16930	-18.97916	-18.78902	-18.59888	-18.40874	-18.21860	-18.02846
-17.83832	-17.64818	-17.45803							

b) Forward surface (canard).

Figure 20. Excerpt of fine grid generation output (sheet 2 of 2).

AD-A171 075 CANARD/TAIL TRANSONIC ANALYSIS(U) GRUMMAN AEROSPACE CORP BETHPAGE NY P AIDALA OCT 85 AFWAL-TR-85-3087 F33615-81-C-3013 2/2

UNCLASSIFIED F/G 20/4 NL

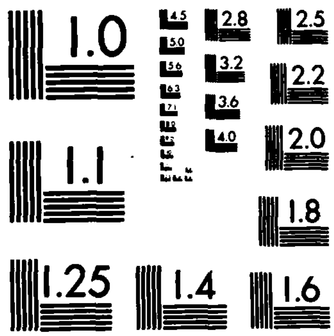

MICROCOPY RESOLUTION TEST CHART
NATIONAL BUREAU OF STANDARDS-1963-A

```
CRUDE ITER NO.  1   DELTA PHI MAX =  -8.534E-02   I =  29   J =  17   K = -12   NSP =   0   W = 1.60

CIRCULATION
LOWER   0.000E+00   0.000E+00   0.000E+00   0.000E+00   5.043E-01   4.976E-01   5.144E-01   5.949E-01   6.231E-01   6.570E-01
LOWER   6.993E-01   7.432E-01   8.125E-01   8.550E-01   8.935E-01   8.642E-01   9.913E-01   8.889E-01
UPPER   0.000E+00   0.000E+00   0.000E+00   6.421E-18   4.620E-01   5.530E-01   4.468E-01   5.108E-01   4.213E-01   4.303E-01
UPPER   3.268E-01

CRUDE ITER NO.  2   DELTA PHI MAX =   4.846E-02   I =  36   J =  17   K =  12   NSP =   0   W = 1.60

CIRCULATION
LOWER   0.000E+00   0.000E+00   0.000E+00   3.748E-02   1.373E+00   1.487E+00   1.549E+00   1.672E+00   1.736E+00   1.800E+00
LOWER   1.858E+00   1.893E+00   1.917E+00   1.863E+00   1.788E+00   1.728E+00   1.343E+00   9.638E-01
UPPER   0.000E+00   0.000E+00   0.000E+00   5.773E-01   7.969E-01   6.958E-01   6.954E-01   5.855E-01   5.710E-01   4.687E-01
UPPER   3.617E-01

CRUDE ITER NO.  3   DELTA PHI MAX =   3.523E-02   I =  44   J =  10   K =  12   NSP =   0   W = 1.60

CIRCULATION
LOWER   0.000E+00   0.000E+00   0.000E+00   8.815E-01   2.161E+00   2.310E+00   2.428E+00   2.465E+00   2.494E+00   2.507E+00
LOWER   2.494E+00   2.445E+00   2.374E+00   2.253E+00   2.095E+00   1.840E+00   1.679E+00   1.344E+00
UPPER   0.000E+00   0.000E+00   0.000E+00   7.938E-01   9.422E-01   1.004E+00   8.723E-01   8.781E-01   7.380E-01   6.870E-01
UPPER   4.684E-01

CRUDE ITER NO.  4   DELTA PHI MAX =  -2.339E-02   I =  64   J =   7   K = -12   NSP =   6   W = 1.60

CIRCULATION
LOWER   0.000E+00   0.000E+00   0.000E+00   1.786E+00   2.629E+00   2.754E+00   2.821E+00   2.842E+00   2.813E+00   2.796E+00
LOWER   2.773E+00   2.732E+00   2.694E+00   2.584E+00   2.443E+00   2.293E+00   1.814E+00   1.252E+00
UPPER   0.000E+00   0.000E+00   0.000E+00   9.987E-01   1.151E+00   1.068E+00   1.076E+00   9.269E-01   8.766E-01   7.029E-01
UPPER   5.326E-01

CRUDE ITER NO.  5   DELTA PHI MAX =  -1.396E-02   I =  64   J =   8   K =   9   NSP =   7   W = 1.60

CIRCULATION
LOWER   0.000E+00   0.000E+00   0.000E+00   2.411E+00   2.868E+00   2.944E+00   2.993E+00   3.026E+00   3.043E+00   3.042E+00
LOWER   3.037E+00   3.000E+00   2.923E+00   2.771E+00   2.560E+00   2.240E+00   1.892E+00   1.479E+00
UPPER   0.000E+00   0.000E+00   0.000E+00   1.163E+00   1.253E+00   1.233E+00   1.134E+00   1.088E+00   9.447E-01   8.190E-01
UPPER   5.644E-01

CRUDE ITER NO.  6   DELTA PHI MAX =   1.389E-02   I =  49   J =   8   K =  19   NSP =  15   W = 1.60

CIRCULATION
LOWER   0.000E+00   0.000E+00   0.000E+00   2.757E+00   3.030E+00   3.096E+00   3.150E+00   3.204E+00   3.230E+00   3.238E+00
LOWER   3.197E+00   3.112E+00   3.016E+00   2.842E+00   2.670E+00   2.475E+00   1.988E+00   1.397E+00
UPPER   0.000E+00   0.000E+00   0.000E+00   1.290E+00   1.380E+00   1.320E+00   1.283E+00   1.163E+00   1.056E+00   8.663E-01
UPPER   6.199E-01

CRUDE ITER NO.  7   DELTA PHI MAX =   1.191E-02   I =  64   J =   9   K =  19   NSP =  21   W = 1.60

CIRCULATION
LOWER   0.000E+00   0.000E+00   0.000E+00   2.950E+00   3.187E+00   3.251E+00   3.303E+00   3.337E+00   3.353E+00   3.345E+00
LOWER   3.316E+00   3.248E+00   3.149E+00   2.980E+00   2.739E+00   2.426E+00   2.011E+00   1.532E+00
UPPER   0.000E+00   0.000E+00   0.000E+00   1.407E+00   1.478E+00   1.419E+00   1.342E+00   1.235E+00   1.114E+00   9.267E-01
UPPER   6.479E-01
```

Figure 21. Flow solution convergence output (sheet 1 of 3).

```
CRUDE ITER NO.   8   DELTA PHI MAX =   8.737E-03   I =  35   J =  18   K =  12   NSP =   34   W = 1.60

CIRCULATION
LOWER    0.000E+00   0.000E+00   0.000E+00   3.099E+00   3.346E+00   3.398E+00   3.434E+00   3.461E+00   3.479E+00   3.477E+00
LOWER    3.456E+00   3.372E+00   3.249E+00   3.025E+00   2.794E+00   2.543E+00   2.055E+00   1.479E+00
UPPER    0.000E+00   0.000E+00   0.000E+00   1.509E+00   1.569E+00   1.505E+00   1.438E+00   1.322E+00   1.178E+00   9.816E-01
UPPER    6.833E-01

     CANARD WAKE UPDATE TO I= 27  X(I)= -26.231

     WING WAKE UPDATE TO I= 34  X(I)= -13.180

CRUDE ITER NO.   9   DELTA PHI MAX =   8.518E-03   I =  47   J =   9   K =  19   NSP =   47   W = 1.60

CIRCULATION
LOWER    0.000E+00   0.000E+00   0.000E+00   3.260E+00   3.489E+00   3.531E+00   3.562E+00   3.585E+00   3.596E+00   3.588E+00
LOWER    3.540E+00   3.457E+00   3.326E+00   3.128E+00   2.862E+00   2.524E+00   2.070E+00   1.555E+00
UPPER    0.000E+00   0.000E+00   0.000E+00   1.602E+00   1.657E+00   1.580E+00   1.504E+00   1.371E+00   1.242E+00   1.025E+00
UPPER    7.170E-01

   FINE ITER  10      AA = 49.157      AASCAL =  1.000      W =  0.800
CCMAX=-3.671E-03 I= 132 J=  4 K=  8 RSAV= 9.794E-05 RSD=-8.920E+00 I=  28 J= 18 K= -8 RESDAV= 5.020E-02 NSP=  178
   CRUDE ITER NO.  10   DELTA PHI MAX =  -6.842E-03   I =  64   J =   1   K =   9   NSP =   56   W = 1.60

CIRCULATION
LOWER    0.000E+00   0.000E+00   0.000E+00   3.238E+00   3.439E+00   3.490E+00   3.516E+00   3.551E+00   3.604E+00   3.550E+00
LOWER    3.530E+00   3.434E+00   3.292E+00   3.092E+00   2.882E+00   2.578E+00   2.059E+00   1.573E+00
UPPER    0.000E+00   0.000E+00   0.000E+00   1.633E+00   1.672E+00   1.592E+00   1.526E+00   1.393E+00   1.254E+00   1.025E+00
UPPER    7.281E-01

   FINE ITER  11      AA = 47.621      AASCAL =  1.000      W =  0.800
CCMAX=-3.893E-03 I= 132 J=  4 K=  2 RSAV= 1.739E-04 RSD= 6.294E+01 I=  28 J= 17 K= -8 RESDAV= 6.168E-02 NSP=  183
   CRUDE ITER NO.  11   DELTA PHI MAX =  -6.109E-03   I =  64   J =   1   K =   9   NSP =   61   W = 1.60

CIRCULATION
LOWER    0.000E+00   0.000E+00   0.000E+00   3.252E+00   3.419E+00   3.490E+00   3.512E+00   3.541E+00   3.609E+00   3.529E+00
LOWER    3.533E+00   3.426E+00   3.275E+00   3.073E+00   2.859E+00   2.565E+00   2.025E+00   1.579E+00
UPPER    0.000E+00   0.000E+00   0.000E+00   1.639E+00   1.667E+00   1.580E+00   1.524E+00   1.398E+00   1.246E+00   1.017E+00
UPPER    7.210E-01

   FINE ITER  12      AA = 44.549      AASCAL =  1.000      W =  0.800
CCMAX=-4.293E-03 I= 132 J=  4 K=  2 RSAV= 2.228E-04 RSD= 6.323E+01 I=  28 J= 17 K= -8 RESDAV= 6.261E-02 NSP=  182
   CRUDE ITER NO.  12   DELTA PHI MAX =  -5.475E-03   I =  64   J =   1   K =   9   NSP =   67   W = 1.60

CIRCULATION
LOWER    0.000E+00   0.000E+00   0.000E+00   3.271E+00   3.406E+00   3.488E+00   3.511E+00   3.537E+00   3.610E+00   3.520E+00
LOWER    3.533E+00   3.423E+00   3.266E+00   3.057E+00   2.847E+00   2.559E+00   2.005E+00   1.579E+00
UPPER    0.000E+00   0.000E+00   0.000E+00   1.645E+00   1.663E+00   1.573E+00   1.524E+00   1.400E+00   1.240E+00   1.012E+00
UPPER    7.176E-01

   FINE ITER  13      AA = 39.940      AASCAL =  1.000      W =  0.800
CCMAX=-4.163E-03 I= 131 J=  4 K=  2 RSAV= 2.715E-04 RSD= 5.343E+01 I=  28 J= 17 K= -8 RESDAV= 6.345E-02 NSP=  184
   CRUDE ITER NO.  13   DELTA PHI MAX =  -5.019E-03   I =  64   J =   1   K =   9   NSP =   72   W = 1.60

CIRCULATION
LOWER    0.000E+00   0.000E+00   0.000E+00   3.298E+00   3.399E+00   3.486E+00   3.511E+00   3.536E+00   3.608E+00   3.518E+00
LOWER    3.533E+00   3.421E+00   3.262E+00   3.049E+00   2.840E+00   2.555E+00   1.996E+00   1.577E+00
UPPER    0.000E+00   0.000E+00   0.000E+00   1.654E+00   1.661E+00   1.569E+00   1.523E+00   1.402E+00   1.238E+00   1.009E+00
UPPER    7.169E-01
```

Figure 21. Flow solution convergence output (sheet 2 of 3).

```
   FINE ITER  14      AA = 33.796     AASCAL =  1.000     W =  0.800
CCMAX=-4.288E-03 I=  43 J=  4 K=  2 RSAV= 3.278E-04 RSD= 4.325E+01 I=  28 J= 17 K= -8 RESDAV= 6.276E-02 NSP=  197
   CRUDE ITER NO.  14    DELTA PHI MAX =  -4.526E-03    I =  64    J =   1    K =   9    NSP =   74   W = 1.60

   CIRCULATION
   LOWER   0.000E+00  0.000E+00  0.000E+00  3.339E+00  3.404E+00  3.488E+00  3.515E+00  3.540E+00  3.606E+00  3.522E+00
   LOWER   3.533E+00  3.422E+00  3.261E+00  3.044E+00  2.835E+00  2.551E+00  1.993E+00  1.575E+00
   UPPER   0.000E+00  0.000E+00  0.000E+00  1.663E+00  1.659E+00  1.567E+00  1.523E+00  1.403E+00  1.236E+00  1.008E+00
   UPPER   7.181E-01

   FINE ITER  15      AA = 26.115     AASCAL =  1.000     W =  0.800
CCMAX=-4.674E-03 I=  39 J=  4 K=  2 RSAV= 4.191E-04 RSD= 3.326E+01 I=  28 J= 17 K= -8 RESDAV= 6.181E-02 NSP=  212
   CRUDE ITER NO.  15    DELTA PHI MAX =   4.212E-03    I =  48    J =   1    K =  22    NSP =   78   W = 1.60

   CIRCULATION
   LOWER   0.000E+00  0.000E+00  0.000E+00  3.400E+00  3.428E+00  3.498E+00  3.525E+00  3.549E+00  3.603E+00  3.526E+00
   LOWER   3.534E+00  3.426E+00  3.263E+00  3.042E+00  2.832E+00  2.548E+00  1.993E+00  1.571E+00
   UPPER   0.000E+00  0.000E+00  0.000E+00  1.672E+00  1.659E+00  1.568E+00  1.524E+00  1.404E+00  1.236E+00  1.007E+00
   UPPER   7.204E-01

   FINE ITER  16      AA = 16.898     AASCAL =  1.000     W =  0.800
CCMAX=-6.099E-03 I=  94 J=  4 K=  7 RSAV= 6.017E-04 RSD= 2.363E+01 I=  28 J= 17 K= -8 RESDAV= 5.968E-02 NSP=  224
   CRUDE ITER NO.  16    DELTA PHI MAX =   3.945E-03    I =  48    J =   1    K =  22    NSP =   87   W = 1.60

   CIRCULATION
   LOWER   0.000E+00  0.000E+00  0.000E+00  3.488E+00  3.480E+00  3.521E+00  3.545E+00  3.569E+00  3.603E+00  3.545E+00
   LOWER   3.536E+00  3.435E+00  3.272E+00  3.045E+00  2.832E+00  2.546E+00  1.997E+00  1.566E+00
   UPPER   0.000E+00  0.000E+00  0.000E+00  1.678E+00  1.660E+00  1.572E+00  1.526E+00  1.406E+00  1.238E+00  1.006E+00
   UPPER   7.235E-01

       CANARD WAKE UPDATE TO I= 28  X(I)= -24.834

       WING WAKE UPDATE TO I= 35  X(I)= -10.758

   FINE ITER  17      AA =  6.119     AASCAL =  1.000     W =  0.800
CCMAX=-1.142E-02 I=  93 J=  4 K=  7 RSAV= 1.271E-03 RSD= 1.430E+01 I=  28 J= 17 K= -8 RESDAV= 6.471E-02 NSP=  232
   CRUDE ITER NO.  17    DELTA PHI MAX =  -7.995E-03    I =  50    J =   6    K = -12    NSP =   89   W = 1.60

   CIRCULATION
   LOWER   0.000E+00  0.000E+00  0.000E+00  3.617E+00  3.575E+00  3.565E+00  3.582E+00  3.609E+00  3.620E+00  3.609E+00
   LOWER   3.554E+00  3.472E+00  3.312E+00  3.075E+00  2.849E+00  2.552E+00  2.020E+00  1.553E+00
   UPPER   0.000E+00  0.000E+00  0.000E+00  1.684E+00  1.671E+00  1.598E+00  1.543E+00  1.416E+00  1.252E+00  1.015E+00
   UPPER   7.334E-01

   FINE ITER  18      AA = 48.956     AASCAL =  1.000     W =  0.800
CCMAX=-9.482E-03 I= 132 J=  4 K=  8 RSAV= 1.804E-04 RSD= 9.019E+00 I=  28 J= 10 K= -8 RESDAV= 4.788E-02 NSP=  232
   CRUDE ITER NO.  18    DELTA PHI MAX =  -5.437E-03    I =  50    J =   6    K =  12    NSP =   97   W = 1.60

   CIRCULATION
   LOWER   0.000E+00  0.000E+00  0.000E+00  3.628E+00  3.597E+00  3.583E+00  3.597E+00  3.620E+00  3.625E+00  3.618E+00
   LOWER   3.557E+00  3.477E+00  3.317E+00  3.082E+00  2.853E+00  2.553E+00  2.025E+00  1.550E+00
   UPPER   0.000E+00  0.000E+00  0.000E+00  1.685E+00  1.673E+00  1.602E+00  1.545E+00  1.417E+00  1.254E+00  1.017E+00
   UPPER   7.347E-01
```

Figure 21. Flow solution convergence output (sheet 3 of 3).

PRESSURE COEFFICIENTS (CP)

STATION 11 J= 11 2Y/B= 0.472 Y= 17.001 LOCAL CHORD= 18.636 CL (CIRCULATION) = 0.382

		UPPER SURFACE							LOWER SURFACE						
I	XWF	X/C	Y/C	CP	MACH	U	V	W	X/C	Y/C	CP	MACH	U	V	W
28	-10.33	0.690	1.182	-0.098	0.738	0.038	0.147	0.680	0.690	-1.182	0.525	0.486	-0.994	-0.711	-1.228
29	-10.07	2.069	2.001	-0.468	0.878	0.190	0.284	0.304	2.069	-2.001	0.756	0.374	-0.722	-0.471	-0.683
30	-9.81	3.448	2.516	-0.607	0.932	0.246	0.326	0.191	3.448	-2.516	0.745	0.380	-0.626	-0.418	-0.542
31	-9.55	4.828	2.918	-0.685	0.963	0.278	0.345	0.124	4.828	-2.918	0.719	0.394	-0.573	-0.393	-0.462
32	-9.30	6.207	3.244	-0.736	0.983	0.300	0.354	0.075	6.207	-3.244	0.693	0.407	-0.537	-0.380	-0.407
33	-9.04	7.586	3.516	-0.769	0.996	0.315	0.356	0.040	7.586	-3.516	0.668	0.419	-0.500	-0.361	-0.367
34	-8.78	8.966	3.748	-0.790	1.005	0.326	0.352	0.013	8.966	-3.748	0.629	0.438	-0.438	-0.313	-0.338
35	-8.53	10.345	3.950	-0.784	1.002	0.327	0.335	-0.009	10.345	-3.950	0.536	0.481	-0.330	-0.217	-0.314
36	-8.27	11.724	4.125	-0.716	0.975	0.305	0.293	-0.028	11.724	-4.125	0.355	0.559	-0.193	-0.092	-0.294
37	-8.01	13.103	4.278	-0.659	0.952	0.287	0.253	-0.045	13.103	-4.278	0.210	0.618	-0.109	-0.018	-0.275
38	-7.75	14.483	4.410	-0.671	0.957	0.295	0.238	-0.060	14.483	-4.410	0.171	0.633	-0.088	-0.007	-0.260
39	-7.50	15.862	4.525	-0.699	0.968	0.310	0.232	-0.072	15.862	-4.525	0.139	0.646	-0.071	0.001	-0.246
40	-7.24	17.241	4.624	-0.722	0.977	0.319	0.239	-0.084	17.241	-4.624	0.094	0.664	-0.048	0.016	-0.234
41	-6.98	18.621	4.710	-0.737	0.983	0.325	0.244	-0.095	18.621	-4.710	0.043	0.684	-0.022	0.036	-0.223
42	-6.73	20.000	4.782	-0.752	0.989	0.331	0.250	-0.105	20.000	-4.782	-0.013	0.705	0.005	0.059	-0.213
43	-6.47	21.379	4.843	-0.764	0.994	0.335	0.257	-0.114	21.379	-4.843	-0.070	0.727	0.031	0.084	-0.203
44	-6.21	22.759	4.892	-0.770	0.996	0.337	0.261	-0.122	22.759	-4.892	-0.124	0.747	0.055	0.108	-0.195
45	-5.96	24.138	4.932	-0.742	0.985	0.326	0.253	-0.130	24.138	-4.932	-0.163	0.762	0.073	0.125	-0.187
46	-5.70	25.517	4.962	-0.648	0.948	0.288	0.218	-0.136	25.517	-4.962	-0.176	0.767	0.078	0.130	-0.179
47	-5.44	26.897	4.983	-0.545	0.908	0.246	0.179	-0.145	26.897	-4.983	-0.155	0.759	0.070	0.119	-0.172
48	-5.18	28.276	4.996	-0.492	0.888	0.224	0.161	-0.151	28.276	-4.996	-0.119	0.745	0.054	0.099	-0.166
49	-4.93	29.655	5.002	-0.462	0.876	0.211	0.153	-0.157	29.655	-5.002	-0.092	0.735	0.042	0.084	-0.160
50	-4.67	31.034	5.000	-0.435	0.866	0.200	0.143	-0.163	31.034	-5.000	-0.080	0.731	0.037	0.076	-0.154
51	-4.41	32.414	4.991	-0.409	0.856	0.189	0.135	-0.168	32.414	-4.991	-0.076	0.729	0.035	0.072	-0.149
52	-4.16	33.793	4.976	-0.385	0.847	0.178	0.128	-0.173	33.793	-4.976	-0.078	0.730	0.036	0.071	-0.144
53	-3.90	35.172	4.955	-0.361	0.837	0.168	0.120	-0.178	35.172	-4.955	-0.083	0.732	0.039	0.072	-0.139
54	-3.64	36.552	4.928	-0.337	0.828	0.157	0.113	-0.183	36.552	-4.928	-0.090	0.734	0.042	0.075	-0.134
55	-3.39	37.931	4.896	-0.319	0.821	0.149	0.109	-0.187	37.931	-4.896	-0.095	0.736	0.044	0.077	-0.130
56	-3.13	39.310	4.858	-0.313	0.819	0.146	0.109	-0.191	39.310	-4.858	-0.096	0.737	0.045	0.077	-0.126
57	-2.87	40.690	4.815	-0.315	0.820	0.147	0.112	-0.195	40.690	-4.815	-0.092	0.735	0.043	0.074	-0.122
58	-2.61	42.069	4.767	-0.307	0.817	0.143	0.112	-0.199	42.069	-4.767	-0.086	0.733	0.040	0.069	-0.118
59	-2.36	43.448	4.715	-0.289	0.810	0.135	0.106	-0.203	43.448	-4.715	-0.081	0.731	0.038	0.065	-0.115
60	-2.10	44.828	4.659	-0.272	0.804	0.128	0.100	-0.206	44.828	-4.659	-0.078	0.730	0.037	0.063	-0.111
61	-1.84	46.207	4.598	-0.256	0.797	0.120	0.094	-0.210	46.207	-4.598	-0.076	0.729	0.036	0.062	-0.108
62	-1.59	47.586	4.534	-0.240	0.791	0.113	0.088	-0.213	47.586	-4.534	-0.076	0.729	0.036	0.061	-0.105
63	-1.33	48.966	4.466	-0.224	0.785	0.106	0.082	-0.216	48.966	-4.466	-0.076	0.729	0.036	0.060	-0.102
64	-1.07	50.345	4.394	-0.209	0.780	0.099	0.077	-0.219	50.345	-4.394	-0.076	0.729	0.036	0.060	-0.099
65	-0.81	51.724	4.319	-0.196	0.775	0.093	0.072	-0.221	51.724	-4.319	-0.076	0.729	0.036	0.059	-0.097
66	-0.56	53.103	4.240	-0.187	0.771	0.089	0.069	-0.224	53.103	-4.240	-0.072	0.728	0.034	0.057	-0.094
67	-0.30	54.483	4.159	-0.182	0.769	0.087	0.069	-0.226	54.483	-4.159	-0.065	0.725	0.031	0.053	-0.091
68	-0.04	55.862	4.074	-0.176	0.767	0.084	0.068	-0.229	55.862	-4.074	-0.060	0.723	0.028	0.050	-0.089
69	0.21	57.241	3.987	-0.167	0.764	0.080	0.065	-0.231	57.241	-3.987	-0.057	0.722	0.027	0.049	-0.087
70	0.47	58.621	3.896	-0.156	0.759	0.075	0.061	-0.234	58.621	-3.896	-0.057	0.722	0.027	0.048	-0.085

Figure 22. Example of fine grid solution output (sheet 1 of 2).

71	0.73	60.000	3.803	-0.145	0.755	0.070	0.056	-0.236	60.000	-3.803	-0.055	0.721	0.026	0.048	-0.082
72	0.98	61.379	3.707	-0.134	0.751	0.065	0.052	-0.238	61.379	-3.707	-0.054	0.721	0.026	0.047	-0.080
73	1.24	62.759	3.609	-0.123	0.747	0.060	0.047	-0.240	62.759	-3.609	-0.052	0.720	0.025	0.047	-0.078
74	1.50	64.138	3.508	-0.113	0.743	0.055	0.042	-0.242	64.138	-3.508	-0.050	0.719	0.024	0.046	-0.076
75	1.76	65.517	3.405	-0.103	0.739	0.050	0.038	-0.244	65.517	-3.405	-0.047	0.718	0.022	0.044	-0.074
76	2.01	66.897	3.299	-0.093	0.736	0.046	0.033	-0.246	66.897	-3.299	-0.042	0.716	0.020	0.041	-0.073
77	2.27	68.276	3.191	-0.085	0.733	0.042	0.030	-0.248	68.276	-3.191	-0.033	0.713	0.016	0.036	-0.071
78	2.53	69.655	3.081	-0.078	0.730	0.038	0.027	-0.250	69.655	-3.081	-0.022	0.708	0.010	0.030	-0.069
79	2.78	71.034	2.969	-0.071	0.727	0.035	0.024	-0.252	71.034	-2.969	-0.015	0.706	0.007	0.026	-0.067
80	3.04	72.414	2.854	-0.062	0.724	0.031	0.020	-0.253	72.414	-2.854	-0.015	0.706	0.007	0.026	-0.066
81	3.30	73.793	2.738	-0.054	0.721	0.027	0.016	-0.255	73.793	-2.738	-0.015	0.706	0.007	0.027	-0.064
82	3.56	75.172	2 619	-0.045	0.717	0.023	0.012	-0.257	75.172	-2.619	-0.014	0.705	0.007	0.027	-0.062
83	3.81	76.552	2.498	-0.037	0.714	0.018	0.008	-0.259	76.552	-2.498	-0.012	0.705	0.006	0.027	-0.061
84	4.07	77.931	2.375	-0.029	0.711	0.014	0.003	-0.260	77.931	-2.375	-0.009	0.704	0.004	0.026	-0.059
85	4.33	79.310	2.250	-0.021	0.708	0.010	-0.001	-0.262	79.310	-2.250	-0.006	0.702	0.003	0.024	-0.057
86	4.58	80.690	2.123	-0.012	0.705	0.006	-0.006	-0.264	80.690	-2.123	0.000	0.700	0.000	0.021	-0.056
87	4.84	82.069	1.994	-0.002	0.701	0.001	-0.012	-0.266	82.069	-1.994	0.010	0.696	-0.005	0.015	-0.054
88	5.10	83.448	1.862	0.010	0.696	-0.005	-0.020	-0.268	83.448	-1.862	0.027	0.690	-0.013	0.004	-0.052
89	5.35	84.828	1.728	0.023	0.691	-0.012	-0.029	-0.270	84.828	-1.728	0.045	0.683	-0.023	-0.008	-0.050
90	5.61	86.207	1.593	0.035	0.687	-0.018	-0.036	-0.271	86.207	-1.593	0.054	0.679	-0.027	-0.014	-0.049
91	5.87	87.586	1.454	0.043	0.683	-0.023	-0.042	-0.273	87.586	-1.454	0.053	0.679	-0.027	-0.013	-0.047
92	6.13	88.966	1.314	0.051	0.680	-0.027	-0.047	-0.275	88.966	-1.314	0.051	0.680	-0.026	-0.010	-0.045
93	6.38	90.345	1.171	0.058	0.678	-0.031	-0.052	-0.277	90.345	-1.171	0.051	0.680	-0.026	-0.010	-0.043
94	6.64	91.724	1.026	0.066	0.675	-0.035	-0.057	-0.279	91.724	-1.026	0.053	0.680	-0.027	-0.010	-0.041
95	6.90	93.103	0.879	0.073	0.672	-0.039	-0.062	-0.281	93.103	-0.879	0.055	0.679	-0.028	-0.011	-0.039
96	7.15	94.483	0.729	0.080	0.669	-0.043	-0.067	-0.283	94.483	-0.729	0.058	0.678	-0.029	-0.013	-0.038
97	7.41	95.862	0.577	0.087	0.666	-0.047	-0.072	-0.285	95.862	-0.577	0.060	0.677	-0.030	-0.013	-0.036
98	7.67	97.241	0.422	0.097	0.662	-0.053	-0.079	-0.287	97.241	-0.422	0.059	0.677	-0.030	-0.012	-0.034
99	7.93	98.621	0.265	0.120	0.653	-0.066	-0.096	-0.289	98.621	-0.265	0.057	0.678	-0.029	-0.010	-0.032
100	8.18	100.000	0.105	0.136	0.647	-0.076	-0.108	-0.291	100.000	-0.105	0.056	0.679	-0.028	-0.008	-0.030

LOCAL SECTION CL (CP INTEG.) = 0.33453
LOCAL SECTION CM (CP INTEG.) = 0.02176
LOCAL SECTION CD (CP INTEG.) = 0.05814

Figure 22. Example of fine grid solution output (sheet 2 of 2).

```
FORWARD SURFACE
               FORCE AND MOMENT BASED ON SEXP=    285.847

               CL            CM            CD(PRESSURE)     CD(FRICTION)

             0.21531      0.07414       0.02890           0.00000

                   CL            CM            CD              BASED ON SREF

                 0.03511      0.01293      0.00471
          PRESSURE DRAG =    0.00471

          FRICTION DRAG =    0.00000

          PITCHING MOMENT DUE TO DRAG =    0.00084

AFT SURFACE
               FORCE AND MOMENT BASED ON SEXP=  1287.256

               CL            CM            CD(PRESSURE)     CD(FRICTION)

             0.25717     -0.09062       0.03575           0.00000

                   CL            CM            CD              BASED ON SREF

                 0.18885     -0.06810      0.02626
          PRESSURE DRAG =    0.02626

          FRICTION DRAG =    0.00000

          PITCHING MOMENT DUE TO DRAG =  -0.00155

               TOTAL FORCE AND MOMENT COEFFICIENTS

                TOTAL CL     TOTAL CM     TOTAL CD

                 0.22396     -0.05517      0.03097

          TOTAL PRESSURE DRAG =    0.03097

          TOTAL FRICTION DRAG =    0.00000
```

a) Lifting surfaces.

```
           BODY LENGTH =     126.000

          BODY WETTED AREA =    5.4328E+03

          BODY PROJECTED AREA =    1.2866E+03

          BODY MAX. CROSS-SECTIONAL AREA =    9.5033E+01

          X-POSITION ABOUT WHICH MOMENTS ARE COMPUTED =     44.000


           BODY FORCE AND MOMENT COEFFICIENTS

                  BODY CL       BODY CM       BODY CD

                  0.03152     -0.00184       0.00465

               BODY PRESSURE DRAG =    0.00465

               BODY FRICTION DRAG =    0.00000
```

b) Body.

Figure 23. Force and moment output.

FORWARD SWEPT SAMPLE CASE

AMACH= 0.700 AOA= 8.000 WINSDS= 1.000 CINSDS= -2.000
AXIT= 9 AXITF= 9 VISMOD= 1

TOTAL CONFIGURATION COEFFICIENTS

CL	CM	CD
0.25548	-0.05701	0.03562

SPANWISE DISTRIBUTIONS

AFT SURFACE

	2Y/B	CLINT	CCL/CAV	CMLOC	CCM/CAV/MAC	CDINT	CCD/CAV	CFINT	CCF/CAV
1	0.00000	0.00000	0.22228	0.00000	0.00000	0.00000	0.00000	0.00000	0.00000
2	0.04374	0.00000	0.23294	0.00000	0.00000	0.00000	0.00000	0.00000	0.00000
3	0.08768	0.00000	0.24365	0.00000	0.00000	0.00000	0.00000	0.00000	0.00000
4	0.13201	0.12643	0.25445	0.01501	-0.12372	0.01124	0.02261	0.00000	0.00000
5	0.17695	0.13932	0.26047	0.01660	-0.12607	0.00826	0.01544	0.00000	0.00000
6	0.22269	0.16366	0.26171	0.02114	-0.12285	0.02472	0.03952	0.00000	0.00000
7	0.26947	0.19073	0.25222	0.02036	-0.12353	0.03184	0.04210	0.00000	0.00000
8	0.31753	0.24769	0.25713	0.02013	-0.12935	0.03050	0.03166	0.00000	0.00000
9	0.36714	0.30453	0.26484	0.03774	-0.12756	0.05086	0.04423	0.00000	0.00000
10	0.41860	0.32487	0.26037	0.02113	-0.12817	0.02822	0.02262	0.00000	0.00000
11	0.47224	0.33453	0.25606	0.02176	-0.11152	0.05814	0.04450	0.00000	0.00000
12	0.52845	0.34765	0.25296	0.00793	-0.10073	0.05676	0.04130	0.00000	0.00000
13	0.58769	0.35092	0.24137	-0.00387	-0.08474	0.05142	0.03537	0.00000	0.00000
14	0.65048	0.35021	0.22610	-0.00910	-0.06541	0.04879	0.03150	0.00000	0.00000
15	0.71752	0.34451	0.20690	-0.01513	-0.04618	0.05295	0.03180	0.00000	0.00000
16	0.78961	0.32339	0.17855	-0.01618	-0.02599	0.05323	0.02939	0.00000	0.00000
17	0.86785	0.34776	0.17372	-0.00604	-0.00810	0.01229	0.00614	0.00000	0.00000
18	0.95366	0.25441	0.11242	-0.01816	0.00341	0.07916	0.03498	0.00000	0.00000
19	1.00000	0.00000	0.00000	0.00000	0.00000	0.00000	0.00000	0.00000	0.00000

Figure 24. Spanload output (sheet 1 of 2).

FORWARD SURFACE

1	0.00000	0.00000	0.00000	0.00000	0.00000	0.00000	0.00000	0.00000	0.00000
2	0.08749	0.00000	0.00000	0.00000	0.00000	0.00000	0.00000	0.00000	0.00000
3	0.17536	0.00000	0.00000	0.00000	0.00000	0.00000	0.00000	0.00000	0.00000
4	0.26403	0.18277	0.12011	0.00244	0.04696	0.03943	0.02591	0.00000	0.00000
5	0.35389	0.18260	0.11425	-0.00158	0.04274	0.03610	0.02259	0.00000	0.00000
6	0.44538	0.20567	0.11645	-0.00413	0.04158	0.00819	0.00464	0.00000	0.00000
7	0.53894	0.22076	0.11155	-0.00355	0.03865	0.03157	0.01596	0.00000	0.00000
8	0.63506	0.23616	0.10457	0.00374	0.03598	0.04549	0.02014	0.00000	0.00000
9	0.73429	0.25094	0.09491	-0.00297	0.03057	0.02983	0.01128	0.00000	0.00000
10	0.83720	0.24699	0.07688	0.00291	0.02412	0.03293	0.01025	0.00000	0.00000
11	0.94449	0.25786	0.06227	0.00043	0.01846	0.00290	0.00070	0.00000	0.00000
12	1.00000	0.00000	0.00000	0.00000	0.00000	0.00000	0.00000	0.00000	0.00000

WAVE DRAG = 0.02819

FRICTION DRAG = 0.00000

LIFT INDUCED DRAG = 0.00742

Figure 24. Spanload output (sheet 2 of 2).

7 - CONCLUSIONS

The CANTATA code shows good performance in the major areas of its development. The embedded grid technique allows arbitrary placement, with arbitrary overlap, of two lifting surfaces. The AF2YZ algorithm provides a substantial improvement in convergence rate relative to SLOR, and can analyze highly swept, highly tapered fighter wings at lift coefficients of 1.0 at transonic speeds. The vectorization of the original scalar oriented code has resulted in an overall scalar-to-vector ratio of 2.6 on the CRAY. The free wake modeling employs a merging of vortex lines to treat wake rollup. This approach works well for potential flow solutions and is easily transferred to other applications of computational fluid dynamics. The comparison of data and analysis indicate that the free wake effects are relatively weak, but their inclusion generally improves agreement with test data. Boundary layer effects are more significant. In particular, flow separation modeling is important for fighter aircraft.

APPENDIX A
FREE WAKE CALCULATION*

Two modifications were developed for the CANTATA code to extend its capabilities to the computation of "free wake" solutions. The first modification introduces a variable grid spacing that can handle non-planar wakes. The second modification introduces an iteration scheme by which the flow computation is carried out for several iterations with a fixed non-planar wake calculated from the flowfield of the previous set of iterations. Taken together these two modifications allow the computation of free wake solutions.

A.1 DISCRETIZATION OF THE WAKE VORTEX SHEETS

Completion of the potential flow iterations yields the distribution of circulation for spanwise grid points J at the trailing edge stations of the wing and canard surfaces. For these distributions the wake is represented by discrete vortices of index L and strength Γ. The details of the discretization procedure are presented in Figure 25 for the wing wake. Computational grid points (X,Y,Z) are represented by the indices (I,J,K) while the Lth vortex line is located by the coordinates (X_I, YV_L, ZV_L), requiring only the indices (I,L). At the surface trailing edge $YV_L = Y_J$ with J = L, i.e., the vortex lines originate from the trailing edge grid points.

A.2 TRACKING OF VORTEX LINES

Vortex lines, which are everywhere tangent to the local vorticity vector are considered the generators of the wake vortex sheet. An element of a line vortex must be tangent to the vector velocity which would result in the absence of that element. In addition, a line vortex element induces zero velocity at its own center. In the limiting case of a two-dimensional continuum of line vortices, i.e., a vortex sheet, these properties require that at all

*by Prof. Jack Werner, Polytechnic Institute of New York, consultant to this study.

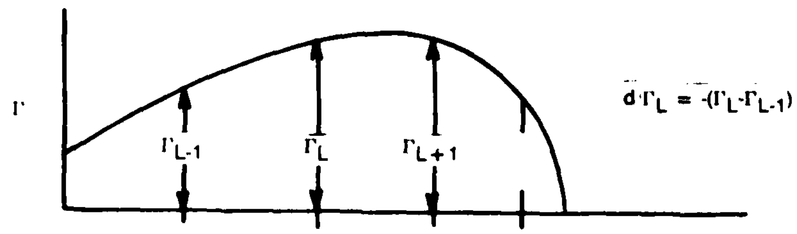

a) *Trailing edge circulation pattern*

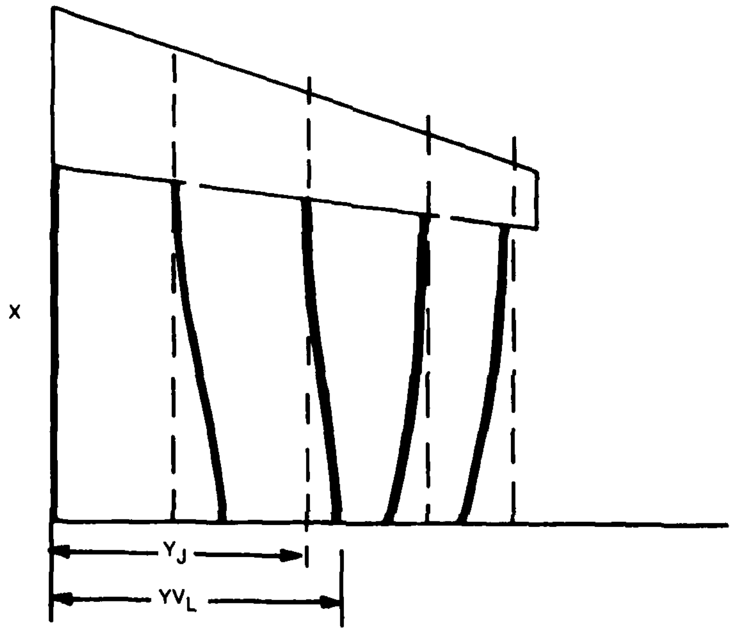

b) Trailing vortex line pattern

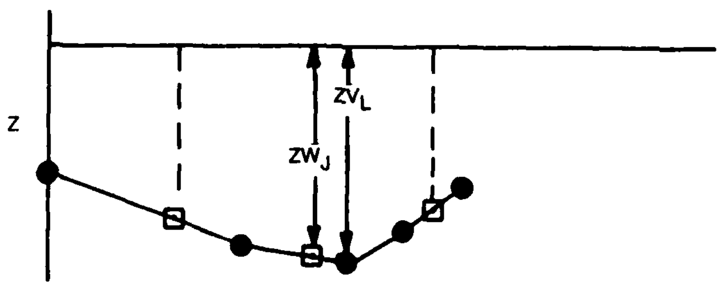

c) Wake cross-section

Figure 25. Discretization of wake vortex sheet.

points the sheet is tangent to the mean of the velocity vectors just above and below the sheet. If $\vec{dr}$ is the displacement vector of a line element corresponding to an increment dx in the downstream direction we have for displacement between stations I and I + 1

$$\vec{dr} = \vec{\vec{VV}}dX/(UV) \tag{A-1a}$$

where

$$\vec{dr} = \hat{i}(X_{I+1}-X_I) + \hat{j}(YV_{I+1,L} - YV_{I,L}) + \hat{k}(ZV_{I+1,L}-ZV_{I,L}) \tag{A-1b}$$

$$\vec{VV}=\tfrac{1}{2}(\vec{VV}_u+\vec{VV}_l)=\hat{i}UV_{I,L}+\hat{j}VV_{I,L} + \hat{k}\ WV_{I,L} \tag{A-1c}$$

$$dX = X_{I+1} - X_I \tag{A-1d}$$

and VV_u, VV_l are velocities above and below the sheet as determined from the potential solution. Thus, a given set of iterations yields values of the velocity vector at grid points just above and below the assumed wake surface. These are linearly interpolated to $YV_{I,L}$ corresponding to the vortex lines L at station I to obtain $\vec{\vec{VV}}$. The equation is then solved for $(YV_{I+1,L} - YV_{I,L})$ and $(ZV_{I+1,L} - ZV_{I,L})$ and an updated vortex line is constructed by integration of these increments.

For the case of unswept trailing edges all vortex lines from a given surface begin at the same index I so that tracking begins simultaneously (the index J is varied for a fixed station I). To consider a case with a swept trailing edge which lies between the extremes of $I = ITE_{MIN}$ and $I = ITE_{MAX}$ the velocities VV, WV are set to values which reconstruct the meanline of the surface points lying between the two indices. The tracking process then begins at $I = ITE_{MIN}$ for all J and proceeds as in the unswept trailing edge.

A.3 ITERATION PROCEDURE

For the first set of potential flow solution iterations, approximate wakes composed of straight line vortices trailing downstream from the canard and wing trailing edges are constructed using the slope at the trailing edge and a streamwise decay of the slope. Subsequently, after each set of iterations the wake shape is updated to only one more downstream station beyond the previous update, i.e., after the latest set of iterations the wake is "updat-

ed" from the trailing edge to I = IM. Beyond this point each vortex line is continued back with a slope at each downstream segment of half the slope of the previous segment. This scheme of slope decay prevents the wake geometry from diverging or becoming chaotic but does not significantly affect the solution in the upstream regions while they are iteratively building up. The above procedure is illustrated in Figure 26. Typically, a set of eight iterations is performed between each wake update.

A.4 WAKE ROLL-UP

It is well known that trailing vortex sheets eventually roll up as they proceed downstream. The procedure employed here for tracking vortex lines allows this phenomenon. As a result, two serious difficulties are encountered in the computational scheme.

First, the flow solution uses a computational space in which the non-planar vortex sheets of the canard and wing are mapped onto parallel planar surfaces. When wake roll-up occurs, the spanwise coordinate, $YV_{I,L}$, of the sheet becomes multiple valued and the mapping function breaks down. Second, the discretization of the wake may result in the interval between vortex lines becoming large compared to the spanwise radius of curvature of the wake. The "tracking" procedure then becomes invalid, producing a chaotic wake surface.

When wake roll-up occurs, the vortex sheet is replaced by one which has single valued coordinates and a vorticity distribution which approximates that of the rolled up wake. This is accomplished by monitoring the spanwise separation between vortex lines at each streamwise station I as the wake is being updated. Roll-up begins as values of $YV_{I,L}$ approach each other. Each downstream station I searches for roll-up with a "proximity test":

$$YV_{I,L+1} - YV_{I,L} \leq DYTEST \qquad \text{(A-2)}$$

where DYTEST is a set parameter (1/2 of the first spanwise grid interval).

When roll-up is detected, the two vortex lines are "merged" to a single line of strength $d\Gamma_L + d\Gamma_{L+1}$ located at the centroid of the magnitudes of their strength:

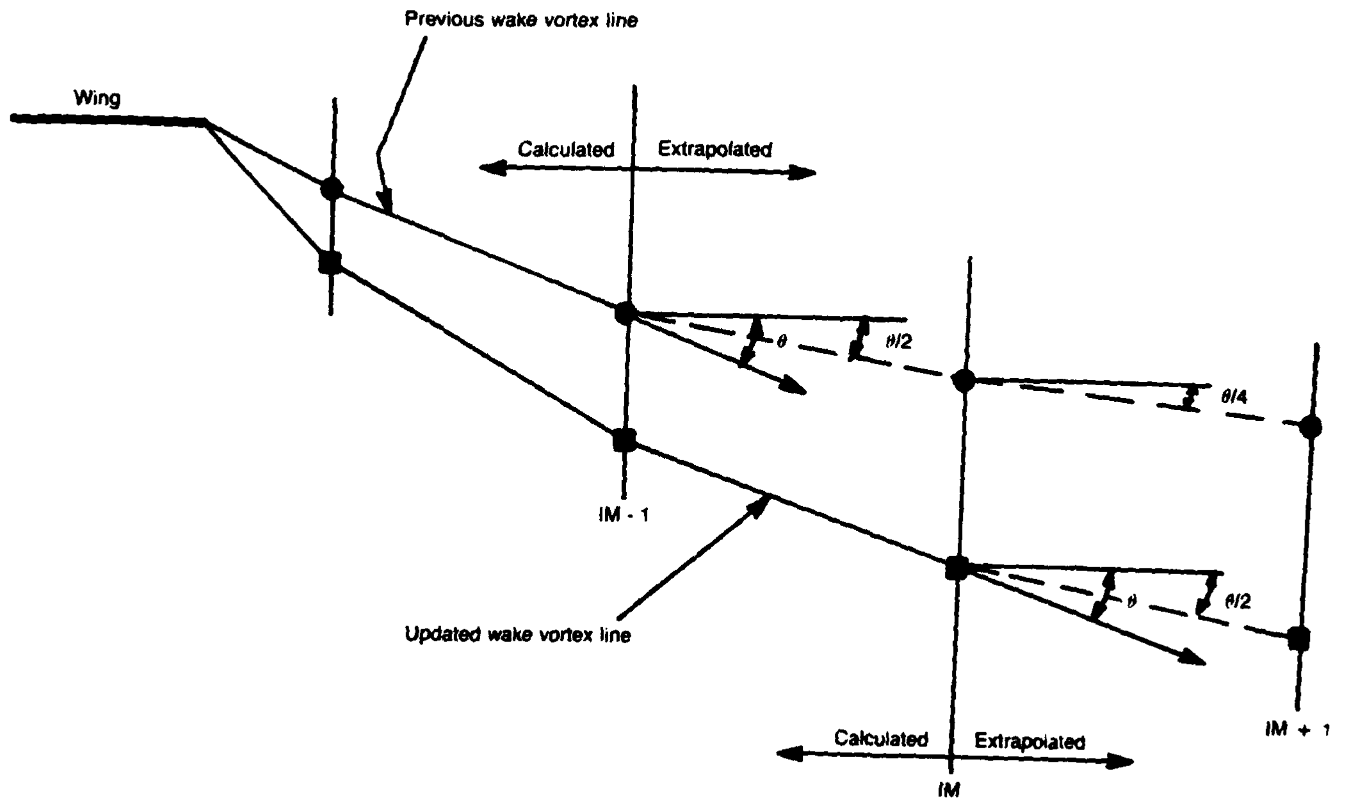

Figure 26. Wake shape iterative development.

$$YV_{I_{MERGED}} = \frac{YV_{I,L+1}\left|d\Gamma_{L+1}\right| + YV_{I,L}\left|d\Gamma_{L}\right|}{\left|d\Gamma_{L}\right| + \left|d\Gamma_{L+1}\right|} \quad \text{(A-3a)}$$

$$ZV_{I_{MERGED}} = \frac{ZV_{I,L+1}\left|d\Gamma_{L+1}\right| + ZV_{I,L}\left|d\Gamma_{L}\right|}{\left|d\Gamma_{L}\right| + \left|d\Gamma_{L+1}\right|} \quad \text{(A-3b)}$$

Scanning over L at a given station I is repeated until the wake coordinates are "single valued," and the vortex lines are renumbered to have consecutive indices. The vortex line tracking (Equation A-1) then continues downstream as before. The vortex line at the symmetry plane or root juncture is continued straight back and never "merged." The proximity test commences with $L = 2$. The merging process is illustrated for a single surface in Figure 27.

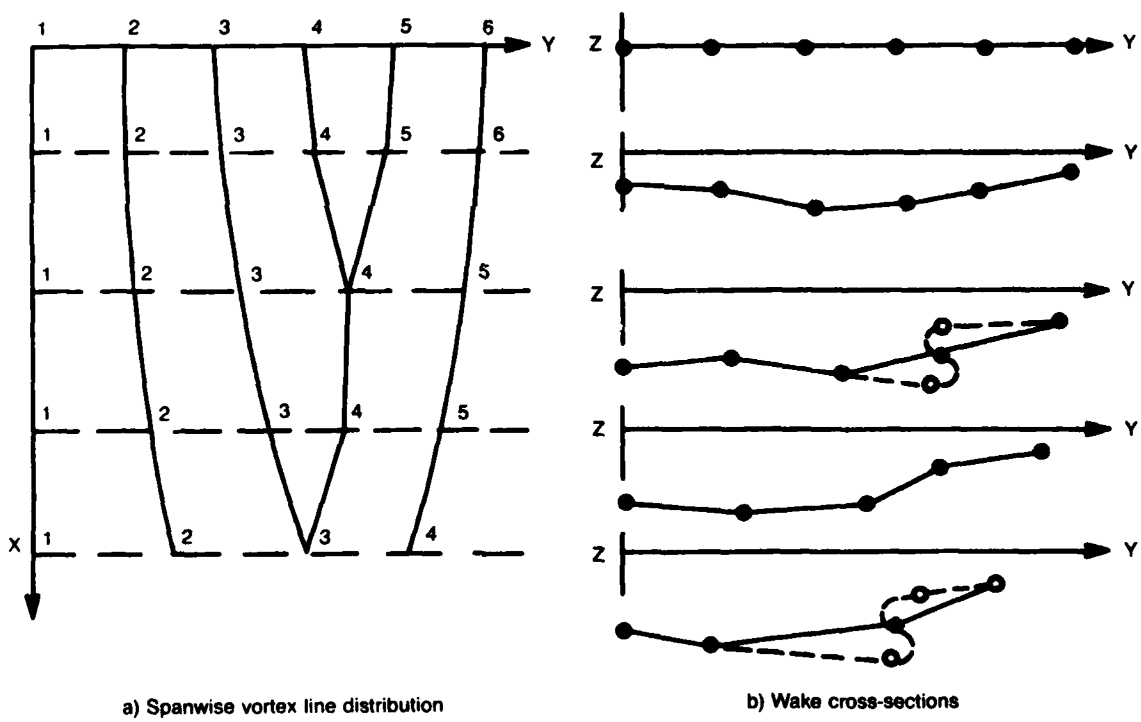

Figure 27. Wake roll-up merging.

A.5 TREATMENT OF LARGE SPANWISE WAKE SLOPE

Even though roll-up is prevented from occurring it is possible for the spanwise slope of the wake to become large and to undergo large changes in the spanwise direction. Both of these circumstances have been found to induce numerical instability in the flow solution. It then becomes desirable to suppress local instances of such occurrences especially in the far wake in order to preserve the solution in the near wake region where it is of importance. This is accomplished by calculating the spanwise slope of the wake at a station I after any necessary vortex merging has been carried out and testing the maximum slope against a reference criterion SLTEST (set at 0.50). If the maximum slope is found between indices J = JKM − 1 and J = JKM

$$\left|\frac{\Delta Z}{\Delta Y}\right| = \left|\frac{Z_{I,JKM}-Z_{I,JKM-1}}{Y_{JKM}-Y_{JKM-1}}\right| \geq \text{SLTEST} \tag{A-4a}$$

a reference line is established

$$Z_{REF} = \tfrac{1}{2}\left(Z_{I,JKM} + Z_{I,JKM-1}\right) \tag{A-4b}$$

and the wake cross-section is scaled about this line:

$$Z_{I,J_{NEW}} = Z_{REF}+(Z_{I,J}-Z_{REF})\ \text{SLTEST}\left|\frac{\Delta Y}{\Delta Z}\right| \tag{A-4c}$$

A modified $Z_{REF}(Y)$ is introduced in the case of swept trailing edges at streamwise stations that intercept the planform. These procedures are illustrated in detail in Figure 28a and Figure 28b. In the latter case $Z_{REF}(Y)$ is chosen to insure that the vortex sheet makes contact with the trailing edge after scaling. If contact is made with only one edge as for the inner section in Figure 28b, Z_{REF} is continued horizontally from the trailing edge.

A.6 PREVENTION OF CROSSING WAKES

Fluid dynamic principles rule out the crossing of wing and canard wakes except along lines of zero vorticity or along stagnation lines. However, due to finite computational grid intervals and the interpolation procedures employed in the numerical solution, the wakes may be found to cross when in fact they should be simply in close proximity. At this point the computational

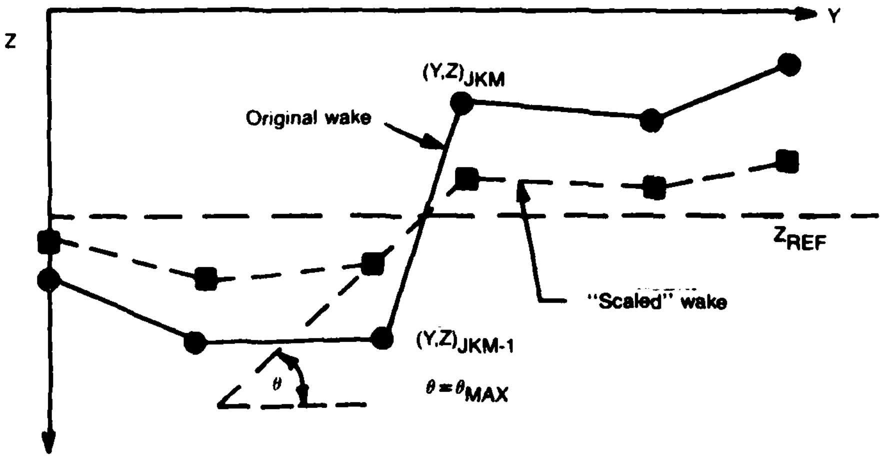

a) Slope correction when not intercepting a swept trailing edge.

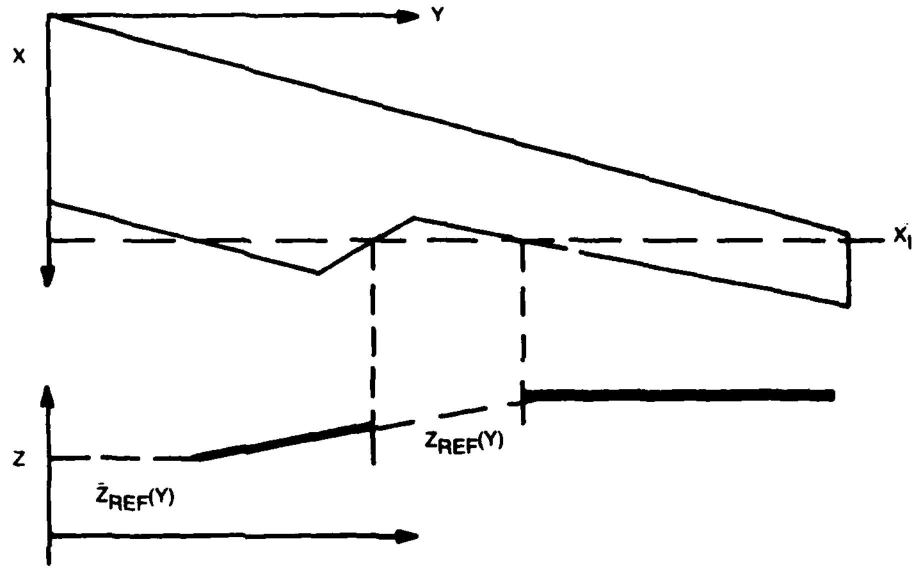

b) Slope correction when intercepting a swept trailing edge.

Figure 28. Spanwise wake slope limitation.

procedure can be expected to break down. To prevent this, the wake is tested by scanning across spanwise grid points J at a fixed streamwise station I after vortex merging and slope corrections have been made. If "crossing" is detected at any J the canard wake is thereafter continued parallel to the wing wake with the separation equal to that at station I-1. In fact, numerical difficulties are encountered when the wakes approach each other too closely before crossing actually occurs. Therefore, the criterion used to detect "crossing" is to compare the wake separation with a minimum acceptable separation SFIX, which is taken to be 0.20 of the original wing-canard vertical separation. Once the canard wake is continued back in parallel fashion, the vortex line generators are assumed to move straight back with constant spanwise distribution of circulation and potential jump.

A.7 WAKE BOUNDARY CONDITIONS

Once vortex merging and slope corrections have been made, the new distribution of circulation, ΓI_L, is found at each streamwise station for all points by simple numerical integration of the vortex strength $d\Gamma_L$. These values of ΓI are interpolated to determine ΓV_L at the vortex line location and further interpolated to determine $\Gamma_{I,J}$ at the grid locations. The wake coordinates at the grid points are also determined by interpolation of the vortex line coordinates. The boundary condition on the wing and canard wake surfaces is the jump in potential equal to $\Gamma_{I,J}$. Beyond the last wake update point no change is considered to occur in the spanwise distribution of Γ. To prevent numerical "kinks" in wake shape at the downstream boundary, the slope in the x direction of the wake is held constant for the three streamwise stations nearest the boundary.

The vertical grid construction considers the wake surfaces to extend beyond the wing and canard tip stations to the outer Y boundary. Thus, beyond the most outboard vortex line of the wake the grid lines are continued with constant values of Z. The edge of the wake is free to expand or shrink as the outermost vortex line is tracked downstream.

APPENDIX B

GLOSSARY OF OUTPUT VARIABLES

CCD/CAV	Spanload drag.
CCF/CAV	Spanload skin friction.
CCL/CAV	Spanload lift.
CCM/CAV/MAC	Spanload pitching moment.
CCMAX	Maximum correction to flow potential for the current iteration.
CCAV	Average of the absolute value of all the flowfield corrections for the current iteration.
CD	Drag coefficient (local or total, as appropriate).
CDINT	Local drag coefficient in spanload tables.
CF	Skin friction coefficient.
CIR	Circulation.
CL	Lift coefficient (local or total as appropriate).
CLINT	Local lift coefficient in spanload tables.
CM	Pitching moment coefficient.
CMLOC	Local pitching moment coefficient (about quarter chord point).
CP	Pressure coefficient.
DRAG	Local drag contribution in the body force output.
ETA	Spanwise computational ordinate.
I	General streamwise index.
IL	Streamwise index of leading edge point in crude grid.
INOSE	Streamwise index of the first point on the body in the body fine grid.
INOSEC	Streamwise index of the first point on the body in the crude grid.
IT	Streamwise index of the trailing edge point at an analysis station in the crude grid.
ITAIL	Streamwise index of the last point on the body in the body fine grid.

ITAILC	Streamwise index of the last point on the body in the crude grid.
ITER	Iteration count.
J	General spanwise index.
JSD	Spanwise index of first solution plane outside the body computational surface.
KLO	Vertical index for bottom of body computational surface.
LOAD	Local lift contribution in body force output.
NSP	Number of supersonic points.
PCT	Fractional cord distance from leading or trailing edge during crude grid shift search.
PHI	Perturbation velocity potential.
RMAX	Maximum body radius.
RSD	Residual with maximum absolute value.
RSDAV	Average of the absolute value of the residual at all grid points for the current iteration.
SEXPC	Canard exposed area.
SHIFT	Grid shift parameter.
U	Streamwise perturbation velocity.
V	Spanwise perturbation velocity.
W	Vertical perturbation velocity or over-relaxation factor.
WCORD	Local cord for wing or canard.
X	Streamwise physical coordinate.
XI	Streamwise computational coordinate.
XLE	Wing or canard leading edge X-location.
XNOSE	Body nose X-location.
XTAIL	Body tail X-location.
XTE	Wing or canard trailing edge location.
XWF	Wing or canard fine grid streamwise physical coordinate.
X/C	Percent fraction of local chord.
Y	Spanwise physical coordinate.
Y/C	Percent chord wing or canard section ordinate.
Z	Vertical physical coordinate.
ZETA	Vertical computational coordinate.
2Y/B	Fraction of semispan (on wing or canard as appropriate).

REFERENCES

1. Aidala, P., "Numerical Aircraft Design Using 3-D Transonic Analysis with Optimization," AFWAL-TR-81-3091, August 1981.

2. Boppe, C.W., "Transonic Flowfield Analysis for Wing-Fuselage Combinations," NASA Contractor Report 3243, May 1980.

3. Vachris, A.F. and Yaeger, L.S., "Quick-Geometry - A Rapid Response Method for Mathematically Modeling Configuration Geometry," NASA SP-390, October 1975, pp. 49-73.

4. Mason, W.H., et al., "An Automated Procedure for Computing the Three-Dimensional Transonic Flow Over Wing-Body Combinations, Including Viscous Effects," Report AFFDL-TR-77-122, Vol. 1, October 1977.

5. Nash, J.F. and Tseng, R.R., "The Three-Dimensional Turbulent Boundary Layer on an Infinite Yawed Wing," The Aeronautical Quarterly, November 1971.

6. Bradshaw, P. and Ferriss, D.H., "Calculation of Boundary Layer Development Using the Turbulent Energy Equation. Compressible Flow on Adiabatic Walls," J. Fluid Mech., Vol. 46, 1971.

7. Hinson, B.L. and Burdges, K.P., "Acquisition and Application of Transonic Wing and Far-Field Test Data for Three-Dimensional Computational Method Evaluation," Technical Report, AFOSR-TR-80-0421, March 1980.

8. Charletta, Roy, "Post Test Report Series I Transonic/Supersonic Testing on a 12.5% Scale Grumman Design 712, X-29A Forward Swept Wing Demonstrator Aircraft Model in the NASA-ARC 11 foot and 9x7 foot Wind Tunnels, at Moffett Field, CA," Grumman Aerospace Report No. 712/ENG-RPT82-021, August 1982.

9. Spurlin, C.J., "Test Report for AFWAL Optimal Transonic Configuration Fighter, Project No. P41T-G6, Test No. TF-570," April 1980.

10. Harris, M.K. and Huie, W.E., "C-5A Aerodynamic Data for Airloads," Lockheed-Georgia Report LG74ER0162, November 1974.

11. Stewart, V.R., "Evaluation of a Propulsive Wing/Canard Concept at Subsonic and Supersonic Speeds," Naval Air Systems Command Report NR82H-85, Vol. 1 and 2, February 1983.

12. Vanderplaats, G.N., "COPES--Control Program for Engineering Synthesis," to be published as a Naval Postgraduate School Memorandum.

13. Vanderplaats, G.N., "CONMIN--A Fortran Program for Constrained Function Minimization," NASA TM X-62282, August 1973.

14. Marconi, F. and Yaeger, L., "Development of A Computer Code for Calculating the Steady Super/Hypersonic Inviscid Flow Around Real Configurations," NASA CR-2676 (Vol. II), May 1976.

U.S. GPO 646-067

END

10-86

DTIC